

Durability of Marine Composites:

A Study of the Effects of Fatigue on Fiberglass in the Marine Environment

by

Paul Holden Miller



Marine Technology and Management Group

Civil and Environmental Engineering

UNIVERSITY OF CALIFORNIA, BERKELEY

Spring 2000

Report Documentation Page		Form Approved OMB No. 0704-0188
Public reporting burden for the collection of information is estimated to average 1 hour per response, including the time for reviewing instructions, searching existing data sources, gathering and maintaining the data needed, and completing and reviewing the collection of information. Send comments regarding this burden estimate or any other aspect of this collection of information, including suggestions for reducing this burden, to Washington Headquarters Services, Directorate for Information Operations and Reports, 1215 Jefferson Davis Highway, Suite 1204, Arlington VA 22202-4302. Respondents should be aware that notwithstanding any other provision of law, no person shall be subject to a penalty for failing to comply with a collection of information if it does not display a currently valid OMB control number.		
1. REPORT DATE 2000	2. REPORT TYPE	3. DATES COVERED 00-00-2000 to 00-00-2000
4. TITLE AND SUBTITLE Durability of Marine Composites: A Study of the Effects of Fatigue on Fiberglass in the Marine Environment		5a. CONTRACT NUMBER
		5b. GRANT NUMBER
		5c. PROGRAM ELEMENT NUMBER
6. AUTHOR(S)	5d. PROJECT NUMBER	
	5e. TASK NUMBER	
	5f. WORK UNIT NUMBER	
7. PERFORMING ORGANIZATION NAME(S) AND ADDRESS(ES) University of California, Berkeley,Civil and Environmental Engineering,Marine Technology and Management Group,Berkeley,CA,94720		8. PERFORMING ORGANIZATION REPORT NUMBER
9. SPONSORING/MONITORING AGENCY NAME(S) AND ADDRESS(ES)		10. SPONSOR/MONITOR'S ACRONYM(S)
		11. SPONSOR/MONITOR'S REPORT NUMBER(S)
12. DISTRIBUTION/AVAILABILITY STATEMENT Approved for public release; distribution unlimited		
13. SUPPLEMENTARY NOTES		

14. ABSTRACT

The growing use of marine composite materials has led to many technical challenges. One is predicting lifetime durability. This step has a large uncertainty as the methods used to design metal ships have never been verified at full-scale for composite vessels. This project systematically extended the isotropic method to the application of fiberglass vessels in the marine environment. The research compared two identical fiberglass vessels having significantly different fatigue histories with undamaged laminates representing a new vessel. Analytical models based on classical lamination theory, finite element analysis, ship motions, probability and wind and wave mechanics were used to predict hull laminate strains. Material properties used in the finite element analysis were based on tested wet and dry conditions. Fatigue tests were used to determine S-N residual stiffness properties. These were compared against strains measured while underway and good correlation was achieved. Fatigue damage indicators were identified which could be used in vessel inspection procedures. Endurance limits were found to be near 25% of static load, indicating a fatigue design factor of 4 is required for these materials. This exceeds ABS and US Navy design guides. Comparisons were made of standard moisture experiments using boiling water versus long-term exposure. Results indicated the boiling water test yielded significantly conservative values and was not a reliable means of predicting long-term effects. Panel tests were compared to a combined coupon and finite element procedure. Results indicated the proposed procedure was a viable substitute, at least for the materials studied. A rational explanation for using thicker outer laminates in marine composites was verified through single-sided moisture flex tests. These showed that the reduced strength and stiffness due to moisture of the outer hull skin laminate could be compensated by increased thickness. Although the resulting non-symmetrical laminate is not ideal from a warping standpoint, the approach leads to consistent tensile failure of the inner skin when subjected to normal loads. Permeability considerations make this desirable for hull laminates. The developed method can be used to design optimized strength-based laminates. This method will yield more weight-efficient vessels than current methods, while in some cases, also increasing safety.

15. SUBJECT TERMS

16. SECURITY CLASSIFICATION OF:

a. REPORT

unclassified

b. ABSTRACT

unclassified

c. THIS PAGE

unclassified17. LIMITATION OF
ABSTRACT**Same as
Report (SAR)**18. NUMBER
OF PAGES**196**19a. NAME OF
RESPONSIBLE PERSON

Durability of Marine Composites

Copyright 2000

by

Paul Holden Miller

Abstract

Durability of Marine Composites

by

Paul Holden Miller

Doctor of Engineering in Civil Engineering

University of California, Berkeley

Professor Robert G. Bea, Chair

The growing use of marine composite materials has led to many technical challenges. One is predicting lifetime durability. This step has a large uncertainty as the methods used to design metal ships have never been verified at full-scale for composite vessels.

This project systematically extended the isotropic method to the application of fiberglass vessels in the marine environment. The research compared two identical fiberglass vessels having significantly different fatigue histories with undamaged laminates representing a new vessel. Analytical models based on classical lamination theory, finite element analysis, ship motions, probability and wind and wave mechanics were used to predict hull laminate strains. Material properties used in the finite element analysis were based on tested wet and dry conditions.

Fatigue tests were used to determine S-N residual stiffness properties. These were compared against strains measured while underway and good correlation was achieved. Fatigue damage indicators were identified which could be used in vessel inspection procedures. Endurance limits were found to be near 25% of static load, indicating a fatigue design factor of 4 is required for these materials. This exceeds ABS and US Navy design guides.

Comparisons were made of standard moisture experiments using boiling water versus long-term exposure. Results indicated the boiling water test yielded significantly conservative values and was not a reliable means of predicting long-term effects. Panel tests were compared to a

combined coupon and finite element procedure. Results indicated the proposed procedure was a viable substitute, at least for the materials studied.

A rational explanation for using thicker outer laminates in marine composites was verified through single-sided moisture flex tests. These showed that the reduced strength and stiffness due to moisture of the outer hull skin laminate could be compensated by increased thickness. Although the resulting non-symmetrical laminate is not ideal from a warping standpoint, the approach leads to consistent tensile failure of the inner skin when subjected to normal loads. Permeability considerations make this desirable for hull laminates.

The developed method can be used to design optimized strength-based laminates. This method will yield more weight-efficient vessels than current methods, while in some cases, also increasing safety.

Acknowledgements

During this study's six-year course numerous people have provided analytical, financial or emotional assistance, and although it is hard to adequately convey my appreciation for all their help, listing them here is at least one small measure of my gratitude!

Professors Bob Bea, Alaa Mansour, Hari Dharan and Ben Gerwick, Jr. of UC Berkeley for their never-ending academic guidance, encouragement and patience.

Professors Dave Kreibel, Bruce Nehrling and Greg White of the US Naval Academy for their support and understanding.

Steve Burke of TPI for unlimited technical assistance regarding the J/24's construction and TPI for providing all the test specimens.

Steve Slaughter of Maricomp for expert technical and practical fatigue analysis advice and for providing a computer and software.

Rich Jepsen and Anthony Sandberg of OCSC for the generous use of two boats and for the opportunity to dig through boxes of files in order to compile the daily history of J6.

Tracy Powell, Thom Henneberger, Tom Sitzmann and Brent Vaughn for their knowledge of sailing J/24's (both technical and practical)

Erich Chase, Susan and Steve Chamberlin, Nancy Pettengill, Dominique Roddier, ENS Tullio Cellano and ENS Katy Westover, USN, for providing assistance during on-the-water testing.

Frank Bucalo, Steve Crutchley, Rusty Foard, Gary Gibson, Roy Goddard, Charlie Hoyt, Gene Miller, Tom Price and Jim Watts of the US Naval Academy for technical and practical testing assistance.

David St. James of WindCall for providing over 1000 daily wind data files on the Berkeley Circle wind conditions.

Gary Mull for providing the initial spark that got me interested in the analysis of small craft structures and materials.

Carl Schumacher for technical support in current small craft practice.

American Bureau of Shipping for financial assistance with testing costs and for project planning.

The US Naval Academy and the Office of Naval Research (through the Naval Academy Research Council) for financial, fabrication and testing support.

And finally, and perhaps most importantly, my sincere thanks to my wife Dawn and my parents, Sarah and Gordon Miller, for all their encouragement and support!

Paul H. Miller

April 2000

Durability of Marine Composites

Table of Contents

Abstract	i
Acknowledgements	iii
Table of Contents	iv
1.0 Introduction	1
2.0 Summary of Marine Composites Applications	5
<i>Figure 2-1: 1993 Marine Industry Market Segments</i>	6
<i>Figure 2-2: Segments of the Recreational Marine Industry</i>	6
3.0 Current Practice in Materials, Analysis and Testing	8
3.1 Marine Composite Materials	8
<i>Table 3-1: Typical Material Properties for Unidirectional Plies Used in the Marine Industry Compared to Traditional Metals</i>	8
<i>Table 3-2: Characteristics of Varying Manufacturing Methods of Marine E-glass/Epoxy</i>	9
3.1.1 Fibers	9
<i>Table 3-3: Market Shares of Reinforcement Fibers for Marine Use</i>	10
3.1.2 Resins	10
<i>Table 3-4: Market Shares of Resins for Marine Use</i>	11
3.1.3 Cores	11
<i>Table 3-5: Effect on Flexural Properties of Switching from Single Skin to Sandwich Construction</i>	12
<i>Table 3-6: Market Shares of Core Materials for Marine Use</i>	12
3.2 Common Design and Analysis Methods	13
3.2.1 Loading Models	14
<i>Table 3-7: Design Loads for Marine Composites</i>	14
3.2.2 Stiffness Models	15
<i>Table 3-8: Stiffness Matrix, C, of a Transversely Isotropic Material</i>	17
<i>Table 3-9: Compliance Matrix, S, in Terms of Engineering Constants of a Transversely Isotropic Material</i>	17
3.2.3 Strength Models	22
3.2.4 ABS Design Codes	23
3.2.5 Fatigue Models	25
<i>Figure 3-1: Comparison of the Fatigue Behavior of Glass, Carbon and Glass-Carbon Hybrid Quasi-Isotropic Laminates</i>	27
3.3 Testing Methods	28
3.4 Limitations of the Current Practice	29
3.4.1 Stiffness and Strength Analysis	29
3.4.2 Load Prediction Limitations	30
3.4.3 Moisture Effects Limitations	31
3.4.4 Testing Methods Limitations	32
4.0 Current Research in Analysis and Testing	34
4.1 Design and Analysis Methods	34
<i>Table 4-1: Levels of Uncertainty in Marine Design</i>	35
4.1.1 Loading Models	35
<i>Figure 4-1: Maximum Pressure Due to Slamming (u=10 fps)</i>	38
<i>Figure 4-2: Slamming Drop Test on Stiffened Aluminum Model in Symmetrical Position</i>	39
<i>Table 4-2: Comparison of Tensile and Shear Strengths of Marine Materials</i>	40
<i>Table 4-3: Types of Loads Used in Metal Vessel Analysis</i>	41
<i>Figure 4-3: Forces on a Sailing Yacht</i>	46
4.1.2 Stiffness and Strength Models	47
4.1.3 Fatigue Models	50

4.1.4 Moisture Effects.....	52
<i>Figure 4-4: Moisture Diffusion Through a Carbon/Epoxy Skin Laminate.....</i>	<i>54</i>
4.2 Testing Methods.....	54
<i>Figure 4-5: Lloyd's Register of Shipping Fatigue Testing Machine.....</i>	<i>55</i>
<i>Figure 4-6: Schematic of FIT Pressure Test Apparatus.....</i>	<i>56</i>
<i>Figure 4-7: Schematic of the Hydromat Testing System.....</i>	<i>57</i>
5.0 Research Overview.....	59
6.0 Coupon Testing Program.....	60
6.1 Moisture Exposure Tests	60
<i>Table 6-1: Abbreviations Used in Coupon Specification.....</i>	<i>62</i>
<i>Table 6-2: Average Weight Gain and COV for Tensile and Shear Coupons</i>	
<i>After 226 Days.....</i>	<i>62</i>
<i>Figure 6-1: Experimental vs. Theoretical Weight Gain for Polyester/E-glass</i>	
<i>Specimens.....</i>	<i>63</i>
6.1.1 Sealed-Edge Moisture Exposure Tests	63
<i>Figure 6-2: Weight Gain Comparison Between Edge-Sealed and Unsealed</i>	
<i>Specimens.....</i>	<i>64</i>
<i>Table 6-3: Change in Tensile Strength Due to Long Term Submergence</i>	
<i>and 24 Hour Boiling.....</i>	<i>66</i>
<i>Figure 6-3: Predicted Weight Gain of J/24 Hull Laminate.....</i>	<i>67</i>
6.2 Tensile Tests.....	67
<i>Figure 6-4: Tensile and Shear Test Set-up Showing Extensometer and</i>	
<i>Strain Gauges.....</i>	<i>68</i>
<i>Figures 6-5 and 6-6 Showing the Effects of Extensometer Calibration.....</i>	<i>69</i>
<i>Figure 6-7: Broken Tensile Specimen.....</i>	<i>70</i>
<i>Table 6-4: Tensile Test Results (psi).....</i>	<i>71</i>
6.3 Shear Tests.....	71
<i>Table 6-5: Shear Test Results (psi).....</i>	<i>72</i>
6.4 Compressive Tests	72
<i>Figure 6-8: Compressive Grips Design.....</i>	<i>73</i>
<i>Figure 6-9: Compressive grips with failed specimen.....</i>	<i>74</i>
<i>Table 6-6: Uncored Compressive Test Results (psi)</i>	<i>75</i>
<i>Table 6-7: Cored Compressive Test Results (psi)</i>	<i>75</i>
6.5 Poisson's Ratio Tests.....	76
<i>Table 6-8: Poisson's Test Results.....</i>	<i>76</i>
6.6 Static Flexural Coupon Testing.....	76
<i>Figure 6-10: 3-Point Test Jig.....</i>	<i>78</i>
<i>Figure 6-11: 4-Point Test Jig.....</i>	<i>78</i>
<i>Figure 6-12: Typical Load-Deflection Curve and Tangent Modulus Line for</i>	
<i>4-Point Bend Test.....</i>	<i>80</i>
<i>Table 6-9: 3 and 4-point Tangent Flexural Modulus and Strength</i>	
<i>(Homogenous Beam Equation) (psi).....</i>	<i>81</i>
<i>Table 6-10: ASTM C393 3 and 4-point Flex Test Results.....</i>	<i>83</i>
6.7 Flexural Fatigue Tests.....	85
<i>Figure 6-13: 4-point Fatigue Test Jig Drawing.....</i>	<i>86</i>
<i>Figure 6-14: 4-point Fatigue Test Jig.....</i>	<i>86</i>
<i>Figure 6-15: Stiffness Reduction Due to Fatigue of Wet and Dry J/24</i>	
<i>Laminates.....</i>	<i>88</i>
<i>Figure 6-16: Fatigue Damage on 50% Specimens After 7500 Cycles.....</i>	<i>90</i>
7.0 Panel Testing Program	92
<i>Figure 7-1: Panel Test Jig Drawing.....</i>	<i>93</i>
<i>Figure 7-2: Panel Test Jig.....</i>	<i>94</i>
<i>Figure 7-3: Load vs. Deflection and Strain for J/24 Panel Test</i>	<i>95</i>
8.0 Full-Scale Testing Program	96
8.1 Vessel Description	96
<i>Figure 8-1: A J/24 (J6) Sailing on San Francisco Bay</i>	<i>97</i>

8.2 Vessel Service Lives	97
8.2.1 J6 Service Life	99
Table 8-1: 1998 Daily Sailing Hours for J6	100
Table 8-2: Month-to-Month Usage of J6 from 1996 to 1999	100
Figure 8-1: Month-to-month Usage of J6 from Jan. 1996 to June 1999	101
8.2.2 Wind and Wave History for J6	101
Figure 8-2: Typical Wind Readings (knots) from the Area of J6's Sailing; 16 July, 1999	102
Figure 8-3: Location of WindCall Anemometer at Berkeley (top left)	103
Figure 8-4: Average Monthly Wind Speed for San Francisco Airport	104
Table 8-3: Comparison of Wind Speed Data for 7/84-7/98 and 7/96-7/98	104
Table 8-4: Monthly Average Wind Speeds for Daylight Hours at Berkeley	105
Table 8-5: Wave Characteristics for Berkeley Circle	107
Figure 8-5: Significant Wave Height (Ht) and Period (Ts) for Berkeley Circle	107
Figure 8-6: Location of Berkeley Circle in San Francisco Bay	108
Figure 8-7: J/24 Polar Speed Diagram	110
Table 8-6: Probability Density Function for Sailing School Vessel Course	111
8.2.3 "Imagination" Service Life	112
8.3 On-the-Water Tests	113
8.3.1 Calibration of Loos Rig Load Gauge	113
Figure 8-8: Test set-up used to correlate Loos Gauge vs. 1x19 and Dyform wire	114
Figure 8-9: Correlation Plots of Loos Professional Gauge for 1x19 and Dyform Stainless Steel Wire	115
Figure 8-10: Load-Extension Plot of 1x19 and Dyform Wire	115
Table 8-7: Stiffness of 1x19 and Dyform Wire	116
8.3.2 Boat Instrumentation	116
Table 8-8: Instrument Locations for Boat Tests	116
Figure 8-11: Location of Below Waterline Strain Gauges	117
Figure 8-12: Interior of J/24 with Gary Gibson and Data Acquisition System	118
8.3.3 Dockside Full-Scale Tests	118
8.3.4 Underway Full-Scale Tests	119
Figure 8-13: Imagination During Testing on San Francisco Bay	120
Figure 8-14: Wind Recording at Berkeley, July 20, 1999	121
Figure 8-15: Accelerometer Data from Underway Testing	122
Figure 8-16: Inside Hull Laminate Strain Gauge Data from Underway Testing	122
9.0 Finite Element Analysis	123
9.1 Tensile and Compressive Coupon Correlation	125
Table 9-1: Final Material Properties for J/24 FEA	125
Table 9-2: Test Values vs. Rule of Mixtures Prediction of Laminate Stiffness	126
Figure 9-1: Tensile Coupon FEA Displacements (in)	127
Figure 9-2: Tsai-Wu Plot of Tensile Coupon at Failure	127
9.2 Flexural Coupon Correlation	128
Figure 9-3: 3-Point Coupon FEA Displacements at Predicted Failure (in)	128
Figure 9-4: Tsai-Wu plot of 3-Point Coupon at Predicted Failure	129
Figure 9-5: 4-Point Coupon Displacement (in)	129
Figure 9-6: Tsai-Wu Plot of 4-Point Coupon at Failure	130
Table 9-3: Tested and Predicted (2-D FEA) Panel Stiffness, Core Shear Modulus and Strength	130
Figure 9-7: Deformed Linear Solid Element Flexural FEA Model (4-point) (in)	132

Table 9-4: Tested and Predicted (3-D FEA) Panel Stiffness, Core Shear Modulus and Strength	132
9.3 Finite Element Panel Study	133
9.3.1 Mesh Density Study	134
Table 9-5: Mesh Density Verification of Deflections.....	135
Table 9-6: Mesh Density Verification of Stresses	135
Figure 9-8: Convergence of Stresses.....	135
Figure 9-9: Final Panel Verification Model Showing Loading and Boundary Conditions.....	137
Figure 9-10: Stress Contours for Deformed Simply-Supported Panel.....	137
Figure 9-11: Stress contours for Deformed Fixed Edge Panel	138
Table 9-7: Comparison of FEA and Linear Plate Theory Predictions	138
Table 9-8: Effects of formulation corrections on 24x24 simply supported panel.....	139
Table 9-9: Effects of formulation corrections on 24x24 fixed-fixed panel	139
9.3.2 Correlation with Panel Tests	140
Figure 9-12: Center Deflection of an Edge-Clamped Panel Versus Pressure Loading.	143
Figure 9-13: Deflections for Deformed J/24 Laminate Simply-Supported Panel (8.4 psi load).....	144
Figure 9-14: Layer 7 Stress Plot for Deformed J/24 Laminate Simply-Supported Panel (8.4 psi load).....	145
Figure 9-15: Tsai-Wu Plot at Predicted Failure (8.4 psi).....	146
Figure 9-16: Load-Deflection Curves for Pressure Loaded J/24 Hull Panel vs. FEA Predictions	147
Figure 9-17: Deformed Displacement Plot of Nonlinear Panel and Frame Model (13 psi).....	148
Figure 9-18: Measured and Predicted Strains in J/24 Hull Panel	148
9.4 Full Scale Test Correlation.....	150
9.4.1 FEA Methodology for Complex Structures.....	150
9.4.2 Global/Local Finite Element Model Methodology.....	153
9.4.3 J/24 Global Finite Element Model	156
Table 9-10: Element Groups and Real Constant Sets for Global Model	157
Figure 9-19: FEA Model of the J/24.	158
Figure 9-20: Interior Components of the J/24	159
9.4.4 Dockside Test Correlation.....	160
Table 9-11: Correlation of Dockside Static Test (Displacements in inches) Versus a Hypothetical New Vessel	161
Figures 9-21 to 9-23: J/24 Unloaded, and Floating with Slack and Tight Rigs (in)	162
9.4.5 Underway Test Correlation	163
Figure 9-24: Wave Elevation and Rig Loads Simulating Test Conditions	163
Figure 9-25: Slamming Pressure Application Point.....	164
Figure 9-26: Slamming Strain Plot for Inner (cloth) Layer, WS=12.5 knots, Hs=1 foot	166
Figure 9-27: Slamming Strain Plot for Outer (mat) Layer, WS=12.5 knots, Hs=1 foot	166
Figure 9-28: Slamming Strain Plot for Inner (cloth) Layer, WS=22.5 knots, Hs=2 feet	168
Figure 9-29: Slamming Strain Plot for Outer (mat) Layer, WS=22.5 knots, Hs=2 feet	168
9.4.6 Cumulative Stiffness Reduction	169
Table 9-12: Predicted and Measured Stiffness Reduction for J6 and Imagination	170
10.0 Conclusions and Recommendations	171
11.0 References.....	175

12.0 Appendices	186
-----------------------	-----

Durability of Marine Composites

1.0 Introduction

Composite materials are used throughout the marine industry for numerous applications including hull shells, internal structure, superstructures, piping, shafts, foundations, ducts, and gratings [1-28]. Most applications are in recreational and small commercial vessels, with composites use in offshore structures and naval vessels rapidly growing.

The history of composites in the marine environment is about 40 years old. During this time empirical rules-of-thumb and experience have developed methods that work adequately, if not conservatively, for long-term service. With the continuing development of new materials however, faster and more reliable methods must be developed to characterize the durability, reliability, and uncertainties of composites for marine use. For example, the first 30 years of marine composites were dominated by single-skin construction, but during the last decade sandwich construction using lightweight cores has found increasingly greater use. This change has required a new, time consuming and expensive learning curve. Durability problems, particularly for below waterline applications, have surfaced as the new construction process became widespread [25, 29]. In addition to safety issues, current empirical methods often do not lead to the most optimized structure [30, 31].

Composite materials are described as a two-phase material that exhibits improved properties over those of each constituent material by itself [32]. The broadness of this statement allows a diverse group of materials to be called "composites." Some traditional marine materials meeting this definition include reinforced concrete, ferro-cement (steel/cement) and even wood (cellulose/lignin). Some analytical approaches work for all these materials.

Macromechanical stiffness analysis of multi-phase materials is well developed and is based on classical laminated plate theories developed by Timoshenko. They work adequately for most thin laminates [33]. Failure criteria were developed for specific material types such as wood, concrete, metal matrix composites and polymer based composites [15, 32-35]. Due to the

current marine industry focus, this paper limits its scope to polymer matrix composites using fibrous reinforcements, with common examples including polyester resin and glass reinforcement laminates.

The reasons these composites have increased in popularity can be traced to fundamental differences between composites and traditional marine materials. These differences include:

- Higher specific stiffness along primary load path compared to metals
- Higher specific strength along primary load path compared to metals
- Greater geometric tailorability
- Better stiffness tailorability
- Higher resistance to the marine environment
- Lower maintenance costs
- Better low temperature properties

The first two attributes relate to the lighter weight structures possible with composites, and are the reason why composites are seriously considered for any high speed or other weight-sensitive marine vehicle [36]. Common composites are not suitable for all marine applications however, as they have significant drawbacks, including:

- Lower quasi-isotropic modulus of elasticity than steel and in some cases aluminum
- Lower heat tolerance
- Higher initial cost
- Lower impact resistance
- Lower UV resistance
- Difficulties with joining

Currently, two drivers focus much of the ongoing marine composites research. One is the dichotomy between lower in-service costs and higher initial cost [37]. In the past, by "overbuilding" initially due to high factors-of-safety, composites have gained a reputation of durability. This causes higher initial costs and makes composites less economically competitive

against other marine materials. The full benefits of weight reduction are also not realized. As with any new material high factors of safety are initially used and are reduced as familiarity and better analysis methods are developed. Current U. S. Navy required factors-of-safety for marine composites range from 2.5 to 4 and illustrate the current lack of confidence mostly due to a lack of data on reliability [18, 30]. Many potential commercial and military buyers of composites are beginning to judge total life-cycle costs rather than the traditional initial costs only when evaluating bids, which will likely lead to greater use of the materials [38].

The other research driver is enhanced environmental legislation, including the Clean Air Act of 1990. Primarily focused on reducing volatile organic compounds (VOC) emissions during manufacturing, legislators and the composites fabrication industry are looking to reduce VOC's while not degrading the finished product's fatigue properties. One of the few studies performed indicated some VOC improvement is possible through modified resin formulation although potential physical properties degradation may occur [39].

Most composites research concentrates on developing theories and methods for aerospace components as those applications enjoy a clearer cost/weight trade-off. Transferring this aerospace experience to marine composites has had some but not widespread success, mainly due to a different operating environment and cost drivers leading to different choices of materials and manufacturing methods [4]

This paper addresses the lack of data in durability by correlating current test and analysis methods with full-scale results. The correct use of this detailed method will allow designers to more accurately predict fatigue effects, eliminating the use of somewhat arbitrary factors included in the industry-standard design guides. The research program included the following components:

1. Review of appropriate laminates, construction methods, analysis methods, and materials representing baseline, current and future industry trends. Selection of a representative material and application for verification.
2. Determination of appropriate fatigue loading for the anticipated application through historical review of the vessels' service lives.

3. Verification and modification of current test methods to better reflect actual load conditions, including strain rate, moisture and boundary conditions.
4. Correlation of test methods to numerical analysis and full-scale results to produce a verified, workable method for fatigue analysis of composite vessels.

This paper is divided into 12 sections:

Section 1: Introduction.

Section 2: Summary of Marine Composites Applications

Section 3: Current State-of-the-Practice: Materials, Analysis and Testing

Section 4: Current Research in Analysis and Testing

Section 5: Project Overview

Section 6: Coupon Testing Program

Section 7: Panel Testing Program

Section 8: Full-Scale Testing Program

Section 9: Finite Element Analysis Correlation

Section 10: Conclusions and Recommendations

Section 11: References

Section 12: Appendices

The first four sections provide background information used in developing the research. Section 5 describes the overall program and Sections 6-9 provide detailed results.

2.0 Summary of Marine Composites Applications

Typical applications for marine composites include recreational craft ranging from sailboards and canoes to speedboats and motor and sail yachts up to 160 feet [17], military vessels up to 180 feet [6, 40], and components of offshore structures [9, 10].

Figure 2-1 shows the total marine market share by government, commercial, and recreational segments [26, 41-43]. *Government* includes the Navy, Coast Guard, Army Corp. of Engineers, Military Sealift Command, foreign military aid and states expenditures. With the exception of minesweepers, utility boats and submarine bow domes, few composites are used in naval applications. *Commercial* includes oceangoing trade vessels, cruise/gambling ships, fishing vessels and small workboats. Generally, commercial vessel uses of composites are limited to fishing vessels and high speed ferries and utility craft. *Recreational* includes yachts, boats and other non-trade or government vessels. Roughly 80-90% of recreational craft are made of composites [44]. An important point is that the cost data includes repairs, which skew the results towards the more expensive government and commercial segments. Based on the data and assumptions stated above, approximately 20-30% of the total marine industry uses composites.

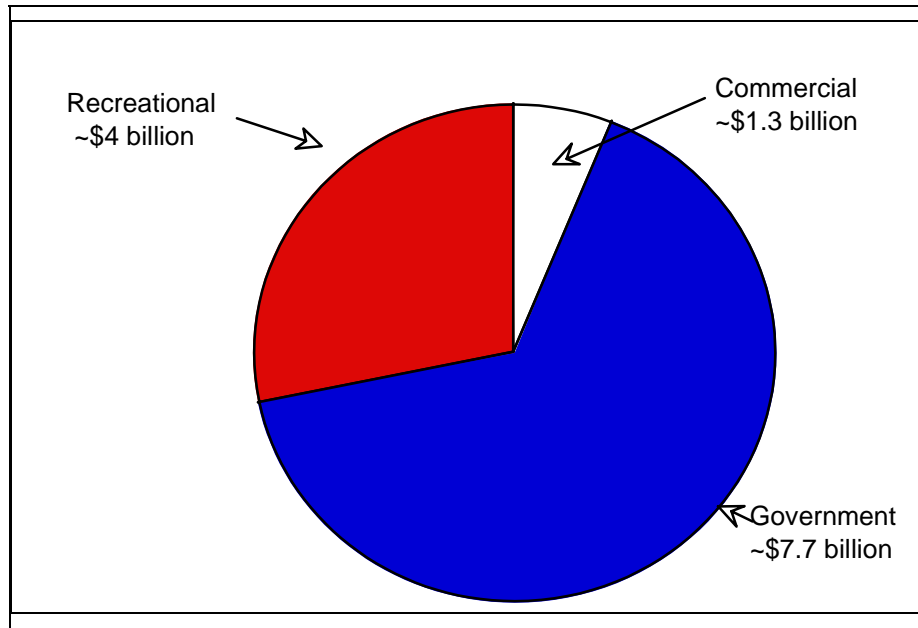


Figure 2-1: 1993 Marine Industry Market Segments

As noted above, the largest use of composite materials in the marine environment is in the recreational market. These products range from canoes, jet-skis and windsurfers, to luxury yachts up to 169 feet. Figure 2-2 shows a breakdown of the recreational market in 1993 [26, 43].

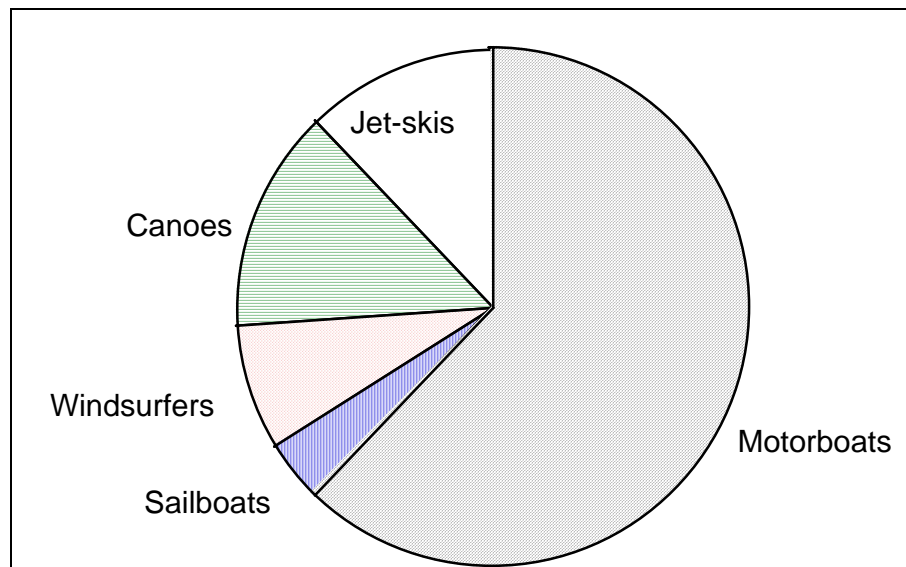


Figure 2-2: Segments of the Recreational Marine Industry

Given the longer history of composites in the recreational industry and the greater availability of samples for study, the research in this project focussed on a common recreational marine composites laminate and application. Although the specific application is from the recreational sector, the materials, testing and analysis methods could apply to any sector.

As with all composites design, marine composites applications are specifically designed and constructed to meet the owner's requirements. The current state of the marine composites industry, including materials, design and construction practices are described in the following section.

3.0 Current Practice in Materials, Analysis and Testing

3.1 Marine Composite Materials

The growing use of marine composites is mainly due to the advantages listed in Section 1. Table 3-1 compares the material properties of two most common marine composite materials and two traditional marine materials [11]. E_x is the longitudinal modulus and X_t is the longitudinal tensile strength. Note that these are for unidirectional plies where all the fibers run in one direction. More realistic laminates have fibers running in multiple directions and the resulting properties would vary from 30-75% of the tabled values, reflecting the percentage of plies oriented in the primary load path. Nonetheless, for stiffness driven design the E_x/ρ column shows that carbon/epoxy laminates have the highest properties, and for strength driven design the X_t/ρ column shows that both composites out perform traditional materials.

Material	Sp. Dens, ρ	E_x (msi)	X_t (ksi)	E_x/ρ	X_t/ρ
Glass/Polyester	1.8	5.6	154	3.1	85.6
Carbon/Epoxy	1.56	20	210	12.8	135
Aluminum	2.8	10	40	3.6	14.3
Steel	7.8	30	80	3.8	10.3

Table 3-1: Typical Material Properties for Unidirectional Plies Used in the Marine Industry Compared to Traditional Metals

The specific formulation of marine composites, both laminate selection and fabrication method, is driven by production requirements, anticipated service-life loading, marine environment effects and cost. Three distinct technology levels are used in marine composites and can be characterized by their fabrication technology, base material selection and cost. Fabrication technologies vary by cure temperature and pressure, from ambient to autoclave temperatures and pressures. Table 3-2 presents the relative differences between different manufacturing

technologies using the same fiber reinforcement [45]. The higher mechanical properties are due to the higher volume fraction of fiber possible with higher pressure cure materials. Analytically these are commonly determined by a “rule-of-mixtures” approach [35].

Tech. Level ⇒	"Low"	"Medium"	"High"
Cure Pressure	ambient	11-14 psi	250-350 psi
Cure Temperature	ambient	150-200F	250-350F
Longitudinal Elastic Modulus (msi)	5.6	6.5	7.6
Longitudinal Strength (ksi)	154	165	169
Relative Unit Cost	1	1.5-2.5	4-10
Examples	utility boats, minesweepers, low cost recreational	naval fairings, high- end recreational	submarine bow domes

Table 3-2: Characteristics of Varying Manufacturing Methods of Marine E-glass/Epoxy

Void content levels are particularly important as they dramatically effect moisture absorption rates and the loss of shear and compressive strengths, particularly in fatigue. Void contents generally range from 8% for the lowest technology to less than 1% for the autoclave-cured composites [4].

3.1.1 Fibers

Reinforcement fibers provide the primary stiffness and strength in polymer composites. In marine applications three basic materials are used for fiber construction: glass, aramid (Kevlar[®]), and carbon. Table 3-3 shows the share of each fiber in the marine industry based on a 1990 industry survey [44]. In general, E-glass is the most common material, with S-glass, (a high strength glass showing strength properties 30% above E-glass) used only in strength-to-weight critical

structures [22] . Kevlar and carbon are generally limited to structures driven by the stiffness-to-weight ratio[11].

Fiber Material	Market Share
Glass	73%
Kevlar	16%
Carbon	8%
others	3%

Table 3-3: Market Shares of Reinforcement Fibers for Marine Use

The material properties of an actual cured laminate made from these reinforcements can vary significantly. In addition to the variances in base material properties this is also caused by differences in manufacturing methods.

3.1.2 Resins

Resins act as the matrix that holds the fiber bundles in alignment. To fulfill this requirement the cured resin must have good bonding and shear properties. Most resin systems used in the marine industry are alloyed with various fillers, extenders and solvents to modify viscosity, improve specific properties, extend shelf life or ease fabrication. On-going improvements and new environmental legislation combine to create continuous reformulation of the resins. Table 3-4 shows the distribution of resins in marine applications in 1990 [44]. Since 1990, and mainly due to costly repairs caused by osmotic blistering, the relative amount of polyester has reduced and vinyl esters and epoxies have increased [46]. Polyester resins remain the most popular due to their low cost. Both polyesters and vinyl esters are cured by catalysts, while epoxies are cured by the addition of a hardener. Vinyl esters and epoxies have mechanical properties exceeding those of polyesters. This will be discussed further in later sections.

Resin Type	Market Share
Polyester	65%
Vinyl ester	19%
Epoxy	12%
others	4%

Table 3-4: Market Shares of Resins for Marine Use

3.1.3 Cores

As mentioned earlier, the first three decades of marine composites were dominated by single-skin construction. By 1990 however, sandwich composites were as common as single skin [44].

The reason was that the higher fiber volumes made possible by vacuum-bagging and tighter woven materials required less resin than was commonly used, resulting in thinner skins.

Although these new materials and methods allowed engineers to easily meet in-plane stress and deflection limits, out-of-plane stresses and deflection limits could not be met. The solution was to go to sandwich construction where the laminate was divided in half and a lightweight core placed in the middle. Table 3-5 shows the impact on out-of-plane properties when switching from single-skin to sandwich construction [47].

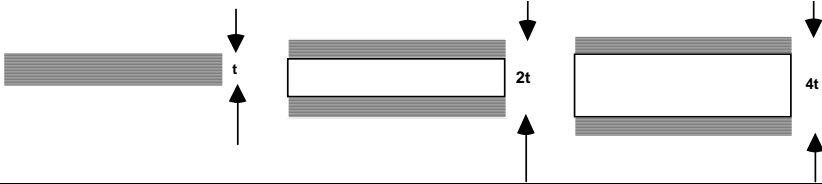
			
Relative Stiffness	100	700	3700
Relative Strength	100	350	925
Relative Weight	100	103	106

Table 3-5: Effect on Flexural Properties of Switching from Single Skin to Sandwich Construction

Common core materials used in the marine industry include foams (mostly PVC) and end-grain balsa wood. Table 3-6 shows the market shares of various cores in the marine industry [44].

Core Type	Market Share
Balsa wood	30%
Foam	47%
Honeycomb	7%
others	16%

Table 3-6: Market Shares of Core Materials for Marine Use

Extensive experience with these core materials has led to satisfactory experience when constructed to classification society guidelines [48-50]. Another material type finding successful applications is honeycomb cores made of Nomex[®] (a para-aramid developed by DuPont) or aluminum. Although not recommended for many below waterline applications, honeycomb materials are attractive due to their lower density (3.5 lbs/ft³ vs. 6-9 lbs/ft³), yet similar material

properties and cost than foams or balsa. Bonding challenges exist however due to the smaller bonding area and the possibility of substantial water intrusion if the outer skin is damaged. This weakness caused problems in naval utility boats in the 1960's and steered the Navy away from honeycomb [16].

Problems with sandwich laminates typically fall into three categories:

- Water absorption. Moisture is absorbed either into the voids within the core or the interstitial areas between core pieces.
- Core shear. Failure occurs through loads exceeding core shear values which typically fall between 100-300 psi.
- Delamination. Separation of the skins from the core usually leads to laminate failure.

All of these phenomena can occur initially or be a function of fatigue life. Delamination caused by insufficient bonding during construction is prevented by using a core bonding material such as a thickened epoxy with a glass carrier cloth and vacuum bagging the skins to the core. Corebond weights of 150 to 300 g/m² are recommended for most materials [20].

3.2 Common Design and Analysis Methods

The solution to every structural problem comprises four basic components:

- Geometry
- Loads
- Materials
- Analysis models

Each of these includes uncertainties, and minimizing these uncertainties to a practical degree allows the designer to create an efficient design. This section presents the current design approaches for loads, analysis and testing used by designers of marine composite applications. As most of these applications are small vessels, and heavily cost driven, this section describes approaches not requiring large amounts of computer or design effort. Later sections describe state-of-the-art approaches.

3.2.1 Loading Models

Selected design methods are related to the types of loads encountered and the design complexity. Forces or loads are application-dependent and many are variable and random, as such, loading values typically comprise the largest uncertainty in marine design [51]. Table 3-7 shows common design loads for marine composites [9].

Category	Specific Type
Static	combined in-plane loads (buoyancy, cargo)
	large out-of-plane loads (pressures, deflections)
	contact loads (docking, assembly, etc.)
	thermal loads (fire)
Dynamic	shock (>150m/sec) (air and water)
	structural dynamics (slamming, whipping, machinery, rigging)
	wave action, cavitation
	noise, acoustics
Fatigue	low cycle (dives)
	high cycle (whipping, vibration, waves)
Creep	hydrostatic
Environment	sea water corrosion
	water absorption
	fire and smoke
	UV exposure

Table 3-7: Design Loads for Marine Composites

Current practice is often dictated by the requirements of insurance acceptability or military standards. For the American designer these essentially mean meeting the requirements of the American Bureau of Shipping (ABS) guides or MILSPECS. For recreational and commercial

vessels the ABS rules and guides apply. The load components in the ABS methods include [48, 49]:

- Hydrostatic head
- Static head augmented by wave height
- Velocity pressure head
- Slamming factor
- Rigging loads

Hydrostatic head is the hydrostatic pressure of the vessel sitting at rest and is the starting point for the ABS calculations. Added to the static head is the head caused by the vessel in waves. The maximum effective wave height is taken as the height of the shearline at its highest point, usually the bow. To increase the accuracy of the static head plus wave train loads, ABS considers the additional pressure effects of speed through the water. Using Bernoulli's equation as a basis, this is handled as a function of vessel speed squared, where the vessel speed is non-dimensionalized by the Froude number.

The slamming load of the forward sections is included through "slamming factors" based on the percentage distance of the panel from the bow. These factors increase through the fore part of the vessel, level off through the midsection, and taper off near the stern. A good summary of ship slamming response is provided in reference [52].

The ABS rules and guides provide a minimum set of scantlings for general offshore use and are based on a comparison of scantlings of vessels that have and have not suffered structural damage [8, 50]. Designers must also consider specialized loads. In the case of sailboats for instance, mast rigging loads are also included. Section 3.2.3 describes the ABS analysis methods in more detail.

3.2.2 Stiffness Models

Loading results in structural deformation and material stresses, and for marine composites the most critical can be grouped as global bending or torsion, panel flexure, and joints [4]. The reason for these becoming the most critical relate to the laminate tailorability and the inherent weakness of the matrix as an adhesive.

The marine composites designer is faced with numerous analysis techniques ranging from simple empirical "rules-of-thumb", to classification society rules, and to advanced numerical modeling through finite element analysis (FEA). The selection of the appropriate method largely depends on the design complexity and owner's requirements. For example, a canoe design rarely justifies the expense of FEA, whereas the Navy requires FEA of most designs. With the increasing power of the personal computer and the wider availability of sophisticated analysis software, more small craft designers are acquiring and applying sophisticated methods [53].

After determining the loads and selecting a composite material system, the designer needs to design a laminate to meet the required performance. Although many small-craft designers use orthotropic plate theory, carpet plots, or even blended properties to determine laminate properties [4, 16, 54], the majority use classical lamination theory (CLT) combined with simple, near static, ASTM tensile tests of unidirectional plies oriented at 0 and 90 degrees to the load. CLT relies on Hooke's law, the linear stress-strain relations for an anisotropic material. For the in-plane properties this is written as:

$$\{\sigma\} = [C]\{\varepsilon\}$$

or

$$\sigma_i = C_{ij}\varepsilon_j, i, j = 1,2,3,4,5,6$$

σ = stress

ε = strain

For a single unidirectional (all fibers running in the same direction) ply, symmetry planes simplify the analysis to transversely isotropic materials [35]. Table 3-8 shows the stiffness matrix C for a transversely isotropic material (a material which has only five independent constants.)

	ε_1	ε_2	ε_3	ε_4	ε_5	ε_6
σ_1	C_{11}	C_{12}	C_{12}	0	0	0
σ_2	C_{21}	C_{22}	C_{23}	0	0	0
σ_3	C_{21}	C_{32}	C_{22}	0	0	0
σ_4	0	0	0	$\frac{(C_{22} - C_{23})}{2}$	0	0
σ_5	0	0	0	0	C_{66}	0
σ_6	0	0	0	0	0	C_{66}

Table 3-8: Stiffness Matrix, C, of a Transversely Isotropic Material

The inverse of the stiffness matrix is the compliance matrix, S:

$$\{\sigma\} = [C]\{\varepsilon\}$$

$$\{\varepsilon\} = [C]^{-1}\{\sigma\} = [S]\{\sigma\}$$

Engineering constants are easiest to input for a transversely isotropic material in terms of the compliance matrix, and are shown in Table 3-9.

	σ_1	σ_2	σ_3	σ_4	σ_5	σ_6
ε_1	$1/E_1$	$-\nu_{12}/E_1$	$-\nu_{12}/E_1$	0	0	0
ε_2	$-\nu_{21}/E_2$	$1/E_2$	$-\nu_{12}/E_2$	0	0	0
ε_3	$-\nu_{21}/E_2$	$-\nu_{21}/E_2$	$1/E_2$	0	0	0
ε_4	0	0	0	$1/E_6$	0	0
ε_5	0	0	0	0	$1/E_6$	0
ε_6	0	0	0	0	0	$1/E_6$

Table 3-9: Compliance Matrix, S, in Terms of Engineering Constants of a Transversely Isotropic Material

E_1 is the elastic modulus of the unidirectional ply in the primary direction. E_2 is the elastic modulus 90° to the primary direction. For a unidirectional ply this is close to the resin modulus. A further simplification can be used as most composites fit the plane stress assumption as composites structures are generally thin in one direction compared to the others. Assuming the 1-2 plane is the plane of interest, the specialized Hooke's law reduces to the 3 x 3 matrix equation:

$$\{\varepsilon\} = [\mathbf{S}]\{\sigma\}$$

or

$$\varepsilon_i = S_{ij}\sigma_j, i, j = 1, 2, 6 \quad (a)$$

The inverse of the plane stress compliance matrix is the reduced plane stress stiffness matrix \mathbf{Q} .

$$\{\varepsilon\} = [\mathbf{S}]\{\sigma\}$$

$$\{\sigma\} = [\mathbf{S}]^{-1}\{\varepsilon\} = [\mathbf{Q}]\{\varepsilon\} \quad (b)$$

In terms of engineering constants, the plane stress compliance and stiffness matrices for the on-axis orthotropic ply are:

$$\mathbf{S} = \begin{bmatrix} \frac{1}{E_1} & -\frac{\nu_{12}}{E_1} & 0 \\ -\frac{\nu_{12}}{E_1} & \frac{1}{E_2} & 0 \\ 0 & 0 & \frac{1}{G_{12}} \end{bmatrix} \quad \mathbf{Q} = \mathbf{S}^{-1} \quad \mathbf{Q} = \begin{bmatrix} \frac{E_1}{1 - \nu_{12}\nu_{21}} & \frac{\nu_{12}E_2}{1 - \nu_{12}\nu_{21}} & 0 \\ \frac{\nu_{12}E_2}{1 - \nu_{12}\nu_{21}} & \frac{E_2}{1 - \nu_{12}\nu_{21}} & 0 \\ 0 & 0 & G_{12} \end{bmatrix}$$

where

$$\nu_{21} = \nu_{12} \cdot \frac{E_2}{E_1}$$

As laminates are made of plies in multiple directions however, the off-axis properties of plies must be determined. The off axis ply properties are calculated through the use of a transformation matrix, where θ is the angle between the fibers and the load:

$$\mathbf{T} = \begin{bmatrix} \cos^2(\theta) & \sin^2(\theta) & 2\sin(\theta)\cos(\theta) \\ \sin^2(\theta) & \cos^2(\theta) & -2\sin(\theta)\cos(\theta) \\ -\sin(\theta)\cos(\theta) & \sin(\theta)\cos(\theta) & \cos^2(\theta) - \sin^2(\theta) \end{bmatrix}$$

To resolve between engineering and true strain an additional matrix is used:

$$\mathbf{R} = \begin{bmatrix} 1 & 0 & 0 \\ 0 & 1 & 0 \\ 0 & 0 & 2 \end{bmatrix}$$

The transformation relations for each ply are then:

$$\begin{aligned} \bar{Q} &= T^{-1} \cdot Q \cdot R \cdot T \cdot R^{-1} \\ \bar{S} &= T^T \cdot S \cdot T \end{aligned}$$

Where the overbars refer to the off-axis stiffness and compliance matrices. To avoid warping during cure and loading, laminates are typically symmetrically stacked, although this is not common in the marine industry. More commonly, marine laminates are designed with the outside skin thicker than the inside. Various reasons, including abrasion and impact resistance are cited. In some cases the inside laminates, although thinner, are made of stiffer materials to help balance the stiffness between the inside and outside skins [7, 55]. If a symmetric laminate is chosen, this means the laminate's in-plane stiffness and compliance are the sums of the individual stiffness and compliance of each ply [35]:

$$\begin{aligned} \{N\} &= [A]\{\varepsilon\} \\ \text{or} \quad [A] &= \int_{-\frac{h}{2}}^{\frac{h}{2}} [Q] dz \\ N_i &= A_{ij} \varepsilon_j, i, j = 1, 2, 6 \end{aligned}$$

where dz = a differential element in the vertical axis

h = the laminate thickness

As the laminate is symmetric there is no warping or twisting and the strain is uniform throughout the laminate. These laminate stiffness and compliance matrices are used in equations (a) and (b) to get the laminate's stress and strain.

For the out-of-plane flexural properties similar relations hold. The moment-curvature relations for the plane stress condition are:

$$\begin{aligned} \{M\} &= [D]\{\kappa\} \\ \text{or} \quad [D] &= \int_{-\frac{h}{2}}^{\frac{h}{2}} [Q] \cdot z^2 dz \quad (c) \\ M_i &= D_{ij} \kappa_j, i, j = 1, 2, 6 \end{aligned}$$

where z = the distance from the neutral axis of the laminate to the neutral axis of the ply

The flexural engineering constants are found from:

$$\begin{aligned} [d] &= [D]^{-1} \\ [d^*] &= [d] \frac{h^3}{12} \\ E_1^f &= \frac{1}{d_{11}^*} \quad E_2^f = \frac{1}{d_{22}^*} \quad E_6^f = \frac{1}{d_{66}^*} \end{aligned}$$

The coupling terms between the in-plane and out-of-plane components are:

$$[B] = \int_{-\frac{h}{2}}^{\frac{h}{2}} [Q] \cdot z \, dz$$

Combining these gives the constitutive relations for the plate [56]:

$$\begin{bmatrix} N_x \\ N_y \\ N_{xy} \\ M_x \\ M_y \\ M_{xy} \end{bmatrix} = \begin{bmatrix} A_{11} & A_{12} & A_{16} & B_{11} & B_{12} & B_{16} \\ A_{12} & A_{22} & A_{26} & B_{12} & B_{22} & B_{26} \\ A_{16} & A_{26} & A_{66} & B_{16} & B_{26} & B_{66} \\ B_{11} & B_{12} & B_{16} & D_{11} & D_{12} & D_{16} \\ B_{12} & B_{22} & B_{26} & D_{12} & D_{22} & D_{26} \\ B_{16} & B_{26} & B_{66} & D_{16} & D_{26} & D_{66} \end{bmatrix} \begin{bmatrix} \epsilon_x^0 \\ \epsilon_y^0 \\ \epsilon_{xy}^0 \\ \kappa_x \\ \kappa_y \\ \kappa_{xy} \end{bmatrix}$$

The most important feature of the “ABD” matrix is the coupling relationships between the in-plane and out-of-plane responses. If the laminate is symmetric, then $B_{ij}=0$ and no coupling between the strains and curvatures exist. Most marine laminates are both asymmetric and unbalanced, however, leading to coupling between bending and stretching.

For unsymmetric laminates the B terms are nonzero and the stress resultants and moments are:

$$\{N\} = [A]\{\epsilon^0\} + [B]\{\kappa\} \quad \{M\} = [B]\{\epsilon^0\} + [D]\{\kappa\}$$

For laminates with a discrete number of plies, m,

$$\begin{aligned} [A] &= \sum_{i=1}^m [\bar{Q}] [z^i - z^{i-1}] \\ [B] &= \frac{1}{2} \sum_{i=1}^m [\bar{Q}] [(z^i)^2 - (z^{i-1})^2] \\ [D] &= \frac{1}{3} \sum_{i=1}^m [\bar{Q}] [(z^i)^3 - (z^{i-1})^3] \end{aligned}$$

To predict “failure”, the laminate stresses and strains are transformed back to ply stresses and strains using (a) and (b). Common causes of failure in marine composites relate to a loss of

stiffness or strength. In the case of stiffness loss this means the lack of meeting a stiffness performance goal, for instance the loss of rig tension in a racing sailboat, or unacceptably large panel deformations in a high speed vessel leading to internal joinerwork debonding. Loss of structural strength has obvious implications.

The loss of stiffness can generally be traced to two phenomena, microcracking and delamination [21]. Microcracking is the generation of small cracks in the matrix which cause discontinuity in load transfer. Larger discontinuities include delaminations between plies or between skins and the core. Delaminations particularly affect flexural and compressive stiffness and microcracking affects shear and tensile properties. Microcracking also increases the diffusivity constant for moisture absorption and if the loads are not reduced, eventually leads to matrix and fiber fracture and complete failure.

Predicting "loss of stiffness" failure is only accomplished through prototype testing [57]. Strength failures are more easily predicted.

3.2.3 Strength Models

The common failure criteria used in design are:

- Maximum stress
- Maximum strain
- Tsai-Wu

The latter defines an elliptic space where failure occurs if the combined stresses fall outside the space [35]. Material strength properties (found from ASTM coupon tests) are:

X_t = Longitudinal tensile strength

X_c = Longitudinal compressive strength

Y_t = Transverse tensile strength

Y_c = Transverse compressive strength

S = Longitudinal shear strength (also called XY_t)

The maximum stress theory is:

$$\text{FOS} = \left| \frac{X_{t,c}}{\sigma_{Y_{t,c}}} \right| \quad \text{FOS} = \left| \frac{Y_{t,c}}{\sigma_{Y_{t,c}}} \right| \quad \text{FOS} = \left| \frac{S}{\tau_{xy}} \right|$$

Factors of safety (FOS) for the maximum strain are identical, with strain terms replacing the stress terms. The lowest FOS is the driver. A MathCad spreadsheet is included in the appendix that calculates the in-plane CLT values and the maximum strain factor of safety. The Tsai-Wu failure criterion for plane stress is:

$$F_{ij}\sigma_i\sigma_j + F_i\sigma_i = 1 \quad i, j = 1, 2, 6 \quad (d)$$

where,

$$\begin{aligned} F_{11} &= \frac{1}{X_t X_c} & F_{22} &= \frac{1}{Y_t Y_c} & F_{66} &= \frac{1}{S^2} \\ F_1 &= \frac{1}{X_t} - \frac{1}{X_c} & F_2 &= \frac{1}{Y_t} - \frac{1}{Y_c} & F_6 &= 0 \\ F_{xy} &= F_{xy}^* \sqrt{F_{11} F_{22}} \end{aligned}$$

The numerical value of the interaction term F_{xy}^* is -1/2 for the generalized Von Mises criterion, and 0 for the Hill-Hoffman criterion [35]. The value of the right hand side of (d) will vary with the actual stress state and relates to the factor of safety. It is not linearly related to the FOS.

Although CLT programs combined with finite element analysis can be used to directly solve for structural stresses and strains, a more common approach in the marine industry uses a different method. The most common approaches are based on linear plate and beam theories, which ABS used to develop its two guides for reinforced plastic vessels and offshore racing yachts [48, 49].

3.2.4 ABS Design Codes

As many American small vessels are built to ABS classification rules to meet insurance or other regulations, current design practices are strongly influenced by the ABS guides [48, 49]. As discussed above, load values used in the ABS guides were determined from back calculation of successful and unsuccessful vessels. The back calculation relied on certain structural analysis models and therefore successfully using the load approximation methods embedded in the guides requires using the same structural models [8]. The basis of these models is linear plate theory.

The two plate equations used in the ABS guides assume a rectangular panel with either simply-supported or fixed edges. The worst bending moment derived from each is then used in section modulus calculations. The basic panel equations are [8]:

Simply-Supported Edges

$$\sigma = \frac{0.75 P_w^2}{t^2 (1 + 1.61 a^3)} \quad \delta = \frac{0.142 P_w^4}{E t^3 (1 + 2.21 a^3)}$$

Fixed Edges

$$\sigma = \frac{0.5 P_w^2}{t^2 (1 + 0.623 a^6)} \quad \delta = \frac{0.0284 P_w^4}{E t^3 (1 + 1.056 a^5)}$$

where,

σ = stress (psi)

p = pressure (psi)

w = short dimension of panel (in)

l = long dimension of panel (in)

t = plate thickness (in)

a = 1/aspect ratio = w/l

δ = deflection at panel center (in)

E = effective panel modulus of elasticity (psi) (calculated using CLT)

These formulas are modified in the ABS guides for curvature. Stiffeners are treated using linear beam equations, and follow the same maximum moment method as the plates.

Fixed	Simply-Supported
$\sigma = \frac{wl^2}{12Z}$	$\sigma = \frac{wl^2}{8Z}$

where,

Z = section modulus (in³)

σ = stress (psi)

w = load(lbs/in)

l = length of beam between supports (in)

To design structure using the guides the engineer determines the basic dimensions, selects a material, and using the above equations and additional restrictions within the rules, determines the plating thickness, frame spacing, and frame height.

3.2.5 Fatigue Models

Fatigue is the accumulation of stress-induced microcracks that gradually increase in size until large enough to cause fracture. Since fatigue is a cumulative process the onset of failure depends on the magnitude and number of cycles of the various stresses placed on the structure [58]. Two types of "fatigue" are generally encountered in marine composites. The first is dynamic or cyclic fatigue caused by varying loads, for instance waves or machinery. The other is static fatigue, or creep, from resisting static loads over a long period of time, for instance, a response to the still water bending moment. For most primary structure applications in marine composites, cyclic fatigue causes more damage [24]. Fatigue is a function of both in-plane and out-of-plane load components. As both generally occur in the linear range of material response, these

components are usually combined through superposition to determine the stress amplitude range [15] .

The basic method to include fatigue effects, for instance in the ABS guides, is to "reduce the material strength properties by a factor of 2 or more." [8]. Although still widely-used today [4], this approach is a carry-over from metal and wood fatigue tests and the resultant design standards developed over 30 years ago [59]. The assumption is that the endurance limit (or "fatigue limit") is half of the static ultimate strength¹. The reason this approach works well is the high number of cycles marine composites are expected to experience in a lifetime, combined with generally high fatigue endurance limits for composites. With many applications facing 10^8 or more cycles, fatigue endurance limits are normally reached [60]. This generalization is not fully justifiable however, as endurance limits vary significantly between different composite materials. Figure 3-1 [61] shows the fatigue behavior of quasi-isotropic² glass, carbon and glass-carbon hybrid laminates in epoxy resin. The all-glass laminate has an endurance limit of 25% at 10^7 cycles, while the all-carbon and hybrid glass-carbon laminates are close to 75%. From this it appears the fatigue reduction value should be between 1.5 and 4, but should be allowed to vary if based on actual material tests.

¹ Although predominantly for fatigue reasons, the factor also includes a margin for creep.

² With the exception of masts and appendages, most marine laminates are nearly quasi-isotropic.

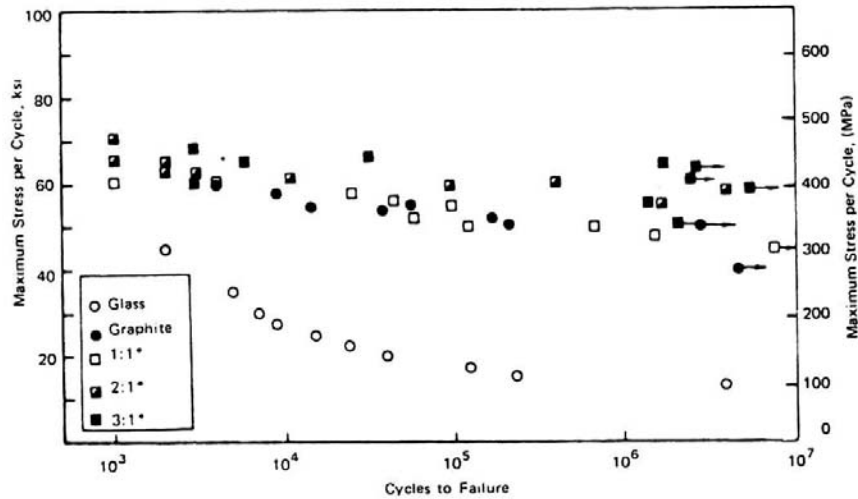


Figure 3-1: Comparison of the Fatigue Behavior of Glass, Carbon and Glass-Carbon Hybrid Quasi-Isotropic Laminates

For structures forecast to face less than 10^8 cycles, two analytical methods are commonly used. One is fracture mechanics, which looks at crack growth and the number of cycles for initial defects to propagate to a critical crack length that leads to fracture [58]. This method is gaining widespread use in metals, but is not yet developed enough for woven composite laminates [62, 63]. The other method uses empirically-developed S-N curves combined with a damage accumulation model.

Both approaches are somewhat risky however, when test data from one material is used as design data for another. The reason is the high dependency on a number of variables, including [60, 64-70]:

- Resin system and cure temperature
- Fiber material
- Fiber format
- Laminate ply sequence
- Void content

- Moisture content

The most common damage accumulation model is the linear Miner Rule:

$$D = \sum_i \frac{n(S_{fi})}{N(S_{fi})}$$

where,

D = the accumulated damage ratio

n(S_{fi}) = the number of stress cycles at stress f_i

N(S_{fi}) = the number of cycles to failure at stress f_i

Usually failure is assumed to occur when D=1, although for some marine composites, tests have shown that this could be as low as 0.25 [15]. For important ship structural details exposed to seawater and easily maintained it is usually 0.3, and if maintenance or inspection is not easily available or accessible then D=0.1 [58]. More recently the Hashin-Rotem logarithmic equation is finding use with composites, although the results appear similar to the linear rule [71].

$$D = \sum_i \frac{\log(n(S_{fi}))}{\log(N(S_{fi}))}$$

3.3 Testing Methods

To determine the fatigue performance of a potential application the most desirable approach is to test a full size prototype. Unfortunately, given the size and cost of most marine applications this is not possible within most design budgets. Information on full-scale testing is rare, although a recent study of composite submarine control surfaces indicated only slight property degradation. Unfortunately the test was performed in dry conditions, which casts doubt on its conclusions for wet service [72].

As full-scale prototyping is rarely possible, designers rely on data from standardized tests. Out-of-plane fatigue testing is usually performed as a modification of the ASTM static tests for composites, or through the use of a specialized composite fatigue test such as ASTM D671, Test for Flexural Fatigue of Plastics by Constant-Amplitude-of-Force [73]. The test is commonly used to determine the flexural fatigue properties of FRP laminates through the use of dogbone cantilever coupons. The test is performed at 30 Hz, which closely approximates the natural frequency of many hull structures, but not the loading input frequency [4]. Dry testing at high frequencies however can cause accelerated damage due to heat buildup [57]

The static test most commonly used for fatigue testing is ASTM D790, Test Method for Flexural Properties of Unreinforced and Reinforced Plastics and Electrical Insulating Materials [73]. This is a three or four point bending test of composite beam samples. This test is widely used to compare the fatigue resistance of various hull laminates as it inexpensively reproduces local panel bending[4].

For sandwich constructions, ASTM C393, Method of Flexure Test of Flat Sandwich Constructions is often used [73]. The test is similar to D790 in that it uses a 4-point bend test. The samples are often wider however, averaging a 4:1 rectangle [73] to reduce edge effects. This test, like D790 is used to verify quality assurance, and since it includes the core and corebond, provides a much better check of the sandwich laminates properties than D671, which only tests the skins [4]. The problem with the three and four point tests is that the laminate usually fails in compression under the load points. This does not reflect conditions where the panel is pressure loaded, such as by wave slap [74].

3.4 Limitations of the Current Practice

3.4.1 Stiffness and Strength Analysis

Numerous problems exist with using orthotropic plate theory or carpet plots or blended properties to determine stiffness and stresses and these methods should not be used except for historical comparisons [35]. Although the uncertainties of CLT analysis are small compared to

manufacturing variances and environmental loading, some problems do exist. These include uncertainties due to the following assumptions:

- Thin laminates (plane stress assumption, span length/thickness >20)
- No curvature
- No cut fibers
- No through-the-thickness fibers (including unidirectional vs. woven laminates)
- Linear stress-strain ratios for both fiber and resin
- No voids
- Perfect interlaminar and fiber/matrix bond
- Uniform layering

Many of these will be addressed in the sections on current research. Voids and bonding issues are generally neglected in analysis as they are "built-in" to the test results, as long as the coupons reflect actual shipyard construction practices rather than laboratory conditions [74].

3.4.2 Load Prediction Limitations

The "design head" method of load determination was based on back calculating a variety of successful and unsuccessful vessels engaged in inland, coastal and offshore service, and extrapolating design loads using first principles. As such, it provides a good empirical reference for boats similar to those in the original study. For vessels significantly varying from those studied, the approach becomes questionable as uncertainties in the extrapolations rise. For example, the initial base for the ABS offshore sailing yacht guide was vessels built to the International Offshore Rule (IOR). These vessels were heavier and had less stability than current offshore racing craft. In practice this means the newer vessels routinely experience significantly

higher speeds and slamming pressures than those used to create the rules [8]. In response, ABS increased the slamming factors³.

3.4.3 Moisture Effects Limitations

The absence of environmental effects on composite materials tests substantially increases the design uncertainty. Although protective coatings counter UV degradation, the effects of moisture absorption can not be as easily prevented or predicted. The extensive and costly problems caused by osmotic blistering indicate the dangers of relying on dry test results to predict the performance of submerged laminates [4, 25, 46, 75, 76]. Although means to prevent blistering were quickly identified through the use of vinyl ester and epoxy resins [65], litigation and repair costs were high.

Numerous researchers have studied moisture effects on composite materials. Results vary however, even for similar materials. Springer [70] looked at the impact on unstressed carbon/epoxy $\pi/4$ laminates (plies oriented 0/45/90/-45 degrees to the load) of moisture contents ranging from "dry" to "saturated." For the dry condition, material properties were unchanged, and at moisture contents above 1%, the tensile strength decreased with increasing moisture content until reaching a maximum decrease of 20%. Comparatively, Sloan [77] found that the effects of soaking samples in seawater increased the tensile strength 5% and decreased fatigue effects through plasticizing of the matrix. One of the differences between the Springer and Sloan results may be related to the use of de-ionized water in the Springer study (as recommended by the ASTM test standards) which may have attacked the epoxy matrix. Another study found no correlation between moisture absorption and strength for three unstressed carbon/epoxy marine laminates, and found degradation of 10-20% for fatigue specimens [78].

³ Note 1 (1997) of the Guide

For sandwich composites the core must also be considered. A study of aluminum cored, carbon skinned marine composites exposed to seawater showed significant degradation from galvanic corrosion in only 19 days [79]. Results from surveys have shown significant degradation of both foam and balsa cores when subjected to moisture for apparently long periods of time [25]. Other studies have shown the effects of high cyclic shear loads on foam cores, and ways of predicting failure through FEA [80].

3.4.4 Testing Methods Limitations

Testing method limitations fall into two categories, laminate construction assumptions and boundary condition assumptions. The first category includes inaccuracies caused by constructing samples to the ASTM "laboratory" standard, which in most cases does not represent actual shipyard construction practices. This can be remedied by having the shipyard construct the samples and increasing the sample batch size to include areas of ply overlaps and other manufacturing variances [74].

Another construction-related problem of the ASTM test methods is the limited range of allowable specimen sizes. As many marine laminates are thicker than the allowable 0.25" tensile test specimens (ASTM D3039) [73], inaccuracies occur as thicker specimens show decreased tensile properties [81]. This problem can be addressed probabilistically using a Weibull distribution approximation [21].

Boundary conditions strongly influence test results. These range from moisture conditioning mentioned above, as the ASTM standards stipulate dry samples, to fixturing, panel sizes, load application, and strain rates. The boundary conditions that differ the greatest from reality are panel sizes and load applications [74]. In the ASTM D790 and C393 tests, line loads are applied rather than distributed pressures. This causes inaccuracies as test sample failure occurs at the load support [82]. In many sandwich construction tests initial failure occurs through core shear, which then propagates to skin failure. This is due to the high shear loading at the load and

support points [80, 82]. For flexural tests the use of four-point instead of three-point fixturing reduces the shear load and hence this problem.

Panel sizes influence test results due to edge conditions, panel aspect ratios and flaw distributions. As laminates are made of plies of varying orientations, the long, narrow specimens used in the ASTM tests do not allow off-axis plies to participate in load sharing. This effectively loads the 0° plies more than in actual panels and reduces stiffness and strength results [74].

4.0 Current Research in Analysis and Testing

The generally successful track record using the practices described above indicates satisfactory designs based on existing designs are currently possible. The limitations discussed above also point out that room for improvement exists and that designs varying from those assumed when the practices were developed need improved methods. As marine composite applications generally have limited budgets, to be successful, refinements must show clear benefit/cost advantages.

The following state-of-the-art refinements use the approach that to improve existing methods one needs to reduce design uncertainties [51]. Uncertainties are divided into two categories. Type I are natural uncertainties, such as randomness, and as such are not information sensitive. Type II uncertainties are modeling uncertainties and can be reduced with better information. Not all refinements are cost-effective for all applications, however, so engineers must understand potential trade-offs before implementation.

4.1 Design and Analysis Methods

Improving analytical accuracy reduces Type II uncertainties. Table 4-1, taken from Det Norske Veritas' (DNV's) "Structural Reliability Methods" gives an example of the relative magnitudes of the major uncertainties in marine designs [83]. Not included in this table are the coefficients of variation (COV) of composite materials test data (due to manufacturing variances), and the COV of test methods. A typical value for data scatter from an ASTM test is 5-8% for quality marine composites [84]. The test data COV does not reflect the complete bias from the material's actual strength due to the test's inherent uncertainty. COV's for testing methods are application dependent, but based on the studies described earlier, can range up to 60%.

Type of Uncertainty	Coefficient of Variation
Wave loads	20-100%
Buckling analysis	100%
Structural analysis	10%
Elastic modulus	5%
Yield strength	8%

Table 4-1: Levels of Uncertainty in Marine Design

The greatest design benefit comes from reducing the areas with the largest Type II uncertainties. Based on the above data, the two leading candidates are loading and test methods for material properties.

4.1.1 Loading Models

Loads comprise one of the largest sources of uncertainty in marine design. The ABS static equivalent wave head method described in 3.2.1 provides a conservative approach for small vessels engaged offshore, as the wave length and wave height are assumed to be in the worst combination. Improvements to the ABS method include service life definition and numerical modeling or prototype evaluations.

Defining the vessel's service life and then using probabilistic methods to calculate anticipated wave spectra and durations has been used by naval architects for years, and accurate wave spectra for the design of ships and offshore structures is available [85]. Spectral wave formulations such as the Pierson-Moskowitz, Bretschneider, ITTC and ISSC apply to offshore conditions, and the JONSWOP spectra approximates inshore conditions [86, 87]. The distribution function can then be correlated to design loads, stress ranges and material S-N curves [88]. This method works well for large vessels and may be appropriate for composite vessels of the largest size.

The large majority of composite vessels are recreational craft under 100' however, and are manufactured in production runs ranging from 10-5,000 or more [44]. Critical extreme design loads are typically caused by impact with docks or foreign objects or capsizing by breaking waves[29, 89]. Critical fatigue loading however, is usually caused by slamming [8], combined with longitudinal bending. Currently the only way to accurately approximate dynamic capsizing loads is through model testing [89]. This method is also the most accurate method to predict slamming loads [13, 90]. The problem with the extreme, one-time loads is that they are very application specific, and often the economics of the application do not justify a detailed analysis or structural strengthening. For high production recreational craft the possible uses and abuses by untrained operators are difficult to predict and design to. Unfortunately, "extreme design loads" are often "selected" not by the engineer but by juries in hindsight of an accident. The US Coast Guard specifies stability minimums for pleasure craft and most insurance companies rely on the Coast Guard and ABS for structural minimums. As compared to one-time extreme loads, fatigue analysis can apply across a number of designs, and is therefore easier to justify economically.

A study comprising analytical, full-scale tank testing and full-scale open water testing of a 16-foot sailing vessel showed close correlation of predicted and actual slamming pressure using an added mass-kinetic energy balance method developed by Von Karmen in 1929 [13]. The method assumes a wedge-shaped body striking a horizontal water surface. The 2-D flow yields the pressure equations:

$$p_{ave} = \frac{1}{2} \rho u^2 \frac{(\pi \cot \alpha)}{\left(1 + \frac{\rho \pi y^2}{2M}\right)^3}$$

$$p_{max} = \frac{1}{2} \rho u^2 (\pi \cot \alpha) \text{ at } y=0$$

where,

p = pressure

ρ = fluid density

u = vertical velocity

α = deadrise angle

M= wedge mass

The maximum pressure from this equation is a single point maximum. To convert this to a pressure surface a sinusoidal distribution based on the vessel geometry is used to calculate the longitudinal and athwartships components [13, 91]. Good correlation was also achieved when the force distribution was found by applying the Morison equation, with the first part used for the velocity dependent term in the equation, and the portion in the parenthesis equivalent to the C_D term [13, 92].

$$\frac{dF}{dl} = -\int p \cdot \vec{n} \cdot d\vec{s} + \frac{\rho}{2} \cdot D \cdot C_D \cdot \vec{u}_n |u_n| + \rho \cdot \pi \cdot \frac{D^2}{4} \cdot C_M \cdot \vec{a}_n$$

The largest uncertainty in the Von Karmen equation is the vertical velocity component, which has a large influence on the predicted pressure. Unlike a free-falling wedge, a vessel's forefoot is supported by the remaining part of the vessel. Depending on wavelength and forward speed, the impact velocity can vary tremendously. Also, due to the cotangent term, the pressure approaches infinity as the deadrise angle approaches zero. The experience of many vessels with flat bottoms does not support this prediction, most likely due to entrapped air providing a cushioning effect. Test data suggests that the worse impact angle is approximately 2-3° [93]. Therefore some uncertainty exists for deadrise angles of less than 5°. Figure 4-1 shows the predicted maximum pressure plotted against the deadrise angle for an impact velocity of 10 fps. As many small craft have flat bottoms this plot shows the uncertainty can be significant.

Note that ABS guidelines predict pressures on the order of 9 psi. At the time the ABS Guide for Offshore Yachts was written (1980) the design rating rules in effect at the time penalized

lightweight vessels. This restricted speeds and the impact velocities. Since then new guidelines allow for greater speeds [94].



Figure 4-1: Maximum Pressure Due to Slamming ($u=10$ fps)

Apart from the air entrapment problem, the equation may also be conservative due to the assumption of a rigid body. Two slight variations of Von Karmen's equation were developed by Payne and Wagner and were compared against test results from large-scale drop tests using actual small vessel structures. Figure 4-2, reprinted from [93], illustrates the conservative bias of these two equations. Payne's and Von Karmen's equations yielded essentially the same results.

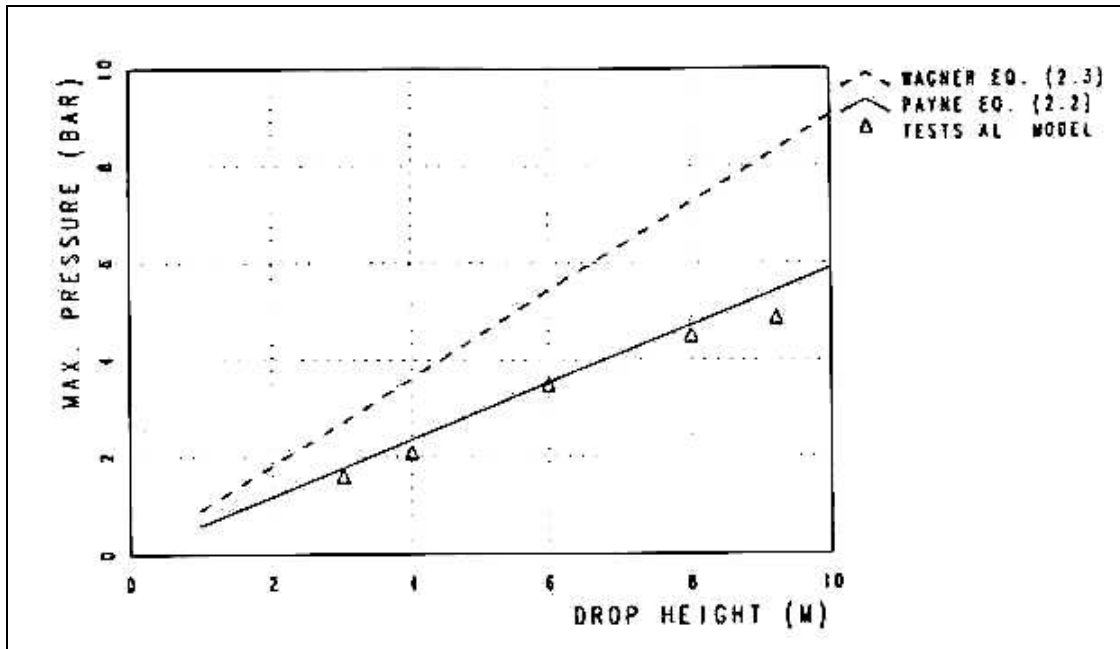


Figure 4-2: Slamming Drop Test on Stiffened Aluminum Model in Symmetrical Position.

To accurately apply Von Karmen's formula will require knowing the impact velocities and the amount of pressure reduction. The first part can be predicted by integrating the results from accelerometers on the test platform. The second part is harder to predict. Alternatively, pressure sensors can be placed on the outside of the test hull.

Since model testing is prohibitively expensive for most applications, alternative methods to model testing are often used. Numerical methods such as "strip theory" and computational fluid dynamics (CFD) are used in large ship analysis and offer promise. Many of the assumptions taken for ordinary strip theory (slab sides, non-breaking waves) limits its usefulness for small craft [88]. Recent modifications to include dynamic wave-induced lift and nonlinear hydrodynamic impact forces have yielded results with sufficient accuracy for design purposes [95]. Slightly non-linear and first-order strip theories based on an assumed constant deadrise slope address the difference in bending moment between hogging and sagging conditions [96-98]. In general, due to bow and stern flare the sagging moments exceeded the hogging moment. For sailing vessels

this is especially important, as the rig loads increase sagging and decrease hogging moments and deflections. Due to the complexity and the lack of market demand, CFD approaches applicable to small craft are rare. Current methods solving the three-dimensional fluids problems require large computer resources and yield results too panel-dependent to be practical design tools[90].

A continuing limitation with strip theories is the port-starboard symmetry assumption. Two factors may make this a non-negligible limitation when considering small vessels built of composite materials. The first is the larger roll angles experienced by small craft. In the case of sailing vessels sailing against the wind, heel angles of 20-40 degrees may exist. The second is the torsion caused by the asymmetric sections, which effect global stress predictions. In the case of metals, shear strengths are typically of the same order of magnitude as the tensile strength. Typical marine composite laminates are often based on a $(0/90)_S$ lay-up, which may result in shear strengths less than 10% of the tensile strength. In these cases, failure may be driven by shear, rather than bending stresses. Using CLT, Table 4-2 compares the shear strength and tensile strength of E-glass/polyester and carbon/epoxy $(0/90)_S$ marine laminates.

Material	Tensile Strength (ksi)	Shear Strength (ksi)	Tensile/Shear
Aluminum	35	17.5	2
E-glass/polyester	60	18.9	3.2
Carbon/epoxy	100	9.8	10.2

Table 4-2: Comparison of Tensile and Shear Strengths of Marine Materials

Failure of a marine structure can be due to a variety of loading histories that include short term extreme loads, such as grounding, collisions, or "freak" weather conditions, or long term fatigue loads. The ABS Guides related to reinforced plastic vessels takes both into account through a

combination of factors of safety and linear plate or beam equations[8]. Although not as rigorous as state-of-the-art analysis, the ABS method produces designs that withstand the anticipated conditions well [94].

Large vessels are generally limited in their operational lives by metal fatigue. Truly extreme loads are rare. General design philosophy for metals leads the designer to check for the failure modes shown in Table 4-3 [99].

Type of Analysis	Loads	Comments
Yielding	Worst Case	Max. Tensile Stress
Buckling	Worst Case	Max. Comp Stress
Crack Initiation	Spectrum	Full Stress Range
Crack Propagation	Spectrum	Tensile Stress Range
Brittle Failure	Worst Case	Max. Tensile Stress

Table 4-3: Types of Loads Used in Metal Vessel Analysis

The extreme loads are worst-case loads specified by the design rules or based on the designer's experience. Fatigue loading is determined by the weather conditions on the vessel's intended route. Fatigue stress levels can be calculated by either using the extreme load as a parameter in a generalized spectrum such as the Weibull, or preferably, calculating the stress spectrum based on the Response Amplitude Operator (RAO) of critical details, using the following relationship between the weather spectrum for the intended route and the stress range [100].

$$S_{stress}(\omega) = S_{sea}(\omega) \bullet |RAO|^2$$

The RAO's for vessels can be calculated using tank models or a combination of strip theory and finite element analysis. Tank test modeling offers greater accuracy at the expense of greater costs and limited flexibility to design changes. By scaling the model to accurately represent the

mass distribution and longitudinally hinging the model, a series of runs in different sea headings and speeds can be used to predict the RAO's [100]. For small craft, and particularly sailing vessels, the use of tank models is particularly important as the limitations of strip theory (heeling, spray, etc.) are addressed. Although tank models of small craft are generally prohibitively expensive they have been successfully used to predict vessel deflections due to rig, keel and hydrostatic and hydrodynamic loads [28]. Unfortunately, using scaling to determine the RAO's does not relieve the need to predict stresses from FEA, as the failure modes of the composite materials do not scale. As an example, the ratio of shear (resin dominated) vs. compressive strength (fiber dominated) changes as the laminate becomes thinner.

In all cases the environment the vessel will operate in must be considered when predicting the wave-induced loads. For ocean waves a logarithmic, Rayleigh, or Weibull distribution is used to correlate the probability of different significant wave heights, and a Pierson-Moskowitz, Bretschneider, JONSWOP, or Ochi 6-parameter spectrum is used to predict the wave energy spectrum[101]. To calculate the deep water wave-induced hogging and sagging bending moments for the FEA, a wave elevation profile of either a Stokes (second order) or trochoidal is used [102]. For inshore craft the Rayleigh distribution is used for the surface elevations and the appropriate energy spectrum is a modified JONSWOP spectrum based on a fetch-limited sea state [101, 103]. The appropriate wave profile is dependent on the fetch and water depth. In shallow water, in addition to the Stokes wave profile, cnoidal and breaking wave profiles are possible [104]. Wave height predictions in shallow water are also predicted using methods developed by the U. S. Corps of Engineers [105].

The University of California at Berkeley is located in the San Francisco Bay Area, an area famous for its varied microclimates [106]. The Bay and its adjacent waters feature winds varying from light to blustery. A steady strong (15-25 knot) westerly sea breeze blows through the only gap in the central portion of the Coastal Range, the Golden Gate, from early spring through fall[106]. Combined with the westerly ebb current, a short, steep chop is common along the San Francisco city front. Studies in the 1950's [86] and 1970's [87] confirmed the appropriateness of using a

narrow-band JONSWOP energy spectrum for central San Francisco Bay. Seabreezes of 25 knots and significant wave heights of greater than two feet are common[86].

The wave profile input to the FEA is a combination of ship motions, wind wave profiles, and fluid-structure interactions. Assumptions are typically made to generate an appropriate profile and pressure distribution. For worst case loads on small craft a wave height equal to the freeboard forward is commonly used[8]. The profile is truncated aft equaling the freeboard. The sagging load condition is used as the rig tension is also forcing the bow upward. Windward and leeward wave profiles are different for sailing craft. Although the combination profile can be constructed using superposition, the results have significant uncertainty.

As described in Section 8.1, the vessel selected for testing, the J/24 sailing yacht, has a freeboard forward of 2.5 feet and a length of 24 feet. For the summer months, the probability of occurrence of a wave height exceeding 2.5 feet on San Francisco Bay is 13% [86]. If the wave length is taken equal to the vessel length (so as to give the maximum sagging moment), the wave period, T, and steepness parameter can be calculated [104].

$$T = \frac{L}{\sqrt{\frac{gL}{2\pi} \tanh(kh)}}$$

$$T = 2.2 \text{ sec}$$

$$\text{where } k \text{ is the wave number } k = \frac{2\pi}{L}$$

h = water depth

$$\text{The wave steepness parameter is } \frac{H}{L} = \frac{1}{9.6}$$

Comparing these values to the 1970's wave data indicates waves of this type are common on Berkeley Circle in San Francisco Bay [87]. Additionally, the value of the steepness parameter indicates a "nearly breaking" wave. (Typically, although a steepness parameter greater than 1/7 is required for breaking of a theoretical wave; "real" waves break at smaller ratios[101].) "Nearly

breaking" waves are easily verified by the commonly seen "white-caps" on the Bay. A breaking wave has a unique non-linear profile and pressure distribution that is not described by equations. For the calculated steepness parameter the wave profile will be either cnoidal [104] or Stokes second order [107], depending on the water depth. The cnoidal wave elevation profile is [107]:

$$Y_s = Y_t + H \cdot \text{cn}^2 \left[2K(k) \cdot \left(\frac{x}{L} - \frac{t}{T} \right), k \right]$$

where Y_s is measured from the ocean floor

$$Y_t = \left(\frac{16h^2}{3L^2} \right) \{ K(k) \cdot [K(k) - E(k)] \} + 1 - \frac{H}{h}$$

cn is the Jacobian elliptic function associated with the cosine function

$K(k)$ and $E(k)$ are the complete elliptic integrals of the first and second kind [108]

The second-order Stokes wave profile is [101]:

$$\zeta = \frac{H}{2} \cos(kx) + \pi \frac{H^2}{L} \cos(2kx)$$

For the water depth and wavelength used in this example the cnoidal and simple cosine wave profiles are nearly identical. As the wavelength to wave height ratio gets higher, the cnoidal wave will have greater steepness than the cosine or Stokes wave. The important factor for vessels is that the steeper the wave profile, the greater the bending moment. For sailing craft however, the depth of the keel prevents the vessel from entering water that would be shallow enough for the cnoidal wave to have a steeper profile. Therefore a realistic wave surface elevation profile for a J/24 in San Francisco Bay is the Stokes second order.

In addition to the uncertainty from using an assumed wave profile is the uncertainty due to the fluid-structure interaction between the hull and the waves. This is a complex problem that is

partially addressed through strip theory and other computational fluid dynamics methods. Another method used with some success is to determine the wave profile by measuring amplitudes off photographs of similar vessels [90].

Besides the hydrostatic and hydrodynamic loads, additional loads on small craft include keel, rudder, and rig loads. The ballasted keel (usually lead) on a sailing yacht typically weighs between 30% and 60% of the vessel's total displacement and extends well below the canoe body, while having a small structural intersection with the canoe body. In extreme cases of capsize the vessel may be on its side with the keel sticking out of the water perpendicular to the canoe body. Similar to the keel, rudder loading must be included. At times the rudder may develop significant forces when course corrections are required. During steady state sailing however, if the vessel's sail plan is "balanced" with the lateral resistance area (meaning negligible yaw moments) the rudder forces will be small as the rudder will be at an angle of attack between $\pm 4^\circ$.

The other major forces on a sailing vessel are rig loads caused by the sails. These are transmitted to the hull through the mast and various pieces of rigging, including shrouds, stays, halyards, and sheets. The largest of these are the compressive mast load, the windward shroud tension and the fore and aft stay loads. The shroud load is directly related to the righting moment, which is function of the ballast, center of buoyancy shift when heeled and crew weight and position. The stay loads are related to the desire to keep the forestay and connected jib luff tight for sailing performance. The combined mast compression load coming from the shrouds, stays and halyards is often about twice that of the vessel's displacement. Shroud loads are of the same order as the displacement, and halyard tensions are roughly 15% of the displacement. The combined fore and backstay load are roughly 85% of the displacement[109].

Figure 4-3 (taken from [109]) shows the windward side of a sailing vessel. The shaded arrows indicate global loads imposed on the hull from the rigging forces. The open arrows are the local forces caused by the hydrostatic and hydrodynamic forces. The global loads increase and decrease (and may change sign) due to the hogging and sagging moments. Note, when the fore

and aft stays are tensioned the vessel is restricted in sagging, preventing the bending moment from changing sign.

The global hull bending is such that the deck and upper topside is put in compression, the hull bottom is in tension and the topsides in shear. The local hull bottom loads from wave slap put the outer skin in compression and the inner skin in tension (for small deflections). These loads happen constantly as the vessel goes through waves, leading to long-term fatigue.

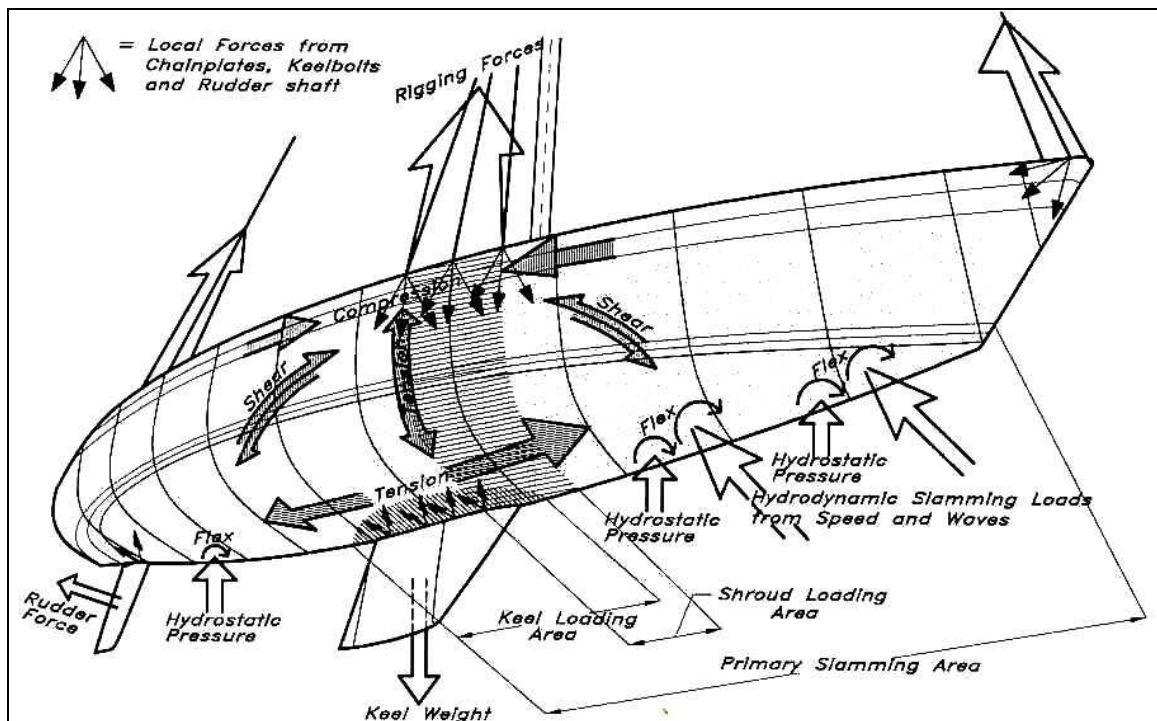


Figure 4-3: Forces on a Sailing Yacht

One possibly significant load not included in this figure is loads caused by trailering and launching. If the vessel is not well supported, significant localized strains are possible. These loads are difficult to quantify as they are dependent on trailer configuration, road condition, tie-down strap tightness and the driver's style!

4.1.2 Stiffness and Strength Models

Although many of the limitations of CLT, including no cut fibers and homogeneity, cannot be modified in any continuum formulation, other analytical uncertainties can be addressed through advances to the underlying theories.

One modification easily implemented to CLT improves calculations of out-of-plane deflections. As described earlier, a plane stress assumption is used to simplify analysis to a 2-D case. The resulting analysis assumes a linear-normal shear deformation approach in line with Kirchhoff plate theory. This approach works well for thin plates where $E_y < 0.1E_x$, and deformations are small. This is generally the case with traditional E-glass/polyester marine laminates, and errors are small.

Thicker laminates, mainly due to the switch to sandwich construction, and higher modulus materials such as Kevlar™ and carbon lead to noticeable errors in CLT. The unbalance of forces in Kirchhoff plate theory led to the development of Mindlin plate theory where a line that is straight and normal to the midsurface is assumed to remain straight but not necessarily normal to the midsurface after loading [110]. Compared to (c) from Section 3.2.2, the revised moment-curvature equations for the Mindlin Theory are:

$$\{\kappa\} = \begin{bmatrix} w_{,xx} \\ w_{,yy} \\ 2w_{,xy} \\ 0 \\ 0 \end{bmatrix} \quad (c) \qquad \{\kappa\} = \begin{bmatrix} \theta_{x,x} \\ \theta_{y,y} \\ \theta_{x,y} + \theta_{y,x} \\ \theta_y - w_{,y} \\ \theta_x - w_{,x} \end{bmatrix}$$

Further developments in composite shear deformation theories (SDT) include higher-order theories. Reddy showed that using the same dependent unknowns as first-order SDT, a parabolic distribution of the transverse shear strains through the thickness could be predicted [111]. DiScuiva showed that assuming a piecewise linear (linear for each ply) shear deformation improved accuracy for moderately thick composites [112].

The most significant improvement over the ABS guides is the use of FEA to predict stresses and deflections. FEA discretizes a geometrical model of the vessel or component into a number of small elements whose stiffness properties are approximated. Individual element stiffness characteristics are combined to approximate the global structural stiffness. A balance of forces solves the matrix equilibrium equations and yields displacements. Strains and stresses follow through constitutive equations. Elements may be designed to assume linear or nonlinear, one, two or three-dimensional elasticity, isotropic or orthotropic, heat or moisture diffusion, and other properties[110]. A generalized description of the FEA method and its application to ship design is included in Chapter 6, Section 5.3, of SNAME's "Ship Design and Construction (1980)" [113]. Although FEA has been used for numerous years in large ship design its application to small craft has been limited by cost [114].

Although initial model construction is often labor-intensive, for marine composites, significant optimizations are possible through laminate tailoring, a benefit not possible when using the ABS method. Numerous studies have demonstrated the advantages of FEA for marine composites applications. For instance, vessels constructed of different materials can quickly be analyzed for cost effectiveness, and optimized through manual or automatic laminate tailoring [7, 13, 18, 20, 72, 90, 91, 114]. A recent FEA project the author worked on yielded a 48% reduction in hull and deck weight compared to the ABS baseline design, while yielding the same deflection and factors of safety[28]. Commercial codes currently include shell elements for thin (Mindlin) and moderately-thick (DiScuiva) laminates, although combinations of brick and shell elements are possible in less sophisticated codes [115].

The maximum stress, maximum strain and Tsai-Wu failure criteria all yield provide reasonably accurate predictions for laminate failure. A problem with the maximum strain and maximum stress theories is that the loading in the X and Y directions is considered independent, while Poisson's effects are known to exist [35]. The Tsai-Wu criterion includes this effect, but loses one of the strong points of the simpler theories, that of predicting the critical failure mode. A

failure criteria which includes both elements was developed by Hashin [116]. The principal failure modes in the Hashin model are:

- Tensile fiber mode described by fiber rupture
- Compressive fiber mode described by fiber buckling
- Tensile matrix mode described by plane failure surface parallel to fibers with $\sigma_{22} + \sigma_{33} > 0$ and compressive matrix mode with $\sigma_{22} + \sigma_{33} < 0$

The quadratic failure criteria corresponding to these modes are:

Fiber Modes

$$\text{FOS} = \left(\frac{\sigma_{11}}{\sigma_x^+} \right)^2 + \frac{(\sigma_{12}^2 + \sigma_{13}^2)}{\tau_{xy}^2} \quad \sigma_{11} > 0$$

$$\sigma_{11} = -\sigma_x^- \quad \sigma_{11} < 0$$

Tensile Matrix Mode $\sigma_{22} + \sigma_{33} > 0$

$$\text{FOS} = \frac{(\sigma_{22} + \sigma_{33})^2}{\sigma_y^+{}^2} + \frac{(\sigma_{23}^2 - \sigma_{22}\sigma_{33})}{\tau_{xy}^2} + \frac{(\sigma_{12}^2 + \sigma_{13}^2)}{\tau_{xy}^2}$$

Compressive Matrix Mode $\sigma_{22} + \sigma_{33} < 0$

$$\text{FOS} = \frac{(\sigma_{22} + \sigma_{33}) \left[\left(\frac{\sigma_y^-}{2\tau_{xy}} \right)^2 - 1 \right]}{\sigma_y^-} + \frac{(\sigma_{22} + \sigma_{33})^2}{4\tau_{xy}^2} + \frac{(\sigma_{22}^2 - \sigma_{22}\sigma_{33})}{\tau_{xy}^2} + \frac{(\sigma_{12}^2 + \sigma_{13}^2)}{\tau_{xy}^2}$$

Unfortunately, no commercial FEA code currently includes the Hashin criteria. For this project the stress output from the FEA was checked using a spreadsheet based on the Hashin criteria.

4.1.3 Fatigue Models

Composite materials exhibit complex failure mechanisms under fatigue conditions. The four basic failure modes for fatigue are similar to the static failure modes. They are [117]:

- Fiber breakage
- Matrix cracking
- Interfacial debonding
- Ply delamination

Which mode applies for a given laminate generally depends on the failure strain of the constituent materials and the ply orientations. The failure strain for glass is generally higher than that of polyester resin, leading to microcracking and failure of the resin before the fibers. Epoxies and vinyl esters have failure strains near that of glass and tend to fail by fiber failure first. As noted earlier, the strong dependence on multiple variables requires the need for specific laminate testing for critical applications. Many marine laminates use similar materials and orientations, allowing for some interpretation of existing data, as well as the data from Section 6.

Failure theories for fatigue of composites are current research topics. Hashin's modified failure criterion covers the first two modes for fully reversed cycling:

$$\text{Fiber mode} \quad \left(\frac{\sigma_{11}}{\sigma_x} \right)^2 + \left(\frac{\sigma_{12}}{\tau_{xy}} \right)^2 = 1$$

$$\text{Matrix mode} \quad \left(\frac{\sigma_{22}}{\sigma_y} \right)^2 + \left(\frac{\sigma_{12}}{\tau_{xy}} \right)^2 = 1$$

where the S-N relations for fully reversed cycling of stress are represented by:

$$\sigma_x = \sigma_x(-1, N) = \text{in the fiber direction}$$

$$\sigma_y = \sigma_y(-1, N) = \text{normal to the fiber direction}$$

$$\tau_{xy} = \tau_{xy}(-1, N) = \text{for shear}$$

These theoretical failure criteria provide good correlation for tensile-tensile tests of epoxy laminates, but have not been verified for compression or tension-compression data[33]. The last two modes do not yet have robust analytical models, preventing analytical evaluation in current design practice.

Various other approaches have been proposed for fatigue design. One simple method proposed by Dharan at U. C. Berkeley uses a limit of 40% of the neat resin ultimate strain as a design endurance limit [118]. This is similar to fatigue methods used in concrete construction. Although data for aerospace laminates fits this model well, no testing of marine composites has been completed.

Other methods used for metal fatigue, such as fracture mechanics, have not proven robust for composites analysis due to the complexities of fiber format and orientation variation. Due to the lack of reliable fatigue theories for composites, analytical analysis is limited to first order approximations. Fatigue testing of proposed laminates is still the only reliable way of predicting performance [4].

With accurate S-N data the next challenge is the prediction of the lifetime under variable amplitude cycling. The standard procedure for high-cycle fatigue is based on a spectral description of the seaway [88]. Using the Miner model, the incremental damage caused by waves centered at frequency, f , during a time interval, T , and stress amplitude, s_i , is:

$$dD = \frac{T \cdot f \cdot p(s_i) ds}{N(s_i)}$$

Where $p(s)$ is the probability density function for the stress based on model tests or finite element analysis through the loading spectrum. The total expected damage during T is:

$$E[D] = T \cdot f \int_0^{\infty} \frac{p(s_i) ds}{N(s_i)}$$

Assuming the S-N curve at high cycles follows the linear piecewise function (if plotted in log-log coordinates),

$$NS^b = C$$

and the probability distribution function for the stress can be approximated by the Rayleigh distribution:

$$p(s) = \frac{s}{m_{os}} e^{-\frac{s^2}{2 \cdot m_{os}^2}}$$

Then using the Gamma function, the expected value of the total damage during T becomes:

$$E[D] = \frac{T \cdot f}{c} \sqrt{2} \cdot m_{os}^2 \cdot \Gamma\left(1 + \frac{b}{2}\right)$$

The largest uncertainty is selecting a distribution that accurately describes the seastate, and hence the responses and loads for smaller vessels.

An alternative model developed by Schaff and Davidson of Wright-Patterson Air Force Base (1994-1995) was successfully applied to the fatigue of aircraft laminates [63]. Their approach included multi-axial variable loading similar to those in marine applications, but did not include any marine materials.

An important consideration in this project's application of the damage accumulation models is the earlier definition of "failure", which included both strength and stiffness criteria. Although the application of these models to strength criteria is well documented, no documentation or research of these models being applied to stiffness criteria for marine composites was found.

4.1.4 Moisture Effects

The differences in moisture effects illustrates the difficulty in predicting laminate performance. The major difficulty is using the current state-of-the-art in moisture diffusion analysis to predict laminate saturation. The basic process through which moisture is absorbed into a polymer composite laminate is assumed to follow Fickian diffusion,

$$\frac{\partial c}{\partial t} = \frac{\partial}{\partial x} D_x \frac{\partial c}{\partial x}$$

where c is the moisture content at some point

The solution can be approximated by [70].

$$M(t) = \frac{G \cdot (M_m - M_i) + M_i}{M_m}$$

$$G = 1 - \exp \left[-7.3 \cdot \left(\frac{D_x t}{s^2} \right)^{0.75} \right]$$

Where,

M(t)= moisture content at time t as a ratio of total saturation

W_m= moist weight of the material

W_i= initial weight of the material

G= a time dependent parameter

M_m= maximum moisture content for the conditions

M_i= initial moisture content

D_x= diffusivity of the material in a direction normal to the surface

s= distance the moisture must travel. For single-sided exposure s=2h, for double-sided exposure s=h, where h= the skin laminate thickness

For a typical high performance carbon/epoxy marine-type laminate, $M_i=0.05\%$, $M_m=1.8\%$, $D_x=7 \times 10^{-7} \text{ mm}^2\text{s}^{-1}$ [70], $s=2h=3\text{mm}$. Figure 4-4 shows moisture diffusion versus time, where the maximum value 1 corresponds to the saturation level M_m .

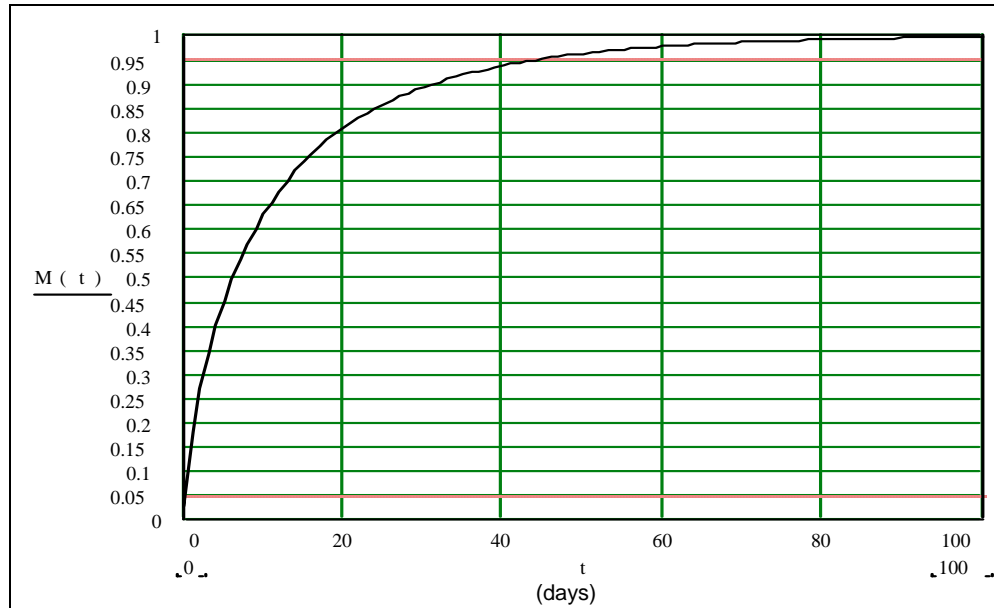


Figure 4-4: Moisture Diffusion Through a Carbon/Epoxy Skin Laminate

This graph shows that theoretically, full moisture absorption would occur in about 80-100 days.

4.2 Testing Methods

As noted above, the greatest gains in improving existing methods are available in areas with the largest uncertainties. For marine composite structures the two largest uncertainties were loads and testing methods. The large uncertainties caused by the standard beam tests prompted development of new test methods in both Europe and the United States. These uncertainties are caused by three main characteristics:

1. Beam boundary conditions
2. Line rather than distributed loads
3. Dry environment

The current state-of-the-art in marine composites fatigue testing is represented by testing machines that successfully address the first two conditions, this research includes all three.

Recent research has followed different approaches. Riley and Isley pressure loaded sandwich panels which were bolted to a rigid frame. The compared laminates were constructed of biaxial and double-bias cloth. The data collected showed improved results over beam analysis. Results fell between FEA predictions for fixed and simply-supported edges, however, suggesting the testing machine boundary conditions were not rigid [119].

Lloyd's Register of Shipping and DuPont cooperated to produce a fatigue testing machine using multiple load points to more evenly distribute the load along the sample length. In addition, the specimen was made square to address the beam boundary condition problem. End conditions were fixed-fixed, which the researchers believed led to premature failure of the laminates at the supports even though the laminate was substantially reinforced in that area [68]. Results indicated improved correlation with theoretical flexural properties for plates over those predicted using beam equations and tests. This improvement became more noticeable as deflections increased past half the laminate thickness to include membrane stresses. Figure 4-5 shows a schematic of the Lloyd's testing machine.

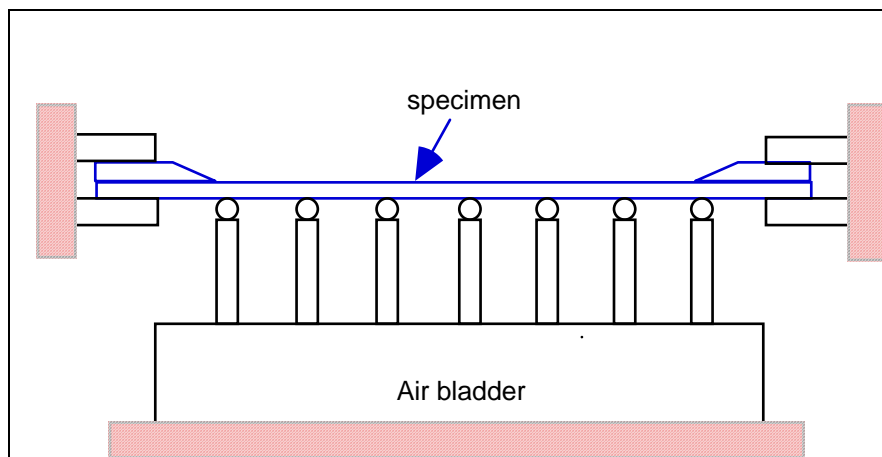


Figure 4-5: Lloyd's Register of Shipping Fatigue Testing Machine

Another improved test method was developed by the US Navy to verify panel designs for the fiberglass coastal minehunter program. Panels 90"x120" were constructed of the full size laminate consisting of skins, core and stiffeners. To represent accurate boundary conditions three bays were constructed, with the distributed load applied only to the center section. Testing was performed to qualitatively select materials rather than verify the testing apparatus, so no data on the machine's performance was reported [120].

Researchers in the Ocean Engineering Department at Florida Institute of Technology (FIT) developed a pressure panel testing machine to test material response to static, fatigue and shock loading. The FIT approach restrained only the panel frames and allowed the panel to extend past the frames to simulate the continuity of the hull shell and reduce stress concentrations at the panel edge. The testing apparatus consists of a water bladder for pressurizing the panel, a box to contain the sides and bottom of the bladder, and framing [121]. Testing provided new insights into core versus skin performance for static and high strain rate loading. Figure 4-6 shows a schematic of the FIT machine set up. This essentially allowed for intermediate ship structures and is similar to equipment developed at the U. S. Naval Academy.

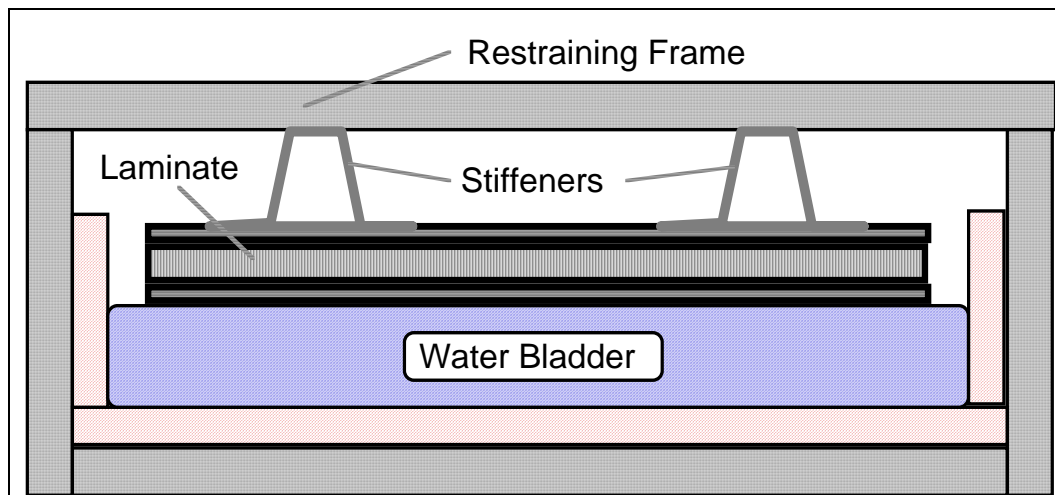


Figure 4-6: Schematic of FIT Pressure Test Apparatus

The most advanced state-of-the-art testing machine was developed by Gougeon Brothers, Inc. in conjunction with Michigan Technological University. Called the Hydromat Testing System (HTS),

it uses a water filled bladder to pressure load the panel like the FIT [122]. Unlike the FIT machine, however, the HTS machine is designed for plates only, rather than stiffened panels. This makes for much less expensive testing, although it limits the results to mostly tertiary rather than secondary structure.

Figure 4-7 shows a schematic of the HTS machine. The upper panel support frame is a truncated pyramid with a load cell in series at the apex. On the pyramid's lower edges a half-round journal bearing is mounted, against which the 24"x24" test panel's top edge rests. The half-round journal bearing also supports the panel from below. The two support frames are bolted together at the corners.

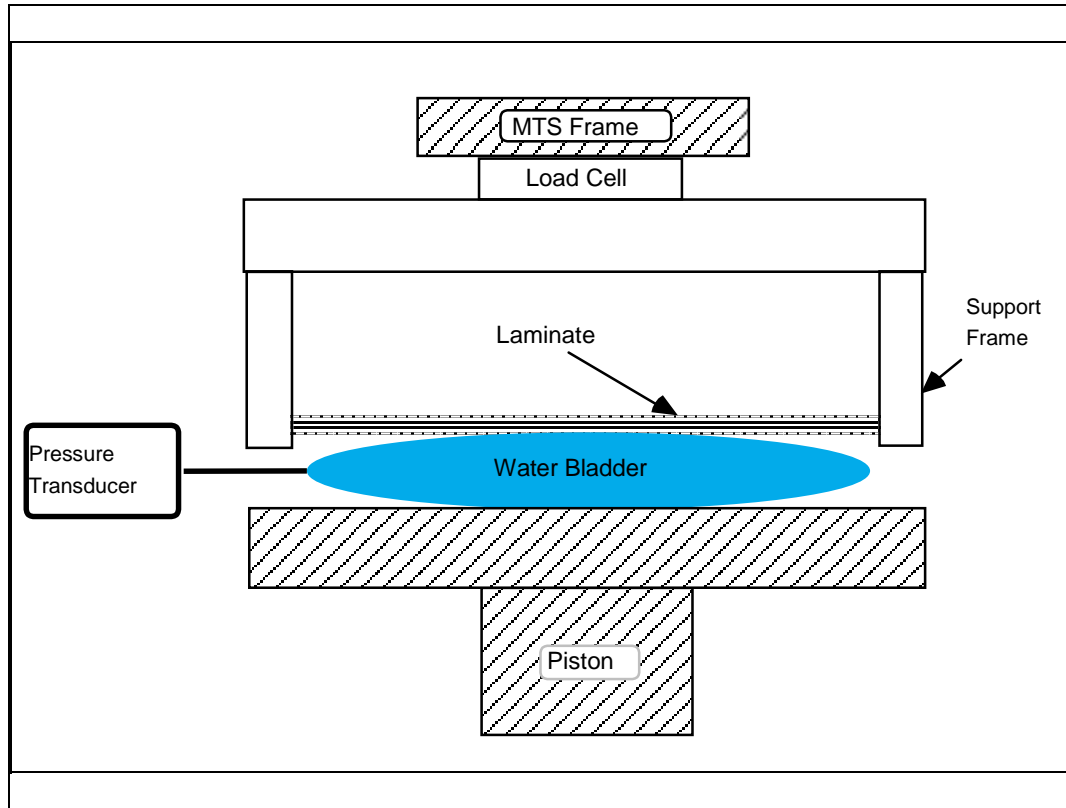


Figure 4-7: Schematic of the Hydromat Testing System

The HTS system was verified by testing carefully machined thin steel plates against thin plate theory matching the HTS boundary condition. Although analytically matching the bladder loading conditions and edge boundary conditions proved complicated, results were excellent. Deflections

and strains were measured for three different loading models. The cosine transition pressure model produced virtually identical values to experimental data and the step pressure model showed differences of less than 4%. The uniform pressure model was off by 20% [122].

The HTS approach has been selected by the USCG and SNAME for further study with the hope of developing a database for marine composites [123]. In addition, it was approved in 1999 as an ASTM test standard, D6416.

5.0 Research Overview

This research addressed the uncertainties in designing for durability of marine composites by correlating test and analysis methods with full-scale results. The research program included:

1. Reviewing appropriate laminates, construction methods, analysis methods, and materials representing baseline, current and future industry trends. Selecting a representative material and application for verification.
2. Determination of appropriate fatigue loading for the anticipated application through review of vessel service lives.
3. Verification and modification of current test methods to better reflect actual load conditions, including strain rate, moisture and boundary conditions.
4. Correlation of test methods to numerical analysis and full-scale results to produce a verified method for fatigue analysis of composite vessels.

Based on the review presented in Section 3, the “standard” material was a sandwich laminate made of polyester resin with E-glass reinforcement and either a balsa or foam core. The selected vessel for the full-scale testing and all comparisons was the J/24 class sailboat, which has a “standard” laminate with a balsa core. The boat is typical of 20-40 foot recreational craft.

The outer skin comprises multiple layers of mat and chopper gun roving. The inner skin is mat and boat cloth. The core is 3/8” end-grain balsa bedded in putty. The vessel is fabricated in an open mold at ambient temperature and pressure. Compared to aerospace or high-performance applications these laminates have higher void contents and significantly more variable properties.

The vessel's construction has not changed much over the years. Although some improvements were made during the last 20 years, the area under study, the bottom hull plating in the slamming area has not changed. The major changes included modifications to some bulkheads and floors. The appendix includes construction drawings and specifications for the J/24.

Testing included coupons in tension, shear, compression and flexure; panels in flexure, and full-scale on-the-water tests. Analysis included spreadsheet, symbolic sheet and finite element analysis using the methods presented in Sections 3.2 and 4.1.

6.0 Coupon Testing Program

The material testing program's goals were to:

- Compare environmental testing approaches
- Determine the material properties needed for the finite element analysis
- Compare coupon and panel test methods to full scale results

The materials tested are polyester/E-glass laminates representing the test vessels' construction. TPI provided coupons representing the forward hull laminate made by shop floor workers. The resin system is 33234-01 PolyLite Polyester by Reichold, Inc., an DCPD isophthalic blend [124]. The only difference between the actual vessel's laminate and the test coupons was the substitution of a layer of clear polyester in place of the pigmented gel coat. This was to allow easier visual inspection of the materials during and after testing. No effects on the material properties were expected from this substitution. Environmental testing included submerged, relative humidity and boiled conditions. The mechanical testing included:

- tensile (ASTM D3039), 21 specimens
- 7 compressive (with core: ASTM C364) and 21 without core: ASTM (Boeing Modified D695)
- shear (ASTM D3518), 21 specimens
- flexural fatigue (ASTM C393)

6.1 Moisture Exposure Tests

To accurately model boats remaining in the water test results providing weight gain and property effects caused by immersion were necessary. These tests also allowed for comparison of standard industry approaches for determining moisture effects. A further benefit was the ability to

compare test results with comments from J/24 owners, who believed the boats gain between 50 and 100 pounds when left in the water.

The basic process through which moisture is absorbed into a polymer composite laminate, Fickian diffusion, was described earlier. For a typical polyester/E-glass marine-type laminate the constants are close to, $M_i=0.05\%$, $M_m=1.8\%$, $D_x=7 \times 10^{-7} \text{ mm}^2\text{s}^{-1}$ [70], $s=2h=3\text{mm}$. Variations of 200% are relatively common for D_x , and W_m appears very sensitive to temperature, with increases of 2-5 times for temperature increases of 10-50°C[70].

To determine the moisture absorption (weight gain and coefficient of moisture expansion) of the J/24 polyester/E-glass laminate, six sets of coupons supplied by TPI were exposed to water. The six sets consisted of two groups of three, representing the ASTM tensile, shear and uncured-compression specimens. Each set had seven individual coupons. The moisture specimens were placed in the steam saturation room in 460 Davis Hall in early March 1998. One group was submerged in tap water at $70^\circ \pm 4^\circ \text{ F}$. The other was exposed to 100% relative humidity and the same temperature conditions. A third set was kept dry. Tap water was used rather than seawater as it was easier to manage and other studies have shown little difference in weight gain amounts or rates between tap (not distilled) and seawater. The edges were not sealed for the baseline tests. The group soaked in the water were kept in plastic containers. The relative humidity specimens were stored on racks. Prior to exposure the specimens were weighed and measured.

Weighing of the exposed specimens involved removing them from the containers, racks and room, light wiping with a towel and weighing on an electronic scale. Prior to each day's weighing the scale was calibrated using a standard weight. The specimens were always weighed in the same order, and the total process took about 45 minutes. Length measurements used the same calipers. The following table (Table 6-1) explains the abbreviations used in the data collection.

TN	Tensile no core
CC	Compressive with core
CN	Compressive no core
SN	Shear no core
FC	Flex with core
D	Dry
R	Relative humidity at 100%
W	Wet

Table 6-1: Abbreviations Used in Coupon Specification

Large variations in the daily weight measurements were noted, although trends were clear.

Table 6-2 shows the average weight gain and coefficient of variation for each set of specimens at the end of 226 days. The Coefficient of Moisture Expansion for the submerged specimens was 0.023%.

Specimens	Weight Gain	COV
TND	0.00%	0%
TNR	1.39%	9%
TNW	1.73%	14%
SND	0.00%	0%
SNR	1.25%	22%
SNW	1.72%	6%
Fickian	1.78%	

Table 6-2: Average Weight Gain and COV for Tensile and Shear Coupons After 226 Days

Figure 6-1 shows the weight gain over time versus the theoretical Fickian diffusion. The submerged specimens gained more weight than the specimens subjected to 100% relative humidity but not a significant amount considering the graph's dip at around day 100 for the relative humidity specimens. This occurred when the steam maker was accidentally shut down. As is common, M_m and D_x used in the Fickian prediction were assumed to make the best plot. The resulting values were $M_m = 0.0173$ and $D_x = 5.0e^{-7} \text{ mm}^2\text{s}^{-1}$. Both are within the published range for these materials[70]. The specimens initial moisture absorption over the first few days however was significantly faster than predicted by the Fickian diffusion equation. Most of the moisture absorption occurred within the first 48 hours. The graph shows the relative humidity

specimens data ending after 177 days. These specimens were removed to participate in the sealed edges study.

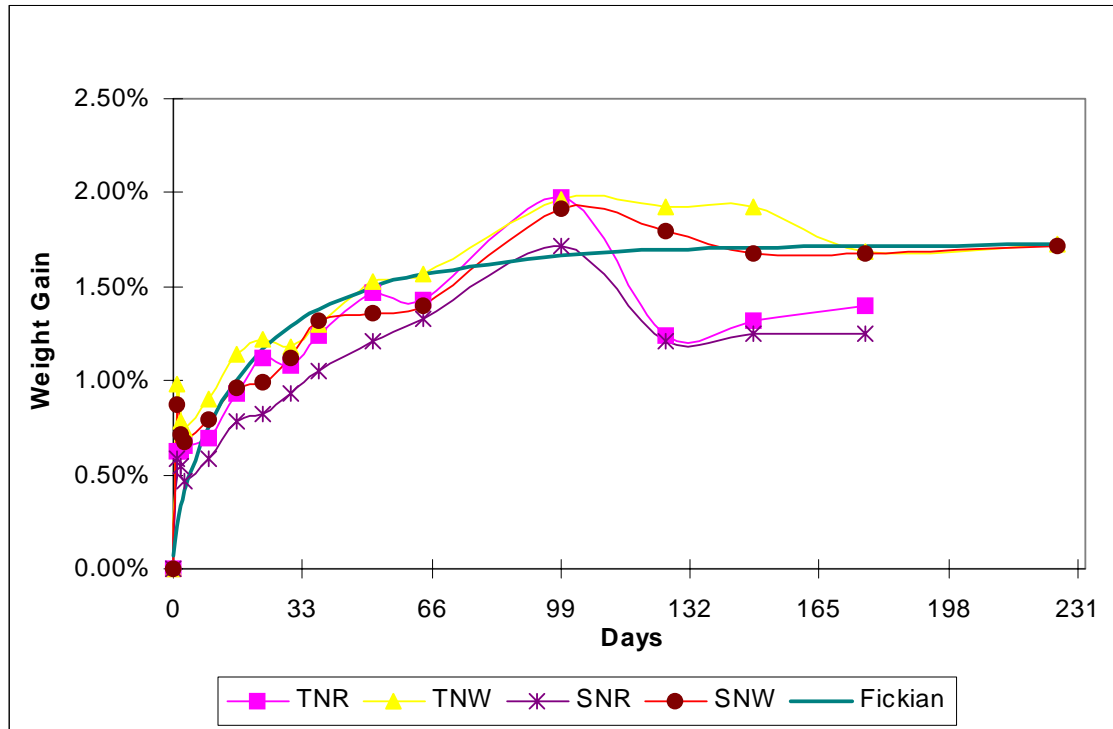


Figure 6-1: Experimental vs. Theoretical Weight Gain for Polyester/E-glass Specimens

6.1.1 Sealed-Edge Moisture Exposure Tests

Controversy exists whether the standard moisture specimens accurately reflect actual conditions on boats. One reason for this is the presence of exposed fiber ends to moisture. This occurs due to the cutting of the laminate which exposes the fiber ends directly to the moisture. The belief is that the moisture reacts with the fiber sizing and wicks along the fiber, reducing the compressive and shear strengths and increasing the rate of water absorption. On most boats these edges would be sealed. This practice has been shown to reduce delamination problems and water incursion into cores, but its value for uncured laminates is not known.

To see the effect of sealing the edges on weight gain, the relative humidity specimens were removed from the steam room and allowed to dry. After one month the weight had stabilized and the edges were then lightly sanded and coated with epoxy. The specimens were allowed to cure for one week, weighed and submerged. The sealed edge specimens were then weighed on the same schedule as the original unsealed specimens and kept in the same environmental conditions.

Figure 6-2 shows the effects of sealing the edges. The weight gains were similar to that seen in the initial study with unsealed edges and there was no appreciable difference between the two sets of specimens after 37 days. What this shows is that edge sealing the laminate will not slow the amount of moisture absorbed into these materials. What is probably occurring is that the polyester resin is absorbing the moisture directly and little or no wicking is taking place.

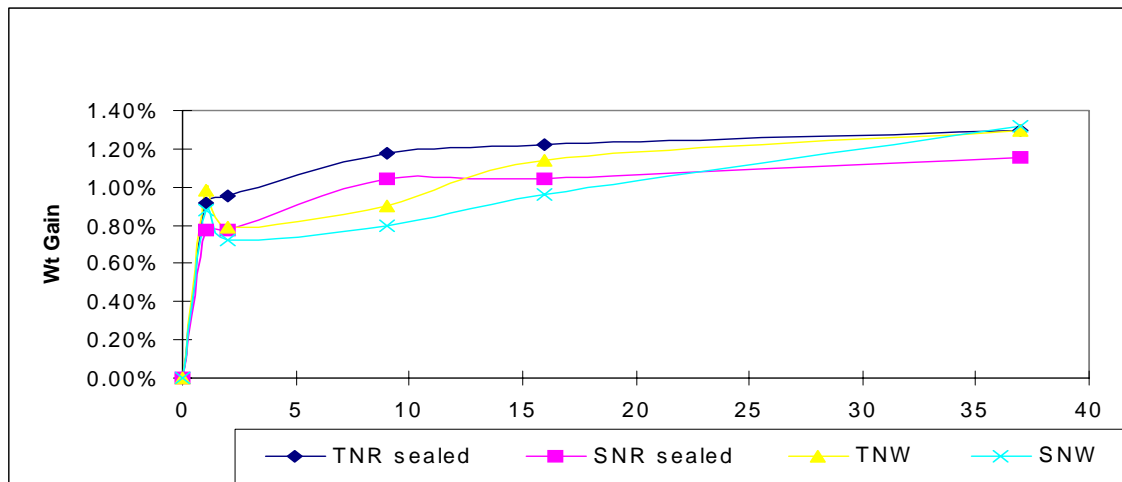


Figure 6-2: Weight Gain Comparison Between Edge-Sealed and Unsealed Specimens

Tests were also performed to determine the effect of different moisture tests on strength. One batch of specimens was kept dry at room temperature. Another was kept submerged in tap water at room temperature for 15 months. The third batch was kept at 100% relative humidity for 15 months and then boiled for 24 hours. This last approach simulates a common method for

accelerated aging. In each case the specimens were tested within one hour after removal from the water to prevent significant moisture lost. The boiling water specimens were allowed to cool to room temperature.

Some controversy exists whether the boiling method accurately reproduces environmental effects. The main reason for this is that at boiling temperatures the coupon is subjected to temperatures 40° F higher than the resin's heat distortion temperature. As this will change the resin's molecular structure it seems unlikely that this would be duplicated by long term exposure at lower temperatures.

The boiling water specimens did show different tensile strength and physical properties from the long term submerged specimens. After boiling the specimens were significantly lighter in color, indicating some change in their physical characteristics. In addition to the 9% lower tensile strengths than the wet specimens, the boiled specimens also exhibited lower levels of audio response. Whereas the dry and wet specimens typically reached a point of 5500-6000 psi before continuous "pinging" was heard from the specimen, the boiled specimens reached this level at 4000-5000 psi. This could be a sign of greater brittleness in the resin causing early microcracking. It appears that using the boiling water test applies an extra level of conservativeness in the physical properties.

Table 6-3 shows the results of the various moisture tests on the coupons tested using ASTM D3039. Note that the wet values are both significantly lower than that seen by Springer and Sloan. This is likely due to the greater resin dominance in the predominantly chopped mat construction. Also, the large decrease in tensile properties is interesting given that typically tensile failures are fiber dominated. Larger differences between the two moisture tests were seen in compressive and shear properties (see Sections 6.3 and 6.4).

Exposure	Average Tensile Strength	% dif.	Average Tensile Modulus	% dif.
	[ksi]		[msi]	
Room Temp - Dry	11.3		1.19	
Room Temp - Wet	9.4	-20%	1.05	-12%
Room Temp - 100% RH/24 Hr Boil	8.6	-24%	1.03	-13%

Table 6-3: Change in Tensile Strength Due to Long Term Submergence and 24 Hour Boiling.

Interestingly, both of the submerged specimen batches showed significantly lower properties than the dry specimens. Typically this is not seen when following the standard specimen preparation guide which suggests 72 hours of drying before testing. Although weaker when wet, like wood, the materials appear to regain their strength when dried. Unfortunately however, vessels in service are rarely dry!

The difference between the submerged and boiled specimens was consistent in that the boiled specimens always showed a marked decrease in properties over the submerged specimens. In addition to the loss of properties, and unlike the unboiled specimens, the boiled specimens changed color from light green to white, signifying some molecular changes. Most likely the boiling, which caused temperatures to exceed the heat distortion temperature of the resin, was the reason. Given the clear differences in properties and the different physical changes there appears to be no justification for using a boiling test to predict long-term properties.

Based on the actual weight gain of the specimens, a calculation was made of the predicted weight gain due to the submerged hull laminate of a J/24 left remaining in the water. Figure 6-3 shows the predicted weight gain over a three-month period. The assumptions were that the weight gain followed the Fickian diffusion pattern, the moisture absorption was one-sided and only effected the outer hull skin that was submerged. The laminate density was 0.042 lb/in³. The rudder was assumed to be removed (otherwise the values would be about 10% larger) and any keel fairing material was neglected. The maximum predicted weight gain if the vessel remained in the water indefinitely was 1.1 pounds.

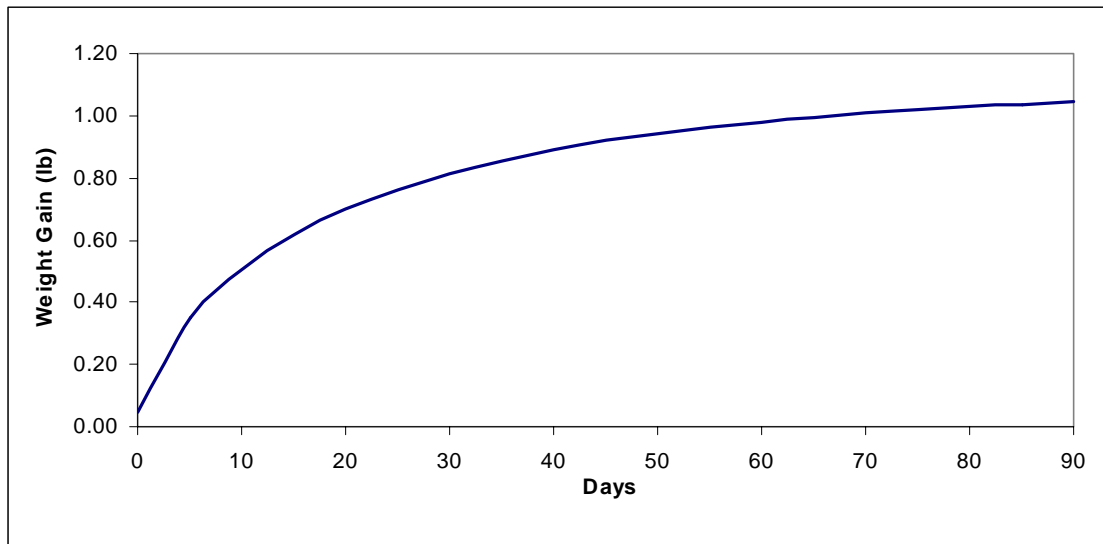


Figure 6-3: Predicted Weight Gain of J/24 Hull Laminate

Clearly the graph and the owner's comments of "50-100 pounds" weight gain are not in agreement. If the entire laminate (inner and outer skins, deck and hull, approximately 1320 pounds) are included by taking the assumption that the boat, due to its proximity to the water, is in 100% relative humidity, then the weight gain would be approximately 23 pounds. The additional weight is likely due to moisture absorption of fairing compounds, cushions, sails, etc.

6.2 Tensile Tests

Twenty-one test specimens were tested for tensile strength and modulus using ASTM D3039. The specimen dimensions were 1 inch wide by 10 inches long (approximately 0.15" thick) and were tabbed with two layers of DB170 on each side within 1" of the ends. As mentioned in the previous section, one batch of seven was cured for 15 months at ambient temperature and humidity. The second batch was kept at room temperature but was subjected to 100% relative humidity for 15 months and then boiled for 24 hours. The third batch was submerged in tap water for 15 months at ambient temperature.

The wet specimens were allowed to cool to ambient temperature but were tested wet to simulate the actual vessel condition. Typical failure loads were on the order of 1400 pounds. Figure 6-4 shows the set-up for the tensile and shear tests. The specimens were tested on the US Naval

Academy's Satec machine using pneumatic grips set at 2500 psi. A 1" gauge length, 20% strain limit extensometer was used as the primary tensile strain measuring device.

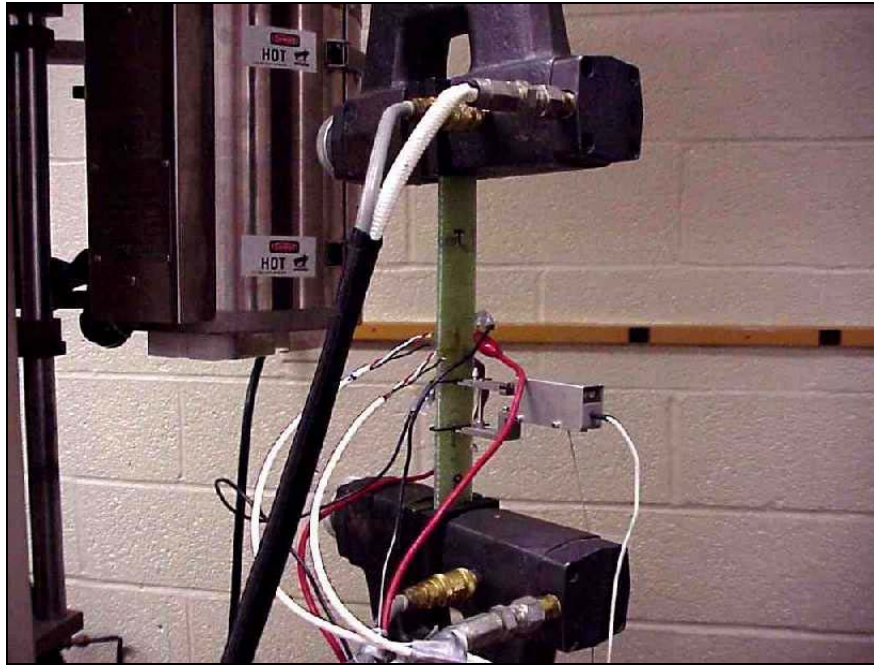
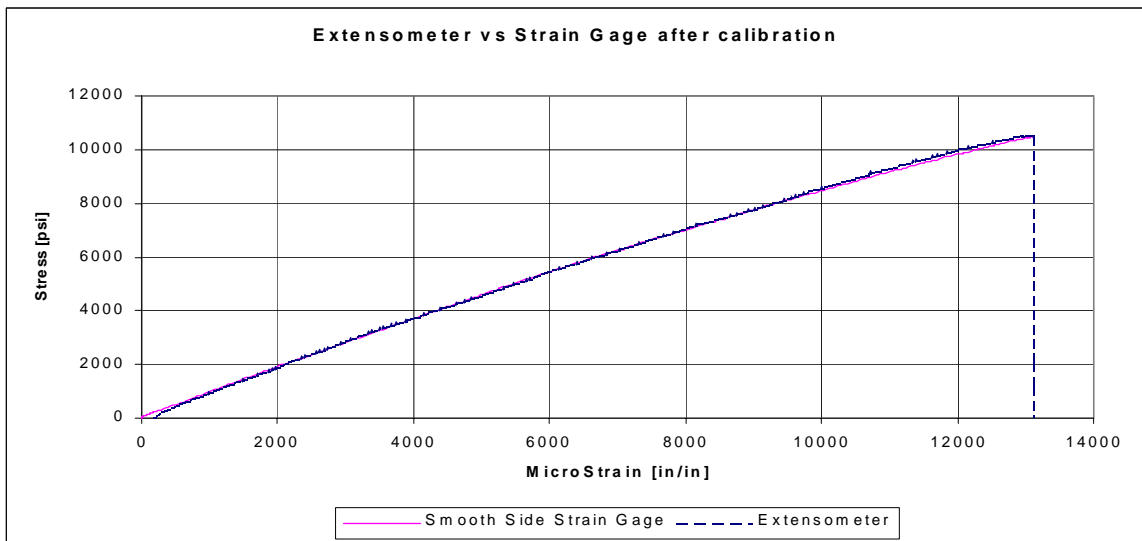
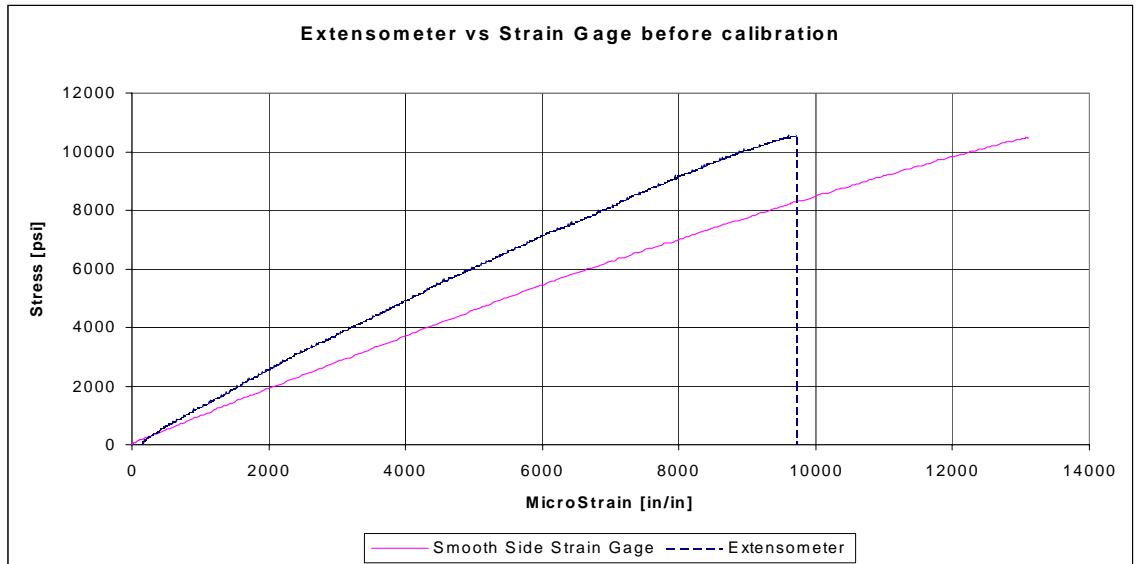


Figure 6-4: Tensile and Shear Test Set-up Showing Extensometer and Strain Gauges

Strain gauges were used to check the extensometer's calibration. The first two specimens in each batch were strain gauged in the horizontal and vertical directions on both sides of the specimen. Additionally all specimens in the dry tensile and dry shear batches were strain gauged. Figures 6-5 and 6-6 show the strain gauge and extensometer results before and after calibration. Calibration was based on comparing deflected positions. After the extensometer calibration only two specimens from each batch were strain gauged. This eliminated the significant difficulties encountered when gauging wet specimens.



Figures 6-5 and 6-6 Showing the Effects of Extensometer Calibration.

Fifty percent of the specimens broke in the middle and the remaining within 1" of the tabbing. Three of 21 specimens broke in the grips. Figure 6-7 shows a close-up of a broken specimen. The design of the tabbing grips may have resulted in the lower-than-normal number of grip failures. Two layers of DB-170 (double-bias) cloth were laminated on each side of the coupon. This provided a surface that could be damaged by the grips but did not give any additional longitudinal stiffness to the coupon.

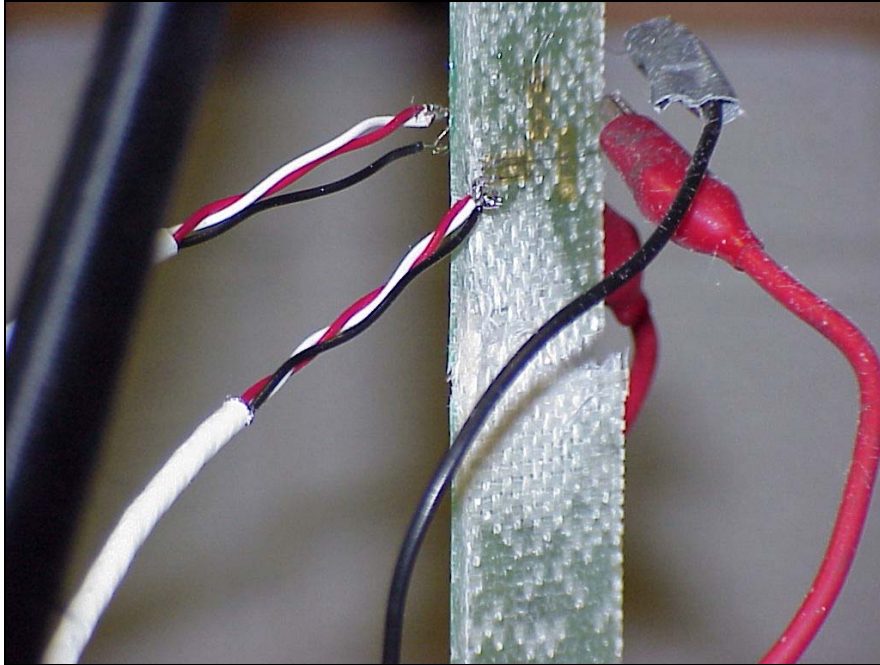


Figure 6-7: Broken Tensile Specimen

Table 6-4 shows the tensile test results. As numerous methods are used to determine the modulus of a given material it was determined that a tangent modulus representing the range from 5-20% of the initial load curve would be used. This compensates for any gauge slip or seating, and also represents that portion of the load curve that is most encountered during operation of these vessels.

An interesting point is the significant difference in strength between the two wet and dry specimens, even though tensile results are considered “fiber dominant” and glass fibers are not effected by moisture. The most likely reason for this is the low fiber volume (approximately 28%) in these laminates and the random mat lay-up.

Coupon #	TND Dry		TNR Boiled		TNW Submerged	
	Mod	Str	Mod	Str	Mod	Str
1			1130100	9150	1069500	8888
2	1140650	10540	1115200	8627	972870	9574
3	1229800	12072	1005500	8974	1003600	9137
4	1164000	8778	1020900	8296	1071300	9792
5	1348900	11894	967220	8747	1058000	10145
6	1161600	11364	968260	8500	1047700	9066
7	1078300	11596	989240	8029	1147300	9384
AVE	1187208	11041	1028060	8618	1052896	9427
COV	7.8%	11.1%	6.6%	4.5%	5.3%	4.7%
<i>Difference from Dry</i>			-13.4%	-21.9%	-11.3%	-14.6%

Table 6-4: Tensile Test Results (psi)

The average dry strength was 11.0 ksi and the modulus was 1.19 msi. Wet, the average strength dropped to 9.4 ksi and the modulus to 1.05 msi. The respective failure strains were 0.93% and 0.90%. The first tensile specimen data was ignored due to software problems controlling the test machine, which caused a greater than expected strain rate and higher strength and modulus values.

6.3 Shear Tests

Twenty-one test specimens were tested for shear strength and modulus using ASTM D3518. The specimens were the same as the D3039 specimens with the exception that the cloth layer was laminated at $\pm 45^\circ$ to the pull axis. The same environmental exposure procedures were used. The tests were run on the SATEC machine with the modulus determined by a 1" extensometer. Typical failure loads were on the order of 1200 pounds.

Table 6-5 shows the shear test results. Like the tensile results the wet specimens showed a marked decrease in strength and some decrease in modulus. The relative decreases were greater than the tensile values, which is to be expected as shear values are more dependent on resin properties.

Coupon #	SND Dry		SNR Boiled		SNW Submerged	
	Mod	Str	Mod	Str	Mod	Str
1	507150	4903	496625	3824	493610	5020
2	599600	5627	471580	4394	433925	4748
3	608450	6135	513950	4474	536300	4758
4	544950	4706	480755	4631	504050	5051
5	538850	5529	453650	4114	520100	5067
6	540700	5822	442485	4250	501350	5089
7	552550	5525	462795	4155	495285	4762
AVE	556035.7	5464	474549	4263	497803	4928
COV	6.4%	9.2%	5.2%	6.2%	6.4%	3.3%
<i>Difference from Dry</i>			-14.7%	-22.0%	-10.5%	-9.8%

Table 6-5: Shear Test Results (psi)

The average dry shear strength was 5.5 ksi and the shear modulus was 0.56 msi. Wet, the average strength dropped to 4.9 ksi and the modulus to 0.50 msi.

6.4 Compressive Tests

Twenty one uncured and seven cured compressive specimens were tested using the ASTM (Boeing Modified) D695 (without core) and ASTM C364 (with core) test standards. The uncured specimens were subjected to the same environmental conditions as the tensile and shear specimens. The cured specimens were tested dry. Modulus was measured by the crosshead movement and checked with strain gauges.

The difference in the two test standards relates to the likelihood of buckling as a failure mode. In the case of the sandwich laminates the core helps stabilize the specimens. To compare the two methods the uncured specimen values were compared to the failure stress of the cured specimens with an allowance for the core removed, making the assumption that apart from buckling resistance, the core provided negligible compressive strength.

One aspect of the testing included designing and building new grips for the cured compressive specimen tests. The grips had to meet the requirements of ASTM C364 while being easier to

build and more versatile than those currently on the market. Figure 6-8 shows the final design drawing and Figure 6-9 shows the grips in the test configuration with a specimen that failed in compression.

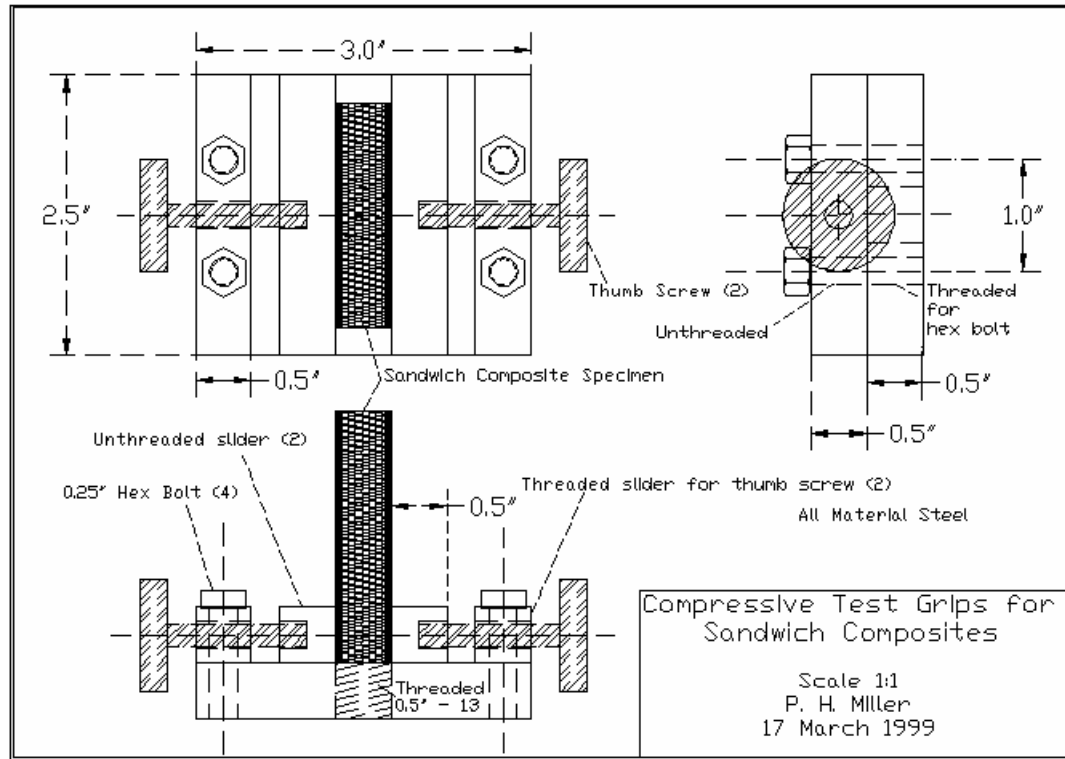


Figure 6-8: Compressive Grips Design



Figure 6-9: Compressive grips with failed specimen

An additional problem occurred with the uncured compressive specimens. The original specimens were fabricated for a standard 4" clamped compressive grip. As the Naval Academy has the more accurate 3" Boeing version test equipment the specimens were modified. This entailed removing 0.4" from each end of the specimen and grinding off the tabbing.

Table 6-6 shows the uncured specimen results. The average dry compressive strength was 25.3 ksi and the modulus was 0.92 msi. Wet, the average strength dropped to 21.2 ksi and the modulus to 0.86 msi. Again the wet specimens showed a significant drop in properties. Of more interest is the difference between the tensile and compressive values, with the compressive strength more than twice that of the tensile values. This again is probably due to the very low fiber volume in the laminate, making the laminate act more like a resin than a glass composite.

Coupon #	CND Dry		CNR Boiled		CNW Submerged	
	Mod	Str	Mod	Str	Mod	Str
1		24856	728520	15838	801780	20966
2	886890	24536	855000	20529	867080	21609
3	901680	28506	845290	19937	872060	21071
4	965130	22477	828360	19699	882700	22591
5	859730	28616	843170	19585	871780	20105
6	957100	25692	730140	17865	854660	20859
7	920610	22561	784520	18814	889360	21463
AVE	915190	25321	802143	18895	862774	21238
COV	4.5%	9.9%	6.8%	8.4%	3.4%	3.6%
<i>Difference from Dry</i>			-12.4%	-25.4%	-5.7%	-16.1%

Table 6-6: Uncored Compressive Test Results (psi)

Table 6-7 shows the cored specimen results with and without allowance for the core. The allowance was calculated by the respective areas of the skins and core. The results show that the core relatively contributes to stiffness, but also decreases relative strength. The latter is most likely due to the added flaws introduced with the core bond and contour cuts.

CCD Dry		CCD-No core correction Dry		Coupon #
Mod	Str	Mod	Str	
270070	4795	945245	16783	1
317159	5590	1110057	19565	2
290140	7615	1015490	26653	3
325040	6579	1137640	23027	4
273150	4634	956025	16219	5
344770	5934	1206695	20769	6
320330	4876	1121155	17066	7
305808	5718	1070330	20012	AVE
9.3%	19.1%			COV
		17.0%	-21.0%	<i>Difference from Dry</i>

Table 6-7: Cored Compressive Test Results (psi)

6.5 Poisson's Ratio Tests

As part of the tensile tests the specimens were strain gauged in the vertical and horizontal directions to determine Poisson's Ratio. All seven dry specimens were gauged for these tests, although the first and fourth specimens succumbed to gauge failure before reliable results could be determined. For comparison, two specimens of the wet and boiled groups were also gauged. For these specimens the surface was toweled dry and the gauges applied. Typical gauge application took approximately 10 minutes, minimizing moisture loss.

As the specimen lay-up was not balanced, some warping occurred during the tests. This meant that each specimen was gauged with one vertical and one horizontal gauge on each side. Negligible differences in Poisson's Ratio were observed from the different sides. The resulting Poisson's Ratio was very similar for both wet and dry specimens and averaged 0.36 (Table 6-8).

Coupon #	TND	TNR	TNW
1		0.378	0.363
2	0.367	0.361	0.354
3	0.384		
4			
5	0.329		
6	0.346		
7	0.348		
AVE	0.3548	0.369	0.359
COV	6.0%	3.4%	1.8%
<i>Difference from Dry</i>		4.1%	1.1%

Table 6-8: Poisson's Test Results

6.6 Static Flexural Coupon Testing

Static flexural testing was performed to determine the out-of-plane properties, validate the FEA, compare test methods and create a baseline for the flexural fatigue tests. These tests are important as out-of-plane loading is the significant loading for small craft [8], and flex tests are often used to qualify small craft laminates [4]. Flex testing included both 3 and 4-point tests

based on the commonly-used ASTM C393 and D790 standards. The major difference between the two standards is that the C393 covers sandwich and the D790 covers solid laminates.

The first tests included three and four point ASTM C393 tests to determine the test effects (uncertainties) on predicted properties and select the method for the planned fatigue testing. The hope was that relatively short 3-point tests would produce acceptable results. This would provide the most number of specimens out of the available stock as the 36-inch pieces gave either three-12" or two-18" specimens. The goal was to find the spans that would cause simultaneous core and face failure, maximizing the apparent strength of the specimen.

When the specimen length changes, the ratio of core shear loading to face sheet loading also varies. In general, the longer the span, the higher the bending moment and therefore the higher the skin stresses. In the 3-point testing the 12" specimen tested using ASTM C393 resulted in a suggested 8" span and 16:1 span-to-depth ratio. The 4-point tests were initially set with quarter-point spacing and a 14" span.

The second test set used both 3 and 4-point C393 tests to find the panel stiffness and core shear modulus. These tests took the specimen to a set load below failure and then tested the specimens to failure in 4-point bending. As will be discussed later, this method allows for determination of panel bending stiffness, face sheet modulus and core shear modulus.

Figures 6-10 and 6-11 show the test set-ups. Specimens were loaded with the thicker outside hull skin (0.095" vs. 0.057" for the inner skin) in compression as this reflects hydrostatic loading. Initial crosshead rate was 0.21 in/min. Supports consisted of 1.25" diameter rods, which fell midway between the minimum and maximum diameters specified by ASTM D790. The combination of the thicker outside skin and the large diameter roller resulted in all failures occurring as either core shear or tensile face failure. Moderate damage was seen under the load points or supports, which indicated a sufficient radius. Additionally, no increase in stiffness at larger deflections indicated the supports did not have a too large radius.

In general the 4-point specimens showed uniform damage in the area between the center supports. This was expected as the maximum bending moment is uniform in this area. This also allows for strain gauging at the maximum bending moment without interference of the load or support points.

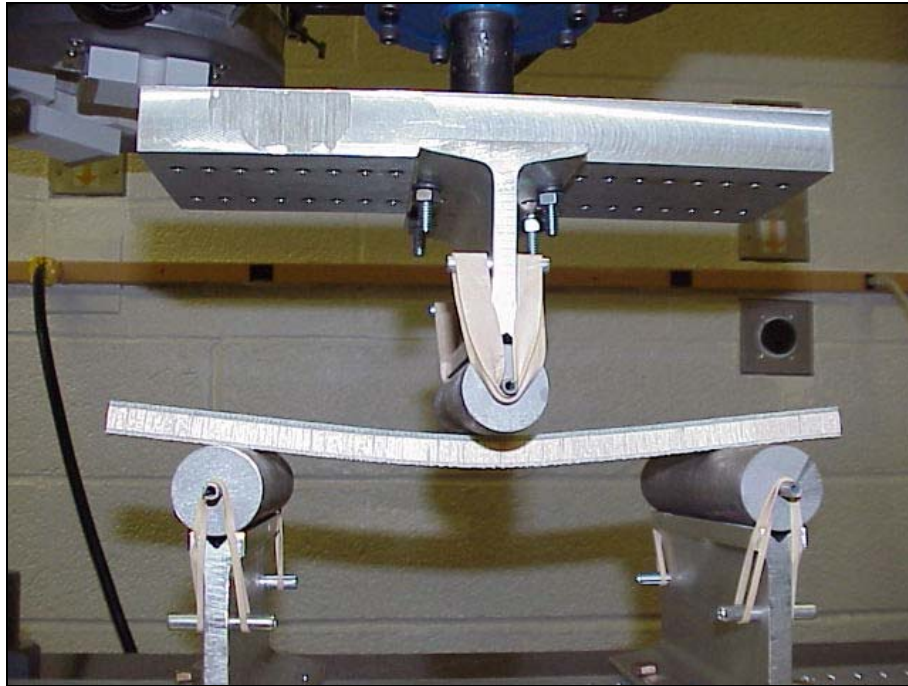


Figure 6-10: 3-Point Test Jig

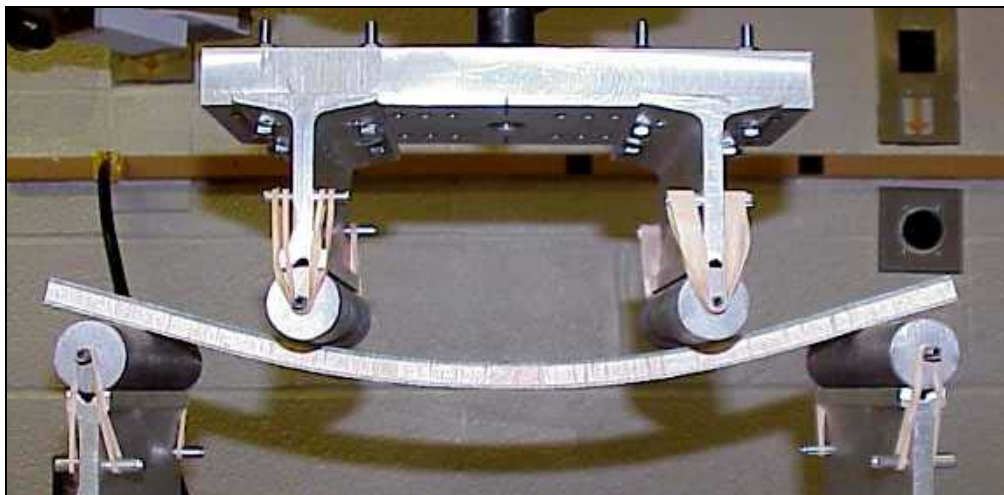


Figure 6-11: 4-Point Test Jig

Numerous methods are used to determine the stiffness of a given material. Two of the most common are the tangent and secant methods. Both use points along the load-deflection curve to determine the slope. For this project a tangent method representing the lower range of the initial load curve was used. This compensates for any grip or gauge slip or seating (toe), and also represents that portion of the load curve that is most encountered during operation of these vessels.

A common method used in the marine industry is to calculate the tangent flexural modulus based on the ASTM D790 test equations and compare it against other laminates. This gives an indication of relative laminate performance but is not useful in determining component properties as it assumes the sandwich is a homogenous rather than a composite material. It is also useful in determining the testing method effects and was used here to compare the 3 and 4-point test methods and determine the correct spans. The flexural modulus from this approach is found from:

$$E_f = \frac{F \cdot m \cdot L^3}{b \cdot d^3}$$

where: E_f = flexural modulus

m = slope of tangent load vs. center deflection line

L = Length of support span

b = specimen width

d = specimen thickness

F = 0.25 for 3-point and 0.17 for 4-point

Figure 6-12 shows a typical-load deflection curve for the flex coupons with an extension of the line used to calculate the tangent modulus. The slope of the tangent line was calculated by taking a linear regression of the points between 25 and 100 pounds. Similar to the tensile, shear and compressive specimens, the curve is linear up to about 2/3rds of ultimate strength. This was the

point where audio response was first heard from the specimen and initial damage was noticed on the tensile face.

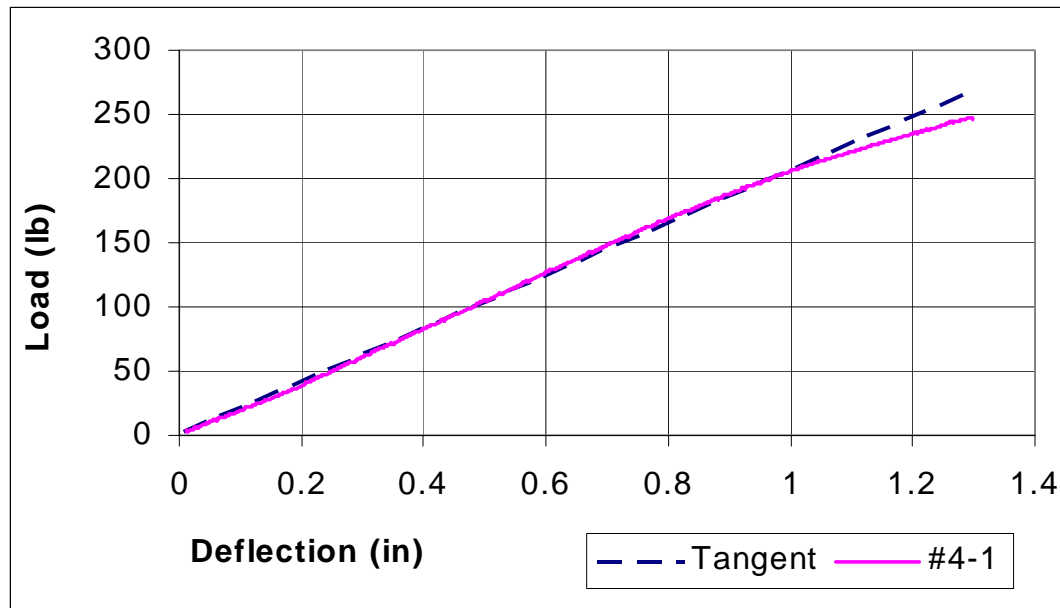


Figure 6-12: Typical Load-Deflection Curve and Tangent Modulus Line for 4-Point Bend Test

Flexural strength was calculated using the Boeing sandwich test (BSS7327) method rather than the ASTM C393 method as it includes the effects of the different skin thickness. This equation also assumes a homogenous skin material, so it too is only valuable for comparative purposes. Actual flexural strength must be backed out from a CLT analysis as was performed in Section 9.2.

$$f_c = \frac{P \cdot L_s}{(W \cdot t_c)(2T + t_t + t_c)}$$

where,

P = peak load (lb)

W = specimen width (in)

L_s = distance between loading nose and support (in)

T = core thickness (in)

t_c = top face thickness (in compression) (in)

t_t = bottom face thickness (in tension) (in)

The failure mode for the first four 3-point tests varied between core shear and tensile failure. The predicted strength using the 3-point test was 12,180 psi and was 12% less for the 4-point test at 10,740 psi. The COV was 5.3% for the 4-point and was 13.8% for the 3-point. All the specimens showed extensive tensile face damage although for 3-point specimens #1 and #4 the actual failure mode was core shear. To increase the face stress relative to the core shear stress the support spans can be moved farther apart to increase the bending moment. The span was increased by 1" to 9" for the last two 3-point specimens and to 14" span with 7" between loading points for the 4-point tests.

A comparison of the 3 and 4-point test results are shown in Table 6-9. The slightly increased stiffness for the 4-point specimen is attributed to the added shear deformation effects for the shorter span between load and support. This would be reduced if the test used the one-third loading span rather than the one-quarter span used, however a trial with a specimen tested with the one-third span had a deformation large enough to cause the specimen to fall between the supports before failure occurred.

Coupon #	3-Point	Strength	4-Point	Strength
1	657428	9290	753262	10762
2	853175	14388	747153	10442
3	708358	12903	749148	9844
4	783509	12588	811014	11262
5	750441	12133	848541	11400
6	783911	11775	766596	10729
AVE	756137	12180	779286	10740
COV	9.0%	13.8%	5.3%	5.3%

Table 6-9: 3 and 4-point Tangent Flexural Modulus and Strength (Homogenous Beam Equation) (psi)

The ASTM C393 test recommends an 8" span for 12" specimens to allow for 2" of overhang past the supports. This ensures that as the coupon bends it does not slip off the supports. By increasing the span to 9" the overhang was reduced 0.5" on each side to 1.5". This did not cause a problem as the specimens failed before the contact slipped. 3-point coupons #5 and #6 both

failed in tensile face failure. 3-point coupon #1 failed early due to the lack of core bond between two balsa blocks.

The other test set determined panel bending stiffness from the ASTM C393 method. This requires a simultaneous solution of the panel bending and shear deflection equations, which is possible only if both 3 and 4-point tests are conducted for the same specimens. The panel bending stiffness, D (lb·in²) is:

$$D = \frac{E(d^3 - c^3)b}{12} \text{ for equal facings, or}$$

$$D = \frac{E_1 t_1 E_2 t_2 (d + c)^2 b}{4(E_1 t_1 + E_2 t_2)} \text{ for different facings}$$

where:

E, E_1, E_2 = elastic modulus (psi)

b = specimen width (in)

d = specimen thickness (in)

c = core thickness (in)

t_1, t_2 = face thickness (in)

The deflection equations for the 3 and 4-point tests include both bending and shear effects:

$$\Delta = \frac{PL^3}{48D} + \frac{PL}{4U}; \text{ 3-point (in)}$$

$$\Delta = \frac{11PL^3}{768D} + \frac{PL}{8U}; \text{ 4-point, quarter loading (in)}$$

$$\text{where } U = \frac{G(d + c)^2 b}{4c}, \text{ the shear rigidity (lb), and}$$

G = the shear modulus (psi)

Solving the two deflection equations simultaneously gives,

$$D = \frac{P_1 L_1^3 \left[1 - \left(\frac{11 L_2^2}{8 L_1^2} \right) \right]}{48 \Delta_1 \left[1 - \left(\frac{2 P_1 L_1 \Delta_2}{P_2 L_2 \Delta_1} \right) \right]} \quad G = \frac{P_1 L_1 c \left[\left(\frac{8 L_1^2}{11 L_2^2} \right) - 1 \right]}{\Delta_1 b (d + c)^2 \left[\left(\frac{16 P_1 L_1^3 \Delta_2}{11 P_2 L_2^3 \Delta_1} \right) - 1 \right]}$$

The “1” subscript refers to the 3-point results and “2” refers to the 4-point. E can then be found from substitution into the earlier equation if it is equal for both faces. For unequal faces either one or the other or a ratio of the two is needed. Although this method has a drawback in that it requires both 3 and 4-point tests to get the panel stiffness, this approach is a viable alternative to a battery of tensile and compressive tests if the face sheets have uniform modulus.

Core shear stress was determined from:

$$\tau = \frac{P}{(T + t_i + t_c)W}$$

Table 6-10 shows the calculated panel stiffness, core shear modulus, failure strengths and shear stress as well as the 4-point failure modes. For these tests the spans were 9” for the 3-point and 16” for the 4-point. The test load for finding D and G was 100 pounds for both tests. Failure modes were tensile in each case, although indications of core shear were appearing before failure occurred. It is interesting to note the manufacturer’s published value of balsa shear strength is 491 psi and the shear modulus is 17,400 psi. The larger COV for the shear modulus is mostly a measurement uncertainty caused by the sensitivity in the calculations of actual deflections.

Coupon #	D	G	Flex Str	τ	Fail Mode
units	lb*in ²	psi	psi	psi	
1	10449	15517	12800	518	tensile face
2	9812	17185	11622	471	tensile face
3	10102	20150	11562	468	tensile face
4	10107	19812	11881	481	tensile face
5	10739	17434	11872	481	tensile face
AVE	10242	18019	11947	484	
COV	3.5%	10.8%	4.2%	4.2%	

Table 6-10: ASTM C393 3 and 4-point Flex Test Results

In this analysis a ratio of the laminate stiffness was estimated from a reverse micromechanics analysis of the tensile coupon results, giving $E_{\text{outer}} = 0.79 E_{\text{inner}}$. The face sheet elastic modulus could then be approximated. Although this is somewhat circular logic, it was used to check the relative tensile and flexural test results. The modulus calculated from this method was 1.38 msi, as compared to 1.19 msi from the tensile tests, a difference of 14.5%. The difference is caused by the homogenous assumption in the calculation. As the actual laminate has its stiffest ply (the boat cloth) on the outside, it creates an apparently higher modulus in bending. The predicted face failure strains were 0.95%, compared to 0.93% for the tensile tests.

The results from the 3 and 4-point static flexural tests indicated the 4-point, 14" span yielded acceptable results and is preferred due to the significantly lower COV. Maximizing the span will more realistically model the vessel loading, as will increasing the number of load points. The greater accuracy of the 4-point is due to the more distributed nature of the load, reducing loading concentrations of shear and bending moment at the center point. A limit is reached however when multiple load points, such as the Lloyd's machine in Figure 4-5 are used. As the equipment for the 4-point is only slightly more complex than the 3-point (requiring a center point deflection reader), the accuracy appears greater, and as it is more versatile than the 3-point, it should generally be used.

As the vessels live in the water a comparison of wet and dry material properties was required. This meant that the outer hull laminate needed to be moisture saturated, but the inner skin did not. To accomplish this the specimens were soaked in a pool of water equal to the thickness of the outer skin. To avoid moisture absorption into the balsa core the exposed balsa was coated with lacquer and varnish. This provided a waterproof yet flexible coating that would not increase the specimen stiffness or strength. After two months of soaking, mildew was present on the specimen edges, but no discoloration or soaking of the balsa was noticed. Using a 16" span, 4-point jig, the dry specimens' static ultimate strength was 11,000 psi versus 10,800 psi for the single-sided wet specimens, a decrease of 1.8%. The COV for both sets was 18%. The flexural

modulus was the same for both at 1.16 msi, with a COV of 8% for the dry and 1% for the wet specimens.

It is interesting to note that the failure of the wet specimens was not significantly lower than that of the dry specimens. Although previous tests showed that all material properties decreased as a result of submergence, for this laminate where the outer skin was substantially thicker than the inside laminate the primary failure mode of both the dry and wet specimens was still tensile failure of the inner skin.

6.7 Flexural Fatigue Tests

After the static flex tests determined that a 14" span, 4-point (quarter point loading) jig would yield results with the least uncertainty a test jig was designed to fatigue load the specimens. As no specimen slippage was observed the span was increased to 16" with a load separation of 8". By spreading the load points further, the bending moment was increased without increasing the shear load. This further ensured failure would initiate in the skins rather than the core, and also more closely represented the vessel's actual frame spacing.

A test jig was designed to load up to 50 specimens at one time in constant deflection loading equaling a percentage of the static strength. Each of the five cam-driven loading stations was designed to handle 10 specimens. Results from these tests yielded a stiffness-based S-N curve. Figure 6-13 shows the test jig drawing and Figure 6-14 the test jig. The drive motor was a Baldor 5 HP, 3-phase "SmartMotor", which included a built-in controller. In-service modifications included removing the cams for the 75% and 50% load cases as these specimens were tested on the Satec 50UD machine.

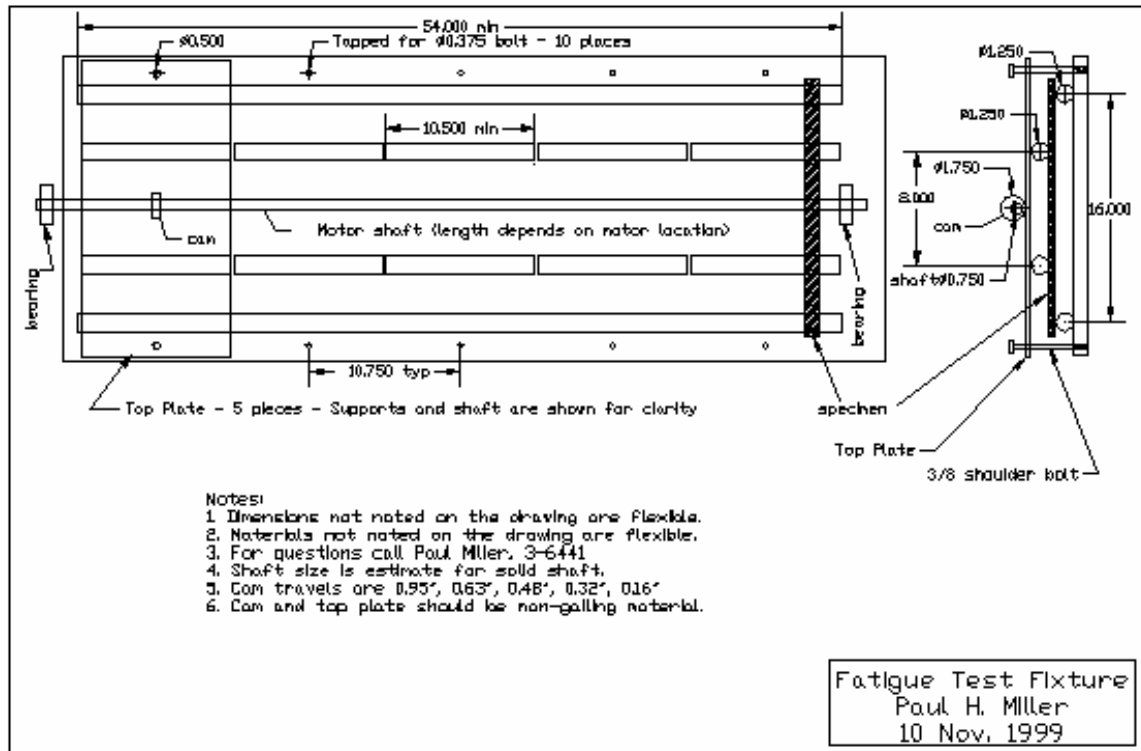


Figure 6-13: 4-point Fatigue Test Jig Drawing

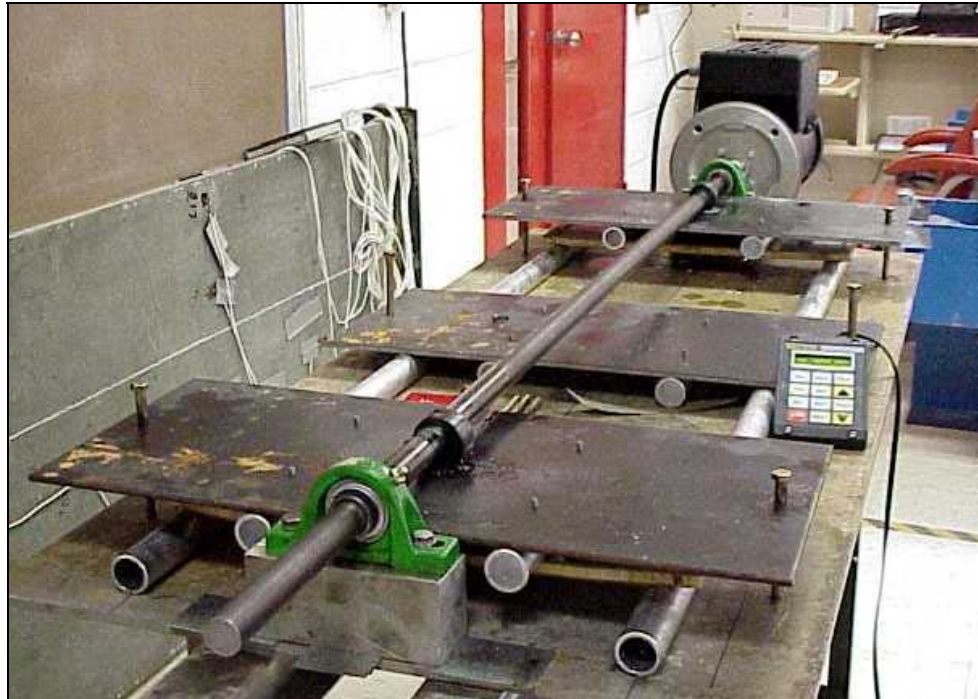


Figure 6-14: 4-point Fatigue Test Jig

The wet specimens were tested out of the water, although they were run for a maximum of six hours each day. The remaining time was spent soaking. Given the low moisture diffusion rate, this was not expected to cause a significant deviation from a fully submerged condition. Indeed, on more than one occasion visible moisture was still apparent on the compression (upper) surface after six hours testing.

One major decision concerned the frequency of loading. Too high a loading rate would cause the specimens to generate high internal heat, which would reduce the predicted strength as the temperature approached the heat distortion temperature. As the goal was to test up to 10^7 cycles, too low a frequency would make the testing last forever! Numerous researchers have looked at this problem and have determined the upper bound as 10 Hz for similar materials [32, 61, 77]. One difference from their tests was that their materials were not cored. As the core would provide insulation, the risk of heat build-up was present.

The “ideal” situation would be to test the materials at the maximum wave encounter frequency [24], which for a J/24 on Berkeley Circle would be 0.71 Hz (see Section 8.2.2). This would duplicate as close as possible the actual loading conditions. The practical solution was to hook up a thermocouple and measure the temperature. The frequency was increased until the surface temperature next to the loading points increased slightly over room temperature. From the manufacturer’s data sheet, the PolyLite 33234-01 resin when tested as a clear casting (no fibers) in December 1998 had an HDT of $158^{\circ} \pm 1.8^{\circ} \text{ F}$ ($70\text{C} \pm 2\text{C}$). The actual HDT of a glass-reinforced laminate would tend to be higher due to the glass fiber [125], so the slight increase over room temperature would not effect strength. Based on the measured temperature and the machine springback limits, the maximum cyclic rate was determined to be 5 Hz for the lowest loaded specimens and 0.5 Hz for the specimens cycled at 75% of the static load. This meant that the tested started out at low frequencies, but the speed increased as the more heavily loaded specimens failed.

The stress level selection was based on the number of available specimens and a minimum batch size of five. With 60 specimens and the need to test wet and dry, this limited the tests to six stress levels. The stress levels were 100% (i.e., “static”), 75%, 50%, 37.5%, 25%, and 12.5%. The baseline “100% Stress” used in the fatigue experiments was the dry static ultimate strength. For the S-N curve construction the approach differed slightly from that used in the static flex tests. Instead of using the labor-intensive C393 combined 3 and 4-point method the specimens were tested using the D790 method. This meant that the calculated moduli were not absolutely

accurate (due to the use of homogenous beam equations described earlier), but the relative sandwich stiffness decreases were accurately represented.

To relate the amount of stiffness measured in the J/24 to the samples, the residual stiffness was determined after a given number of cycles at the various stress levels. Stiffness measurements were taken on the Satec 50UD after various cycle amounts⁴. The measurements used a force control limit of 30 pounds, which equaled the 12.5% loading level. The crosshead rate was 0.5 in/min. Figure 6-15 shows the effect of multiple cycles on the hull laminate. In both illustrations the stiffness is normalized to the single-cycle dry stiffness at that percent load stress. The COV for all the measured stiffness of a given test group ranged from 2% to 6%. In Figure 6-15 the wet and dry specimens of each load have the same color and marker type, with the wet specimens having dashed lines and hollow markers.

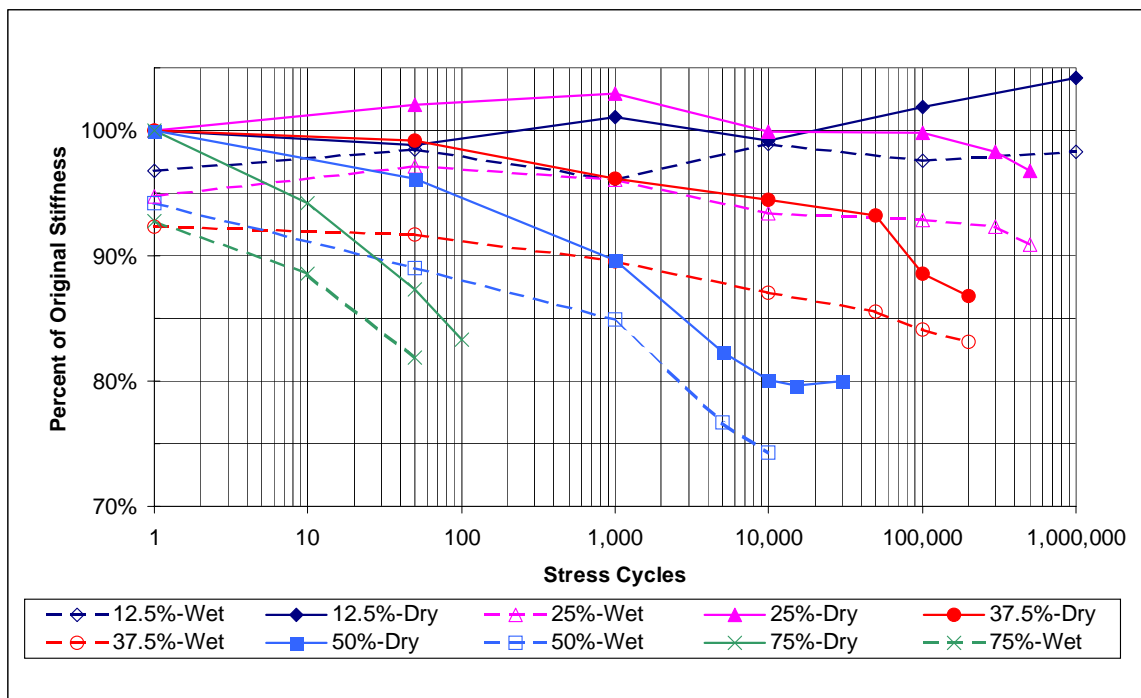


Figure 6-15: Flexural Stiffness Reduction Due to Fatigue of Wet and Dry J/24 Laminates

⁴ Only enough cycles at each stress level were tested so as to produce the data required for the full-size correlation. Additional testing to predict out to a 50-year life is on-going.

The results indicate some general trends. First is the influence of moisture on the outer skin. All the single-sided moisture exposure specimens had lower initial and final stiffness values than the comparable dry specimens. This was due to the reduced stiffness values on the moist side. The loss of stiffness however was not significantly different between the wet and dry specimens. This was likely due to the consistent failure mechanism, which was tensile failure on the inside skin. As this skin was always dry, the moisture's effect was to shift the neutral axis toward the outer skin, increasing the stress on the inner, tensile face.

Significant audio response was heard during the initial cycle of the 75% and 50% specimens, and to a small extent with the 37.5% specimens. Continued audio response was heard during each of the 75% specimens cycles all the way to failure. A small response was also heard with the 50% specimens during most cycles. These responses corresponded to a "whitening" of the laminate's tensile face, indicating microcracking of the resin and some fiber fracture. The progression to failure included an initial audio response combined with whitening under the cloth layer (the outer layer was cloth, the inside layers were mat), followed by whitening of the cloth layer. Failure tended to occur when the flexural stiffness dropped 20% from its initial value. In some cases (most notably the 50% dry specimens), the stiffness stabilized while crack size propagated.

Figure 6-16 shows the 50% specimens after 7500 cycles. (Most of the wet specimens failed near 5000 cycles and the dry specimens did not fail until after 25,000 cycles.) The "whitening" is clearly visible in the area of uniform bending moment. It was interesting to see that the initial visual clues occurred randomly in this area and did not appear to be influenced by edge effects. The initial visual clues were small, white spots of roughly 2 mm x 2 mm, which corresponded in size to one crimp site of the cloth weave. These appeared to occur between the cloth and mat layer. As this visual clue always occurred prior to the onset of rapid failure this could be used as a visual inspection indicator of fatigue onset. Also noticeable is the random location (within the constant moment section) of final failure.

Like the static tests, the fatigue failures were tensile face failures, but unlike the static tests the fatigue tests were low-energy release events. A typical failure was preceded by 50-100 cycles of increasing audio output (a tearing sound) combined with a tear forming in the cloth. In most cases the tear started at one edge and slowly progressed across the specimen. In roughly 25% of the cases the tear began near the middle and spread transversely in both directions.

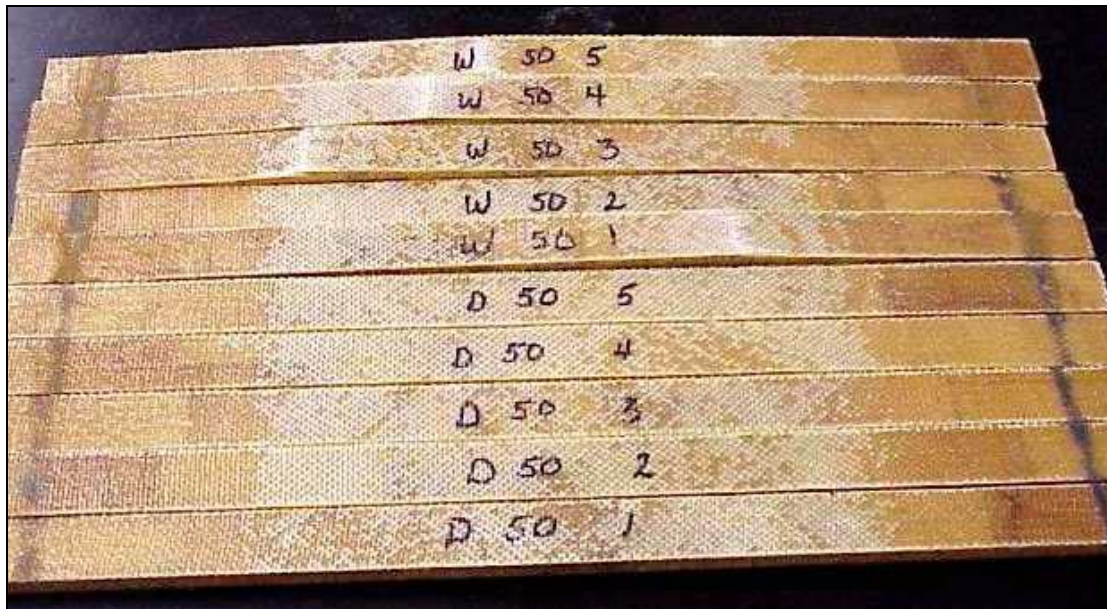


Figure 6-16: Fatigue Damage on 50% Specimens After 7500 Cycles

As expected, the specimens loaded to 75% of static strength failed after a very limited number of cycles. The first dry specimen failed during the second cycle and the last at 906 cycles. The average for the five specimens was 323 cycles, with a COV of 173%. This was substantially higher than for the wet specimens, which had an average failure at 43 cycles, with a COV of 62%. The likely reason for this is the effectively higher stresses on the tensile side due to the apparent shift of the neutral axis toward the wet skin.

In each of the specimens when an audio response was heard, the specimen acquired a “set” and did not return to its unloaded state. This was similar to a “yield” type metal characteristic, although the analogy is not accurate in that in metals the modulus does not change and with the fiberglass the stiffness dropped appreciably.

Low cycle fatigue clearly effected the 75% and 50% specimens. High cycle (for the number of cycles tested) fatigue clearly effected the 37.5% specimens and slightly effected the 25% specimens. The 12.5% specimens did not appear effected by fatigue. This indicated the “stiffness endurance limit” for these materials would require a fatigue factor of safety near 4, while as noted earlier, ABS requires 2.3 and the U. S. Navy, 2.5 - 4, depending on application. This implies a vessel built to either guide may experience fatigue failure if its service life includes a sufficient number of cycles.

A final note about the flexural fatigue coupon testing. The stiffness reduction of sandwich structures is highly dependent on the core thickness, as the core thickness drives the section modulus. Thicker cores would see smaller stiffness reductions before failure.

7.0 Panel Testing Program

The panel testing program's main goal was to compare FEA predictions based on coupon tests with actual panels. This had two intentions. First, it would give a good indication of the FEA's accuracy to predict full-size vessel responses and indicate whether linear or non-linear analysis would be required for sufficient accuracy. The secondary goal was to determine if FEA combined with coupon test results could be a viable substitute for the panel test methods discussed in Section 4.2. Four 24" x 24" panels were produced by TPI at the same time and with the same fabrication techniques as the flexural coupons.

Testing included pressure loading a panel that had moisture conditions representing a boat that is either "dry-sailed" or left in the water. Specifically this had the inner skin dry (80-100% relative humidity) and the outer skin either wet or dry. As with the flexural specimens the balsa edges were sealed with varnish to prevent moisture entering the core or inner skin and the panels were soaked for at least two weeks in 0.1" deep water (the outer skin thickness is 0.095"). The boundary conditions were simply-supported around the perimeter. To allow the specimen to overhang the edges, the restraining jig was made 23" square. The jig is similar to the HydroMat rig described in Section 4.2.

A normal pressure load was applied from 0 to 15 psi ⁵ and string pots measured the panel center point and frame deflections. A strain gauge (of the same type used in the coupon and on-the-water tests) also measured the center strain. Figure 7-1 shows the test jig fabrication drawing. The final jig differed from the drawing in two ways. First, steel channels were not available so larger (5 x 2) aluminum channels were substituted. Secondly, during welding the ends of the jig toed out slightly which caused the bolt holes to lose alignment with the base. As re-drilling the jig was not possible due to interference with the webs, an additional beam was placed over the jig to provide a clamping surface.

⁵ The maximum allowable bag pressure was 15 psi as measured at the tap.

The jig was clamped to a rigid steel base with a pressure bag placed between the base and the panel and the panel lying between the bag and the jig. Figure 7-2 shows the full test rig in the Naval Academy's ship structures lab with 15 psi pressure applied. Three string pot attachment points and the strain gauge wire can be seen. As only three pots were available, multiple runs were performed with one pot moved to different positions on the frame. This gave a clear picture of frame deflections, which could then be duplicated in the FEA.

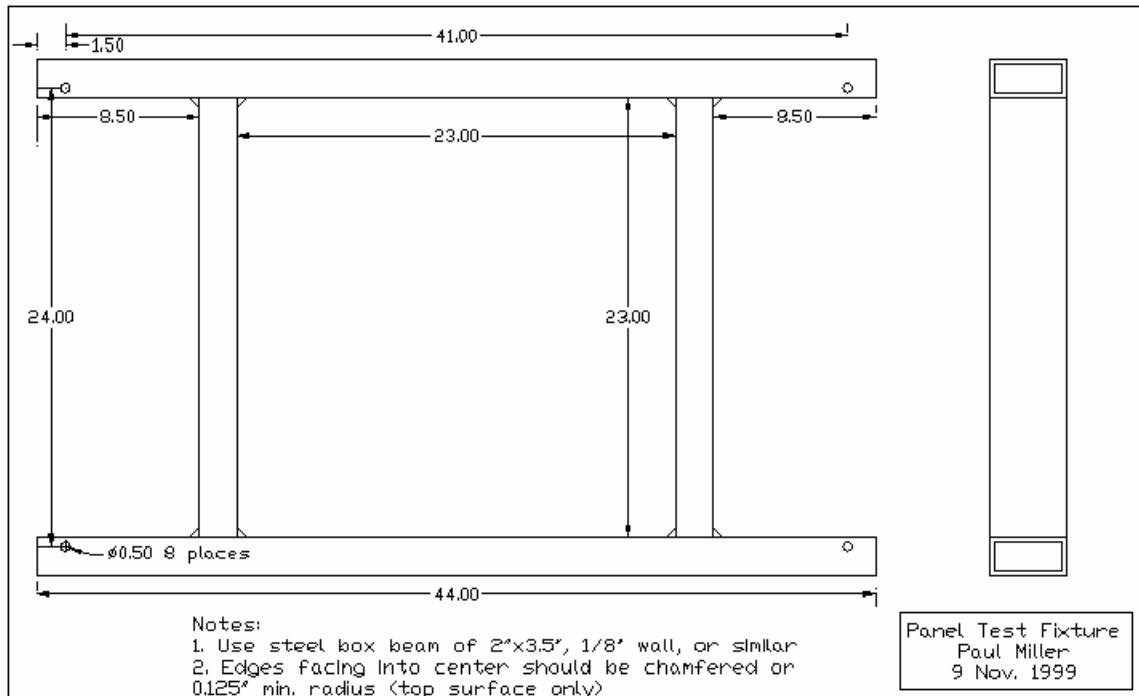


Figure 7-1: Panel Test Jig Drawing

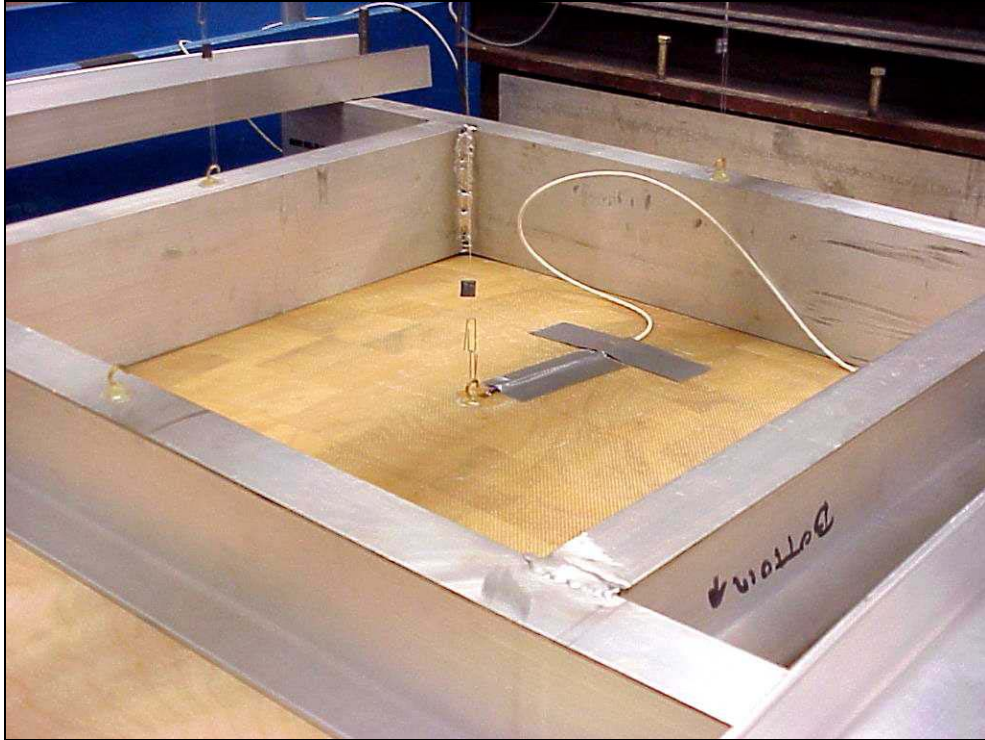


Figure 7-2: Panel Test Jig

Measurements were recorded of the panel center and jig deflections and the center strain versus the water pressure. The relative center displacements and strains for the panels versus the load are shown in Figure 7-3. These show that the dry panel had a slightly higher bending stiffness and that the deformations are nonlinear, with the stiffness increasing with load. This is typical of a structure responding to membrane in-plane stiffness increases, but was not seen in the flexural coupon test results (see Figure 6-12) due to the absence of constrained edge effects. The dry plot showed two jumps, which were likely caused by stiction release between the panel and jig. At the maximum pressure of 13.5 psi, localized damage was seen along the contact edges, but no damage was seen in the center or corners. This occurred as the maximum strain was about 0.5% and the material's failure strain is close to 1.0%.

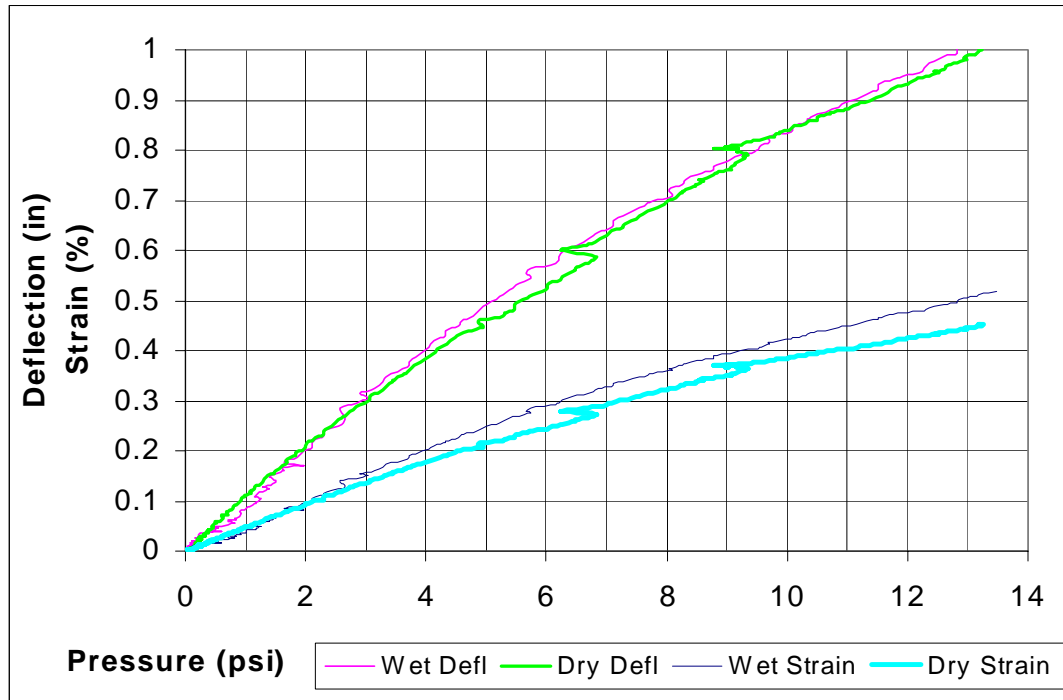


Figure 7-3: Load vs. Deflection and Strain for J/24 Panel Test

The small difference in stiffness between the wet and dry panels is not surprising given the small differences in tensile and compressive moduli found in the coupon tests. Also, as the thinner face (which was dry in both panels as it represented the inner hull skin) was farther from the panel's neutral axis, it exerted a proportionately larger influence on the results. A discussion of the membrane-stress action and a comparison to the FEA predictions is presented in Section 9.3.2.

8.0 Full-Scale Testing Program

The goal of the full-scale testing was to get actual data from vessels in service (one “high mileage” vessel and one “low mileage”) to compare against laboratory results. In this marine composites project the approach to identifying suitable test vessels followed these steps:

1. Identify appropriate laminate and construction practices representing common marine composites. This was presented in Section 3.1.
2. Identify vessels constructed of these materials.
3. Locate representative vessels in the San Francisco Bay Area and contact their builders for information on construction details.
4. Determine an order-of-magnitude fatigue study based on construction details and available boats known to be of “high mileage” and “low mileage”.
5. Study means of fatigue measurement on the potential vessels.
6. Select best candidate.

A number of vessel designs were identified and reviewed in steps 1-4. Many of these were ruled out due to a lack of cooperation by the builders in providing construction details, or a lack of documented quality control such that a valid comparison could be made between two vessels. By step 4 the list included: Boston Whaler 13 and 17, Catalina 27, J/24, J/30, Express 27 and 37, Laser, International Canoe, and Soling. The predominance of sailing vessels was mostly due to the better quality control documentation resulting from racing rule requirements.

Step 5 removed many vessels due to the need to keep the strain gauging data acquisition system dry and supplied with power. The final candidates were the J/24, Express 27 and Express 37. The selection of the J/24 was based on its greater availability through the support of OCSC, the great support from the builder, TPI, the reduced crew requirements, and its widespread use internationally.

8.1 Vessel Description

Over 6000 J/24's have been built, making them the second most popular sailing keelboat in the world. Designed by Rod Johnstone in the mid-70's, the boat is considered a one-design racer

with overnight accommodations for four. Although predominantly used for racing, sailing schools also use the boats for instruction and day charters. The boat is built throughout the world and marketed by J/Boats. The major US builder was TPI, Inc. of Warren, Rhode Island, who built 5,186 boats, with the last one in 1995 [126]. Production resumed at a different U. S. builder in late 1999. The construction and the sail plans are included in the appendix and more information is included in the global finite element model discussion in Section 9.4. Figure 8-1 shows a J/24 sailing on San Francisco Bay.



Figure 8-1: A J/24 (J6) Sailing on San Francisco Bay

After the type of vessel was identified the next steps were to a) find two vessels meeting the “high” and “low” mileage requirements and document their service lives, and b) develop the finite element models.

8.2 Vessel Service Lives

Through the assistance of various members of the J/24 class association in the San Francisco Bay Area two vessels meeting the criteria were located at the Berkeley Marina. The “high mileage” boat was named “J6” and the “low mileage” boat, “*Imagination*”. The two vessels

compared in the analysis have seen significantly different conditions during their lives. The procedure for each boat was similar:

- a) determine how many hours of sailing the vessel saw
- b) correlate those hours to weather data (wind and waves)
- c) determine the number of strain cycles and ranges seen

In both cases, the vessel owners, the J/24 Class Association and various weather-recording groups were contacted for information.

The need for hours spent sailing and the wind and wave data relate to the fatigue strain amplitude and cycles encountered. The strain ranges experienced by the boats were driven by two factors: rig tension and wave height. Rig tension itself includes two components: shroud tension and backstay tension. Shroud tension on the sailing school boats is set when the mast is stepped, and OCSC policies set the shroud tension at 400 pounds. Shroud tension has little impact on longitudinal bending and varies depending on whether the shroud is on the windward or leeward side (the leeward shroud goes slack as the vessel heels). Windward shroud tension begins with the preload and grows to a value based on the righting moment achieved by hull shape, ballast, and crew weight. The FEA global model showed negligible impact on strains through the full range of shroud tension.

The significantly larger impact on longitudinal deflections due to rig tension is backstay and forestay tension. In general, more backstay tension is applied when the sails are deemed too powerful. This occurs when sailing against the wind on breezy days. Although in racing situations the backstay is slackened when sailing downwind, this is not commonly done while cruising or in class. On the sailing school boats the maximum backstay and forestay tension was measured during the two boat tests.

Also driven by wind conditions is the amount of strain induced by wave impacts. During the summer months the waves are large enough that the entire bow can be immersed or exposed. This can induce significantly larger rig loads in addition to the slamming loads. To determine the

wind speeds in the boats' sailing area wind reading were taken from a weather station located at the Berkeley Marina on HS Lordships restaurant and correlated to National Weather Service data.

8.2.1 J6 Service Life

Early in the project the need was identified to find a vessel that had a large number of documented sailing hours resulting in a significant number of high stress cycles. As few privately owned sailing vessels see significant use, the search led to commercial sailing schools and rental operations. OCSC, a sailing school and club located at the Berkeley Marina proved to be an excellent source for test vessels as they closely document each vessel's use (for billing purposes) and are located in a spot known for consistently high winds and chop. A vessel was selected from the OCSC fleet based on the most number of documented sailing hours.

J6⁶ entered the OCSC fleet as a new vessel in December 1984 and began operations in January 1985. Her only trailering experience was from the dealer to OCSC. Detailed daily records of boat usage were available for January 1996 to May 1999 and were used to develop monthly totals for morning, afternoon and evening use. These were then used to correlate wind speeds and wave heights as the winds in Berkeley generally follow a consistent daily thermal cycle.

The same data was compared to overall figures from 1985 to 1998, which indicated the annual usage was relatively consistent from year to year. Table 8-1 shows the amount of usage per daily time period and month for 1998, and is typical of those from 1996-1999. "AM" hours are 9 AM to 1 PM and "PM" hours are 1-5. "Evening/Night" hours are after 5 PM. Typical usage included sailing lessons, charters by members and the occasional special event. Only those hours spent sailing outside the breakwater were included. Table 8-2 and Figure 8-1 show the month-to-month

⁶ Vessel ID TSP 43759M84D

usage of J6 from 1996 to 1999. The total predicted hours sailed since new is 11,300 with a COV of 12%.

1998 Month	Hours Used			total
	AM	PM	Eve/Night	
January	6	16	3	25
February	8	8		16
March	10	28		38
April	32	57	4	93
May	26	48	3	77
June	28	34	5	67
July	31	49	4	84
August	32	39	2	73
September	26	46	6	78
October	32	41		73
November	24	42	3	69
December	8	12		20
Totals	263	420	30	713

Table 8-1: 1998 Daily Sailing Hours for J6

Month	Total Hours Used				Average	COV
	1996	1997	1998	1999		
January	32	32	25	26	29	13%
February	53	77	16	53	50	51%
March	66	76	38	86	67	31%
April	89	68	93	55	76	23%
May	76	73	77	74	75	2%
June	64	78	67		70	11%
July	92	86	84		87	5%
August	85	100	73		86	16%
September	59	61	78		66	16%
October	84	76	73		78	7%
November	51	94	69		71	30%
December	26	18	20		21	20%
Totals	777	839	713	294	776	8%

Table 8-2: Month-to-Month Usage of J6 from 1996 to 1999.

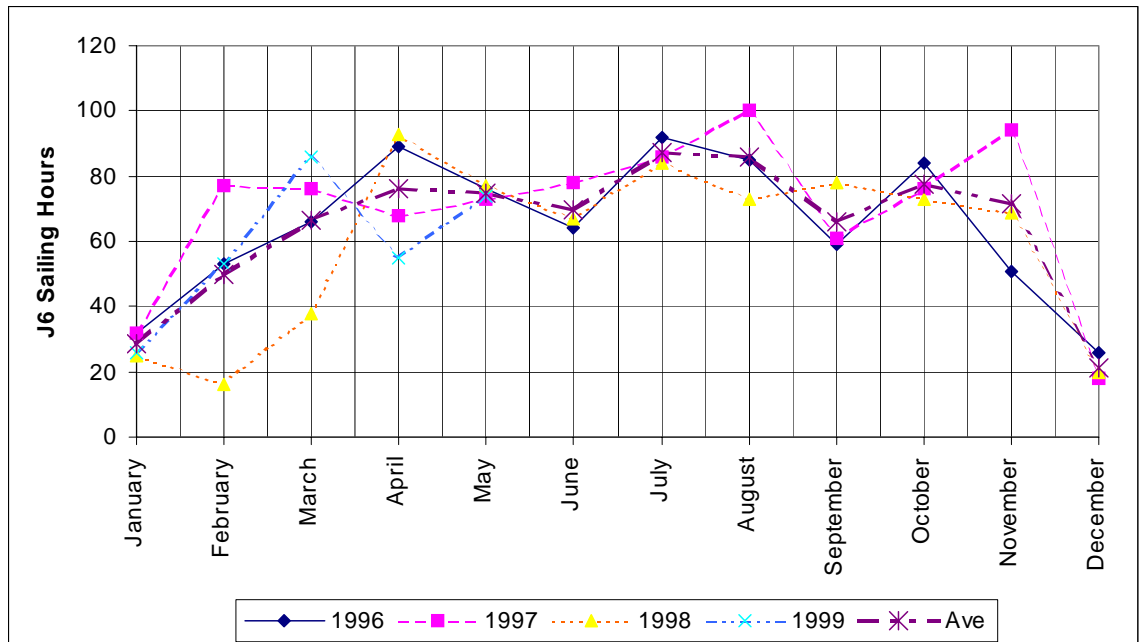


Figure 8-1: Month-to-month Usage of J6 from Jan. 1996 to June 1999.

Note the trends are consistent from month-to-month and year-to-year. The largest COV's occur during the winter, which is the rainy season. This time period also has the lowest average wind speeds (hence lower stress cycles), and lower usage. The windier summer months have COV's ranging from 2-16%. The particularly low usage in February and March 1998 can be attributed to the above-average rainfalls associated with El Niño. This is a weather pattern that repeats every 4-5 years, so including it in the averages is not unreasonable.

To determine the weather conditions encountered by J6 a two-step approach was developed:

- Use wind data for Berkeley on the days sailed from 1996-1999 to determine wave height and stress range
- Compare regional wind patterns from 1985-1999 to determine appropriateness of extrapolation.

8.2.2 Wind and Wave History for J6

The detailed wind data for Berkeley was provided by Call of the Wind, a privately owned company providing wind data for sailboarders around the country through their WindCall data

stations [127]. Two WindCall weather stations are located near J6's sailing location. One is the "Berkeley Marina" located 0.5 to 1 mile southeast of Berkeley Circle, on the southwestern edge of the Berkeley Marina. The other is "Point Isabel", located 1 mile northeast of Berkeley Circle. Readings with a portable wind gauge taken on board J6 during the on-the-water tests and checked against the WindCall data showed close correlation with both data sets.

Figure 8-2 is a typical plot of wind data (taken on July 16, 1999 during the on-the-water tests). The top row shows the wind direction, which was from the typical southwest direction on this day. The red line shows the gust peaks and the green line the lulls. The blue bars represent the mean wind speed.

The Berkeley station was established by WindCall in 1996 and records all wind values above 10 knots. Winds below ten knots generate waves that are small enough to have little influence on global bending (more about this later). Figure 8-3 shows the location of the anemometer (top left). Data was provided by WindCall in daily files that included time, lull wind speed, gust wind speed, and 15-minute average wind speed. As the boat records indicated J6 only rarely sailed after dark (<2%), the data was filtered to include only those wind readings taken between 9 AM and sunset.

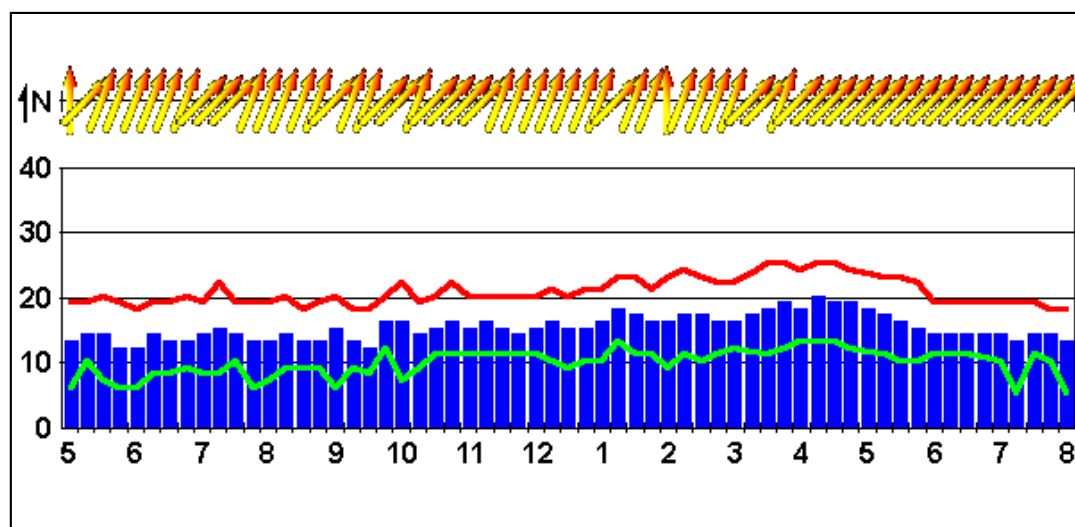


Figure 8-2: Typical Wind Readings (knots) from the Area of J6's Sailing; 16 July, 1999



Figure 8-3: Location of WindCall Anemometer at Berkeley (top left)

As the WindCall data began in 1996 and J6 had been sailing in Berkeley since 1984, a comparison was made of historical data at San Francisco Airport for winds recorded between 1984 and 1998[128]. This was done to see if the 1996-1998 data was representative of the entire period. Figure 8-4 shows a plot of the average monthly wind speeds for the period. This was developed from the average daily wind speeds which themselves were based on two-minute averages. A clear trend is the higher wind speeds during the summer months. Table 8-3 shows the correlation between the WindCall data period and the complete period of J6's career. Both the average wind speed and COV are close enough to conclude the shorter period is representative of the longer period.

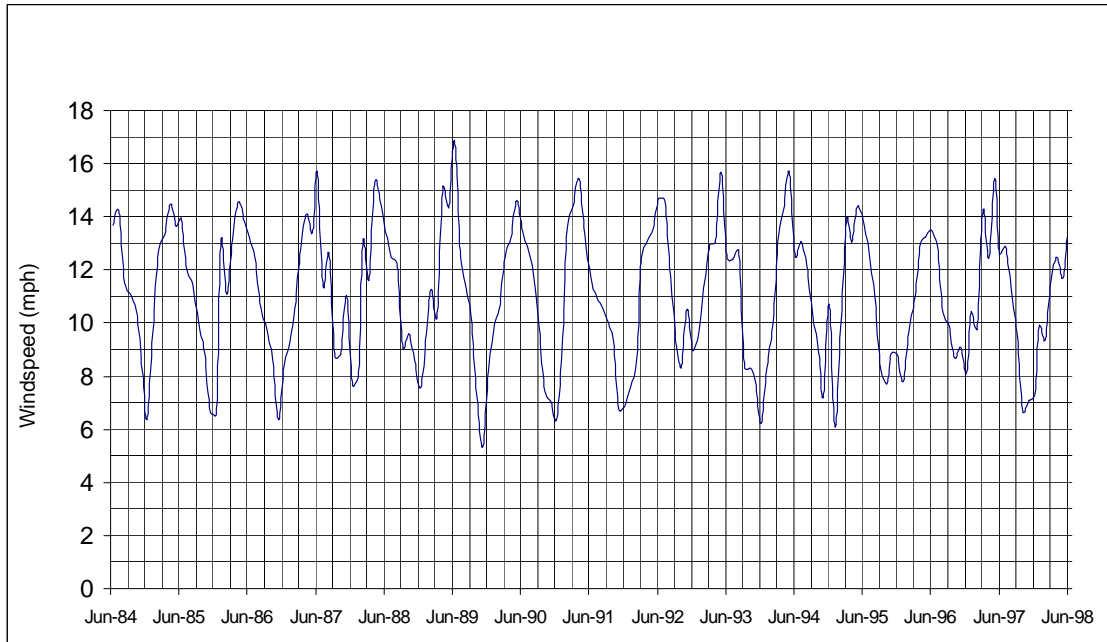


Figure 8-4: Average Monthly Wind Speed for San Francisco Airport

Average of July 84 to July 98	11.02
COV of July 84 to July 98	23%
Average of July 96 to July 98	10.84
COV of July 96 to July 98	22%

Table 8-3: Comparison of Wind Speed Data for 7/84-7/98 and 7/96-7/98

The Berkeley WindCall data was used as the input for the wave height predictions. The wave data would then be used for two purposes; determining the stress response operators from the finite element analysis and determining the number of wave encounters or stress cycles experienced by the vessel.

As noted earlier, the WindCall data was truncated at 10 knots. This was acceptable for this study as both a) small waves would be developed in lighter winds, and b) less longitudinal rigging loads would be applied as the need to flatten the sails would be less. These would both lead to low stress levels on the vessel's bottom plating.

Table 8-4 shows the monthly daylight wind speed probability density function for Berkeley as generated from the Berkeley Marina WindCall data. Although the table shows a relatively high

percentage of winds of less than 10 knots, these were typically in the morning and evening hours. Virtually every day from March through October saw winds of at least 10 knots and most afternoons between March and October saw winds of 15-20 knots.

Month	<10 knots	10 to 15	15-20	20-25	>25 knots
Jan	80%	12%	6%	1%	1%
Feb	73%	15%	6%	3%	1%
Mar	59%	27%	11%	3%	<1%
Apr	49%	30%	18%	3%	<1%
May	32%	32%	27%	8%	1%
Jun	34%	34%	24%	8%	<1%
Jul	29%	35%	32%	5%	<1%
Aug	35%	34%	28%	3%	<1%
Sep	40%	30%	27%	3%	<1%
Oct	61%	25%	12%	1%	<1%
Nov	79%	12%	6%	2%	1%
Dec	81%	10%	6%	2%	1%

Table 8-4: Monthly Average Wind Speeds for Daylight Hours at Berkeley

As discussed in Section 4.1.1, studies in the 1970's [87] showed the wave spectrum that best approximates that found in the central portion of San Francisco Bay is the JONSWOP spectrum. This spectrum was developed for the shallow North Sea where the fetch is limited but deep water waves can develop [129]. Although this spectrum does a good job for the deeper portion of the Bay (where the earlier study was located), the depth in the Berkeley Circle averages near 10 feet, which gives a typical wavelength to water depth ratio of 2.4. This implies the wave dynamics follow an "intermediate-wave pattern" [104].

Since the earlier study on San Francisco Bay, the US Army Corps of Engineers extended the JONSWOP spectrum for intermediate and shallow water effects [105]. As outlined in the *Shore Protection Manual*, the Corps' method uses an empirically-verified set of equations that "provide a transition between the revised deepwater forecasting equations and the shallow-water forecasting model." The equations developed for the significant wave height, H_s , wave period, T_s , and duration of time, t , that is needed to get fully-developed waves are:

$$\frac{gH_s}{U_A^2} = 0.283 \tanh \left[0.530 \left(\frac{gd}{U_A^2} \right)^{\frac{3}{4}} \right] \tanh \left\{ \frac{0.00565 \left(\frac{gF}{U_A^2} \right)^{\frac{1}{2}}}{\tanh \left[0.530 \left(\frac{gd}{U_A^2} \right)^{\frac{3}{4}} \right]} \right\}$$

$$\frac{gT_s}{U_A} = 7.54 \tanh \left[0.833 \left(\frac{gd}{U_A^2} \right)^{\frac{3}{8}} \right] \tanh \left\{ \frac{0.0379 \left(\frac{gF}{U_A^2} \right)^{\frac{1}{3}}}{\tanh \left[0.833 \left(\frac{gd}{U_A^2} \right)^{\frac{3}{8}} \right]} \right\}$$

$$\frac{gt}{U_A} = 537 \left(\frac{gT_s}{U_A} \right)^{\frac{7}{3}}$$

where $U_A = 0.589 \cdot U_s^{1.23}$, the wind stress factor

F = Fetch, ft

d = Depth, ft

g = Acceleration of gravity

U_s = Observed wind speed, mph

Table 8-5 and Figure 8-5 show the predicted wave characteristics for Berkeley Circle for winds ranging from 0 to 30 knots based on the Army's model. The assumptions were the water depth was 10 feet and the fetch was 42,000 feet (8 miles). The actual depth of the Berkeley Circle ranges from 7-12 feet depending on the tide. Figure 8-5 assumes that the waves have had time to become fully developed. Note that to become fully developed waves with 25-knot winds, the wind must have been blowing for over an hour. The maximum wind speed was set at 30 knots as this approximates the limit at which the sailing school restricts sailing.

Windspeed	Sig Wave Ht	Period	Wind Stress	Time to Develop
knots	ft	sec	mph	min
Us	Hs	Ts	Ua	t
0	0	0	0	-
5	0.5	1.5	5.1	-
10	0.94	2.1	11.9	110
15	1.41	2.5	19.6	90
20	1.81	2.81	27.9	75
25	2.21	3.1	36.7	65
30	2.51	3.3	45.9	55

Table 8-5: Wave Characteristics for Berkeley Circle

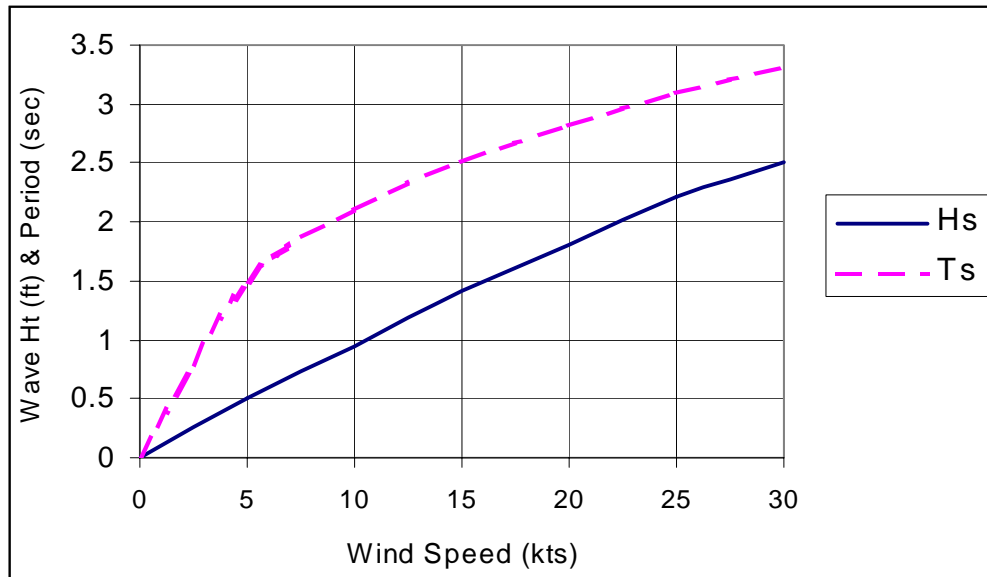


Figure 8-5: Significant Wave Height (Ht) and Period (Ts) for Berkeley Circle

Note that in the typical summer afternoon breeze of 10-25 knots the wave period ranges from 2 to 3.2 seconds and the significant wave height ranges from 1 to 2.25 feet. With a steepness ratio ranging from 1:10 to 1:20 for intermediate waves, this gives wavelengths of 10 to 45 feet. As the J/24 has a waterline length of 22 feet and a freeboard of 2.5 feet forward, the vessel will often experience waves creating the maximum longitudinal bending moment.

Figure 8-6 shows the location of Berkeley relative to the Golden Gate (where Highway 101 crosses the Bay). Berkeley Circle, where the boats sail, is located in the Bay just west of Berkeley (north is at the top of the map). The cause of the typical southwesterly wind on the circle is clear as the wind blows through the Gate and over Berkeley in response to a thermal low

pressure that develops as interior valleys warm during the day [106]. The fetch was determined as the distance from the Gate to the middle of the Circle. This could lead to some uncertainty in the wave characteristics prediction as the central Bay's depth is greater than 80 feet in spots, leading to wave heights and periods corresponding to deep-water waves. Counteracting this however is the fact that the Berkeley shoal starts roughly 1 mile to the west of the sailing area. This would tend to drive the wave characteristics back to an intermediate type.

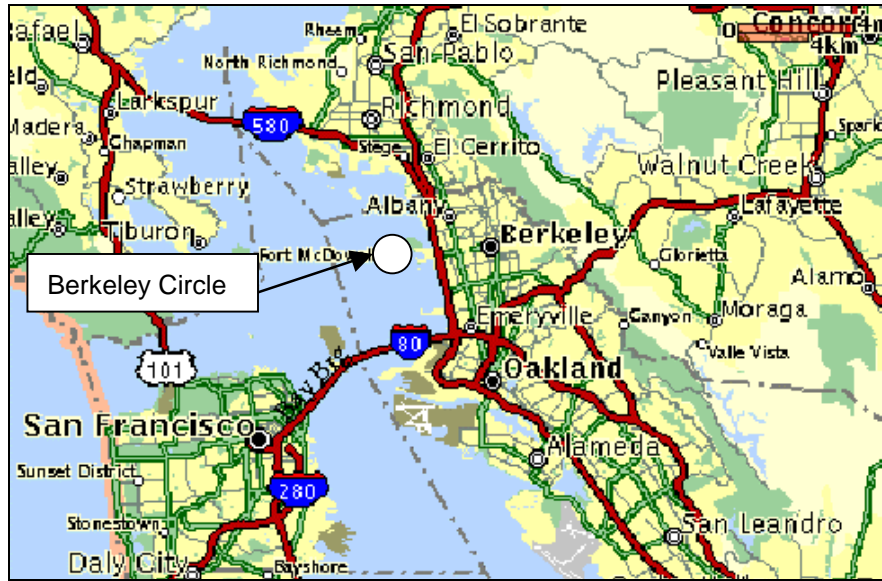


Figure 8-6: Location of Berkeley Circle in San Francisco Bay

Recalling from Section 4.1.3 that the total expected fatigue damage can be found from

$$E[D] = T \cdot f \int_0^{\infty} \frac{p(s_i) ds}{N(s_i)}$$

Where T is the time duration and f is the linear stationary encounter frequency with the waves (not to be confused with ω , the circular wave frequency). The portion $T \cdot f$ is the number of wave encounters experienced by the vessel. For a vessel with multiple courses and speeds the total number of wave encounters is the summation from each course and speed combination. The linear wave encounter frequency, f_e , is [130]

$$f_e = f + \frac{U \cos \phi}{U_w T_s}$$

$$\text{where, } f = \frac{\omega}{2\pi} \text{ or } \frac{1}{T_s}$$

U = boat speed

U_w = wave speed

φ = heading angle relative to upwind

T_s = significant wave period (see Figure 8-5)

Or, in terms of functional components,

$$T \cdot f = T(\phi, m, U_{ws}) \cdot f_e(U, \phi, U_w, T_s)$$

$$T \cdot f = p(\phi) \cdot p(m) \cdot p(U_{ws}) \cdot \left[f(U_{ws}) + \frac{U(\phi, U_{ws}) \cdot \cos(\phi)}{U_w(U_{ws}) \cdot T_s(U_{ws})} \right]$$

T is a probability density function combining the amount of time spent at each wave angle, the amount of usage per month, and the wind speed distribution per month. As the vessel is sail powered, the terms in the linear wave encounter frequency equation can all be related to wind speed and course if the depth is assumed constant.

The wave speed is dependent on the wave length and water depth. Close approximations for deepwater and shallow-water waves are [104]:

$$U_{w-deep} = \sqrt{\frac{gl}{2\pi}}$$

$$U_{w-shallow} = \sqrt{gh}$$

where,

g = acceleration due to gravity

l = wave length

h = water depth

Note that although the Berkeley Circle is shallow, the limited fetch does not allow for long wavelengths to develop. This means the deep water wave speed equation is a reasonable approximation of the actual waves.

To complete the determination of the number of wave cycles encountered by the boat, the boat's speed and angle relative to the waves must be determined. The speed of a sailing vessel is dependent on numerous variables, including the apparent wind angle, wind speed, sail selection and sail trim. A velocity prediction program (VPP), which optimally solves the force and moment equilibrium equations, is used to predict these values [109, 131]. Figure 8-7 shows a VPP-generated polar diagram for the J/24 showing the predicted boat speed vs. wind speed and true wind angle [132].

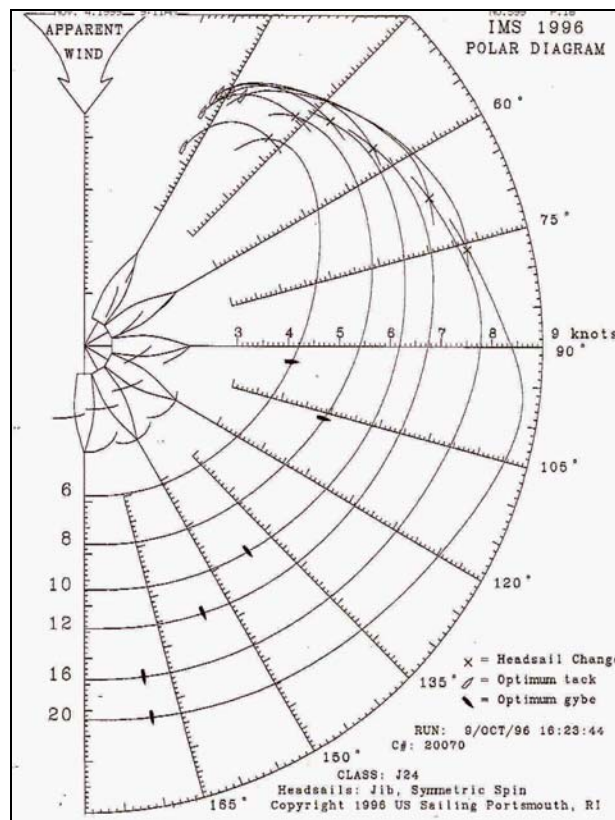


Figure 8-7: J/24 Polar Speed Diagram

The VPP assumes the boat will be sailed at maximum potential. This would include proper trim, full crew weight in “hiking” positions, and the largest sails appropriate to the conditions. For the sailing school boats, the actual speeds will be less as the students are not trimming the sails to

perfection, the crew is not hiking out, and sail selection is based on skill level rather than speed. In particular, special purpose sails such as spinnakers are rarely used. This reduces the speeds in certain conditions significantly.

To check the actual speeds against the VPP, GPS measurements were taken during sailing lessons in June and July 1999. These showed that upwind speeds averaged 90% of VPP predictions and downwind speeds averaged 65% of the predictions. The low downwind values were due to the absence of a spinnaker.

The results from the polar diagram and sailing observations were combined with a probability density function of the wind speeds and true wind directions for boats on charter or lessons from OCSC (Table 8-6). The distributions were based on times taken by during lessons during the summer of 1999:

Beating (true wind angle = 45 degrees)	60%
Reaching (true wind angle = 90 degrees)	25%
Broad Reaching (true wind angle = 135 degrees)	15%

Table 8-6: Probability Density Function for Sailing School Vessel Course

A total wave encounter prediction for J6 was determined by solving the expanded $T \cdot f$ equation and taking the assumption that the wind and wave directions coincided. The resulting summation over the period 1985-1999 gave a total lifetime estimate of significant wave encounters of 10.2 million for J6. Wave encounter frequencies ranged from 0 Hz (for broad reaching with the waves) to a maximum of 0.71 Hz when beating into the waves at an apparent angle of 45 degrees.

The portion of the accumulated damage equation that includes the stress density function were based on significant wave height and are described in Section 9.4.

8.2.3 “Imagination” Service Life

A search of boatyards, dealers, J/24 sailors and the J/24 Class association yielded a list of a dozen boats thought to have “low mileage”. A December 1981 built-boat named “*Imagination*”⁷ was located and selected as:

- She was available in Berkeley, having joined the OCSC fleet one week earlier
- During a large part of her life she was located on lakes or in climates that reduced the number of sailing hours per year, or was inactive
- She was clearly in excellent condition, indicating a lack of serious wear (including having her original mast)
- No indications existed of any damage
- She had been in the water long enough to reach moisture equilibrium
- Her construction details were nearly identical to J6’s

Correspondence with her owner indicated about 20 hours use annually from 1993-1999 [133].

Reviews of the J/24 Class Association data did not reveal her sail number in any major championship prior to that, so it is unlikely she was campaigned hard, or trailered a significant amount. No other records of her were available, so the assumption was made that she averaged 50 hours per year from 1982 to 1993 and sailed in predominantly light air venues. This corresponds to market research performed by J/Boats of their typical customer[134]. The total hours “*Imagination*” has spent sailing is estimated at 740, as compared to 11,300 for J6.

Using a similar approach to calculating wave encounters as was used for J6, but with a reduced wind range to account for her known and estimated history, the total number of wave encounters for “*Imagination*” was estimated as 600,000 at the time of testing, or roughly 6% of J6’s.

⁷ Vessel ID TSP42560M81E

8.3 On-the-Water Tests

A major component in correlating the coupon and panel tests to full-size vessels was to perform dockside static bending tests and underway dynamic tests. This was accomplished during the summer of 1999 on the Berkeley Circle. The two boats were strain gauged on the hull and rigs and checked using static load and deflection measuring devices. Underway readings were recorded on a laptop. The following sections describe the process in detail.

8.3.1 Calibration of Loos Rig Load Gauge

Rigging loads on the vessels were measured during the sailing by strain gauges mounted to the rigging chainplates. To calibrate the strains to loads and to set the preloads, non-recording "Professional" load gauges manufactured by Loos were used. As some uncertainty existed in the Loos rig gauge calibration charts accuracy, a series of tests on an Instron machine compared the stiffness and load of the standard 1x19 and Dyform rigging wires to the gauge readings. The tests consisted of six wire strops. The 1x19 wire sizes were 1/8", 5/32" and 3/16". The Dyform sizes were 3mm, 4mm and 5mm. The 26" wire strops were tensioned in an Instron machine at the Naval Academy and the gauge reading noted versus the indicated load cell value. Figure 8-8 shows the test set-up.



Figure 8-8: Test set-up used to correlate Loos Gauge vs. 1x19 and Dyform wire.

Figure 8-9 shows the resulting correlation plots. The values for the 1x19 wire corresponded almost exactly with the calibration table supplied by Loos, but the Dyform was 12-26% stiffer. Figure 8-10 shows a typical load–extension plot. The non-linear modulus is due to the twisted wire strand construction. Table 8-7 compares the measured stiffness values of the 1x19 and equivalent Dyform. These values were derived from the tangent modulus in the range of vessel loading. The “Area Modulus” is the modulus of elasticity using the nominal area based on the wire diameter when assuming a rod construction, rather than the actual area.

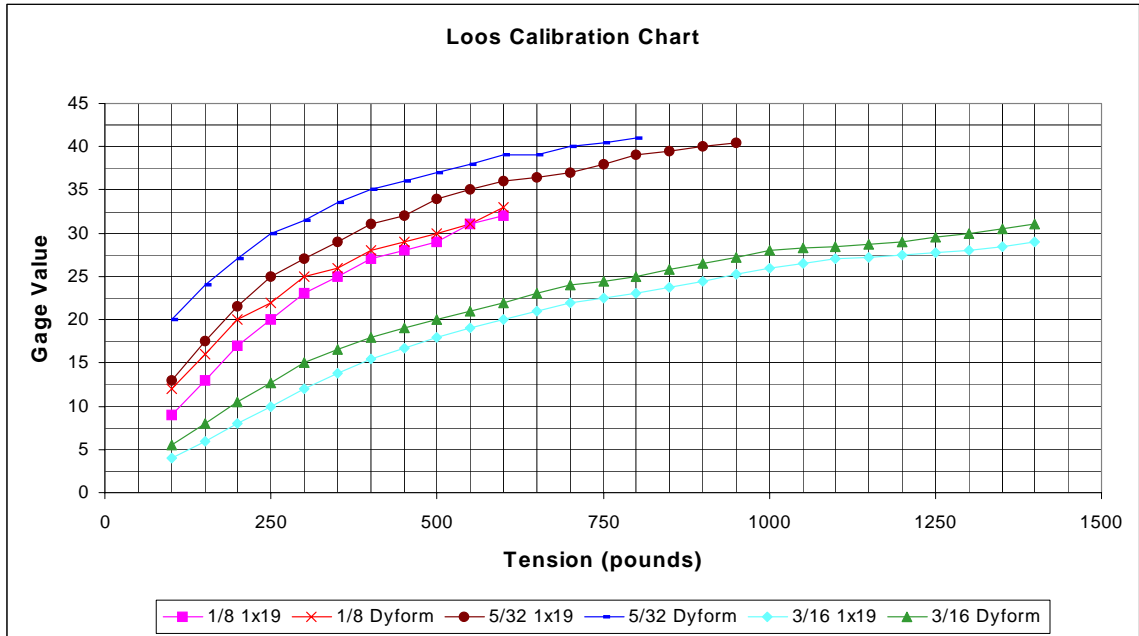


Figure 8-9: Correlation Plots of Loos Professional Gauge for 1x19 and Dyform Stainless Steel Wire.

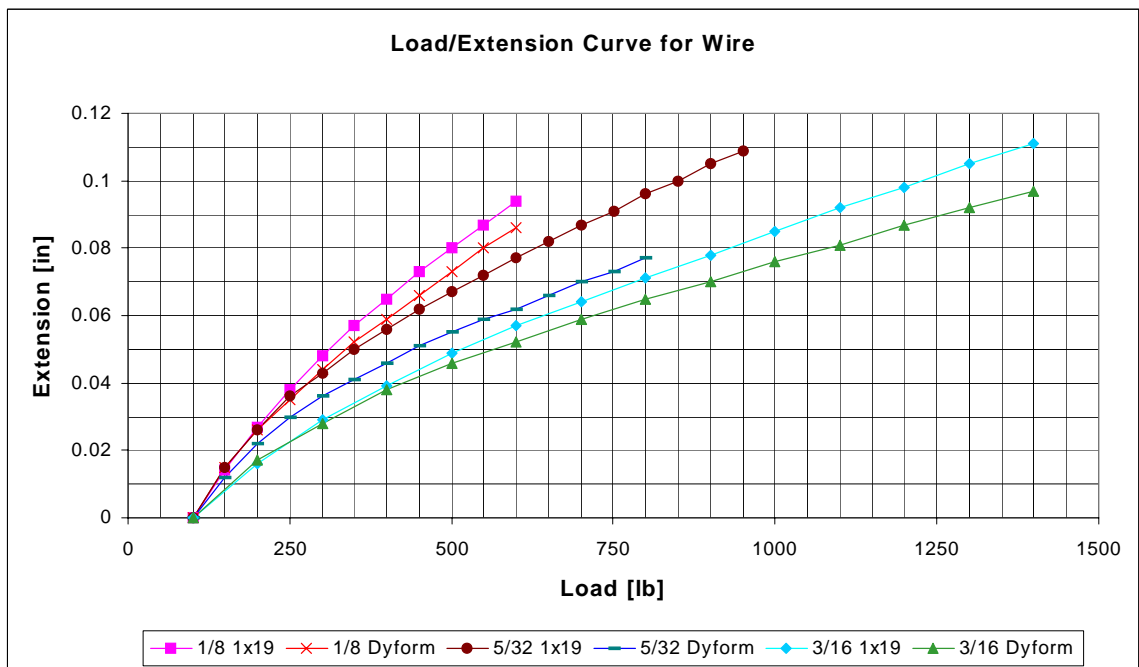


Figure 8-10: Load-Extension Plot of 1x19 and Dyform Wire

Wire Dia.	1/8"		5/32"		3/16"	
Construction	1x19	Dyform	1x19	Dyform	1x19	Dyform
Area Modulus	1.29E+07	1.44E+07	1.34E+07	1.69E+07	1.29E+07	1.53E+07
% diff		12%		26%		19%

Table 8-7: Stiffness of 1x19 and Dyform Wire

8.3.2 Boat Instrumentation

Instrumentation also included six strain gauges and one accelerometer. Table 8-8 shows the locations of the gauges and accelerometer. The gauges mounted on the inside and the outside of the hull were located a) on centerline, 25" aft of the bow bulkhead, and b) 6.5" off centerline to starboard, 25" aft of the bow bulkhead. The hull-mounted strain gauges were oriented longitudinally, corresponding to the x-axis in the FEA models.

Instrument Locations for Boat Tests	
<i>Instrument</i>	<i>Location</i>
Strain Gage #1	Portside shroud chainplate
Strain Gage #2	Forestay chainplate
Strain Gage #3	Inside hull on centerline
Strain Gage #4	Inside hull off centerline
Strain Gage #5	Outside hull on centerline
Strain Gage #6	Outside hull off centerline
Accelerometer	Bulkhead aft of strain gages

Table 8-8: Instrument Locations for Boat Tests

The gauges were GFLA-3-70, 3 mm., 120-ohm single-axis models manufactured by Tokyo Sokki Kenkyujo Co., Ltd. Figure 8-11 shows the wires leading from the outside gauges through the through-hull fitting for the galley sink.

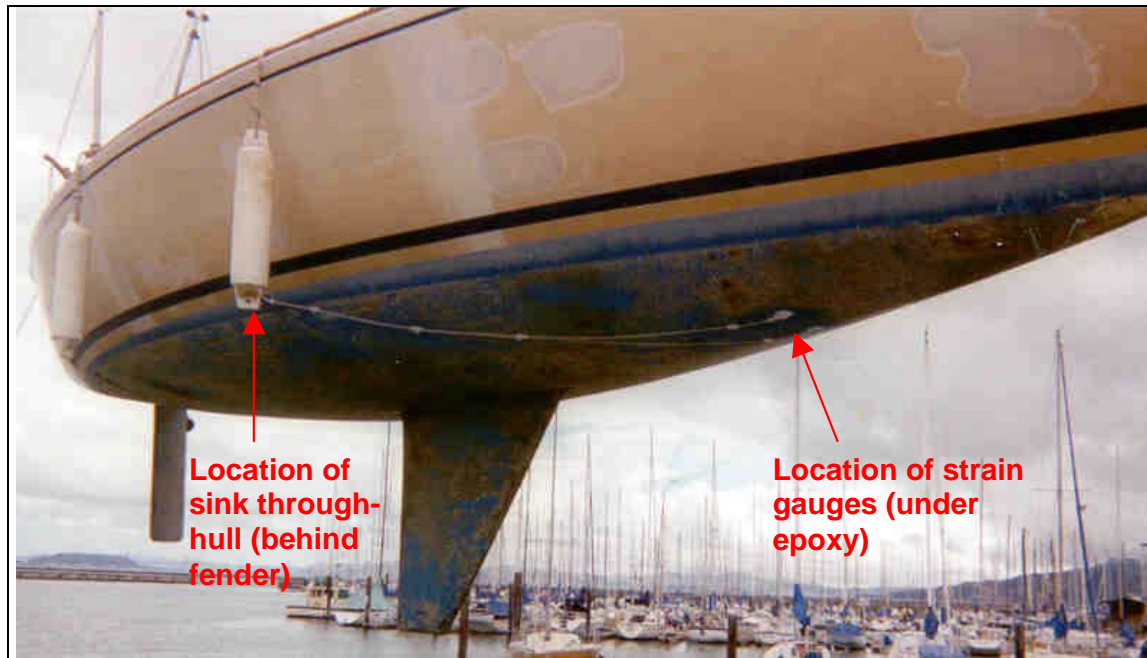


Figure 8-11: Location of Below Waterline Strain Gauges

Both the gauges and the accelerometer had the data recorded through an IOTech Personal Daq connected to a laptop through the computer's USB port. This innovative product significantly simplified and reduced the size of the data acquisition system. A faulty board in the new Daq #56 however, caused significant delays. IOTech provided a demo #55 unit combined with an expansion module that allowed for test completion on the last day available for testing. Figure 8-12 shows the interior of the J/24 with Gary Gibson, the Naval Academy's Lab Technician, and parts of the data acquisition system. All components were waterproofed to avoid damage and all power was provided by the vessel's "group 24" 12-volt DC battery. Unfortunately, the linear accelerometer gave sporadic readings and required manual adjustment to compensate for the angle of heel during sailing.



Figure 8-12: Interior of J/24 with Gary Gibson and Data Acquisition System

8.3.3 Dockside Full-Scale Tests

To provide a further verification of the global model and a baseline for the sailing tests, dockside bending tests on the boats were completed. The dockside test included two parts; an on-the-water test performed at dockside that measured the global hull change due to imposed rig loads, and correlation of those results to the global FEA models (see Section 9.4.5 for results). The steps included in the dockside tests were:

1. Note trim of vessel by measuring distance of knuckles at bow and stern out of the water.
2. Release tension in forestay, backstay, and upper and lower shrouds on both sides.
3. Stretch a lightweight twine between the bow and stern pulpits such that it passed close alongside the mast. Tension the string until no discernible sag was noted. Mark the position of the string along the mast.
4. Tension backstay to maximum reading and measure tension in all shrouds and stays. Measurement was made using the Loos & Co, Inc. Professional Model Tension Gauges PT-1 and PT-2. See Section 8.3.1 for calibration information.
5. Retension string and mark on mast.
6. Measure distance between marks.

7. Release tension in the backstay and compare mark to original mark.
8. Repeat.
9. Retension rig to OCSC policy.

While the shrouds were slack the instrumentation was turned on to zero the strain gauge readings. When the shrouds were tensioned and measured with the Loos gauge the instrumentation noted the strain in the chainplates due to static rig tension. This provided a baseline correlation between chainplate strain and rig tension.

8.3.4 Underway Full-Scale Tests

Underway testing included sailing the vessels upwind (closehauled) and downwind (broad reaching) in San Francisco Bay on both tacks and recording the data. A course that took the boats from Buoy F (leeward) to Buoy G (windward) in the Berkeley Circle was chosen. This placed the testing directly upwind of the Point Isabel WindCall station and at the northern edge of the Berkeley Circle. The same helmsman, sail trimmers and crew were used for both boats, minimizing the variation in sailing techniques. On each leg the crew positioned themselves in the same location to minimize differences in righting moment. Figure 8-13 shows *Imagination* during testing on July 20. The strain gauge wires can be seen underneath the feet of the forward crew. Berkeley can be seen on the left.

Testing was accomplished over two days. On July 16, 1999 “J6” was tested in 15-18 knots (2-foot significant wave height) with a reduced number of strain gauge channels (the expansion module had not yet arrived). Figure 8-2 showed the wind record for July 16. On July 20 both “J6” and “Imagination” were tested in 10-12 knots (1-foot significant wave height).



Figure 8-13: *Imagination* During Testing on San Francisco Bay

After the first boat recorded about 20 minutes of data, the acquisition system, crew and sails were moved to the other boat and testing repeated. This ensured the testing was completed in as near identical conditions as possible. The first data set was taken between 1 and 2 PM. The second was taken between 3:30 and 4:30. Figure 8-14 shows the Pt. Isabel WindCall plot for July 20 [127]. The plot shows similar average winds during the two test periods although the gust peaks were higher at the end of the first period. The higher average wind speed between the test periods may have caused an increase in wave height. Using a hand-held wind gauge the sailors noted similar wind speeds and directions for the two tests but thought there was possibly a slightly higher significant wave height. Photos of the testing however, did not indicate a change in wave height.

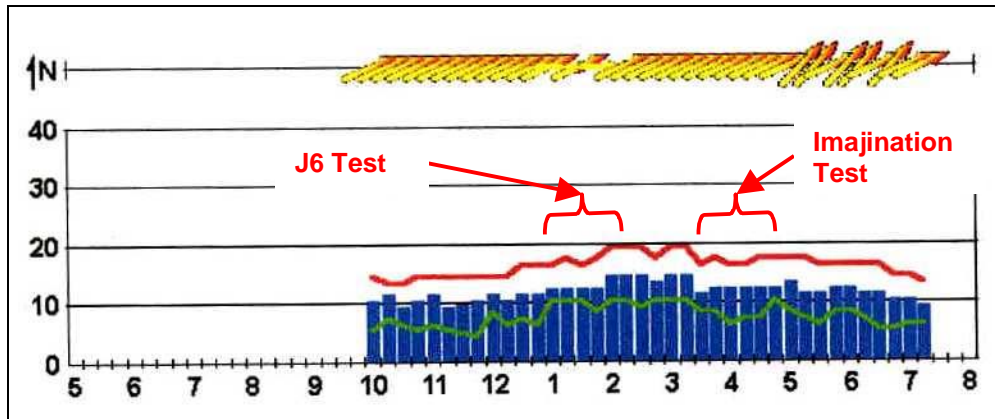


Figure 8-14: Wind Recording at Berkeley, July 20, 1999

Note that this figure shows the WindCall data truncation when the average wind speed dropped below 10 knots. At the conclusion of the second test set the wind was noted to begin getting shifty and lose its consistent velocity. This was reflected in the WindCall data by the change in wind direction arrows at the top.

Data was recorded to the laptop as voltage differences. Figures 8-15 and 8-16 show a one minute portion of the data recording. Figure 8-15 shows the accelerometer data. The values reflect the variation of “G” forces experienced by the strain gauges. This data was used to predict the slamming pressures. Figure 8-16 shows the strain on the inside hull laminate (on and off centerline). The peak strain was 0.136%. In both plots the peak period closely corresponds to the predicted wave encounter period.

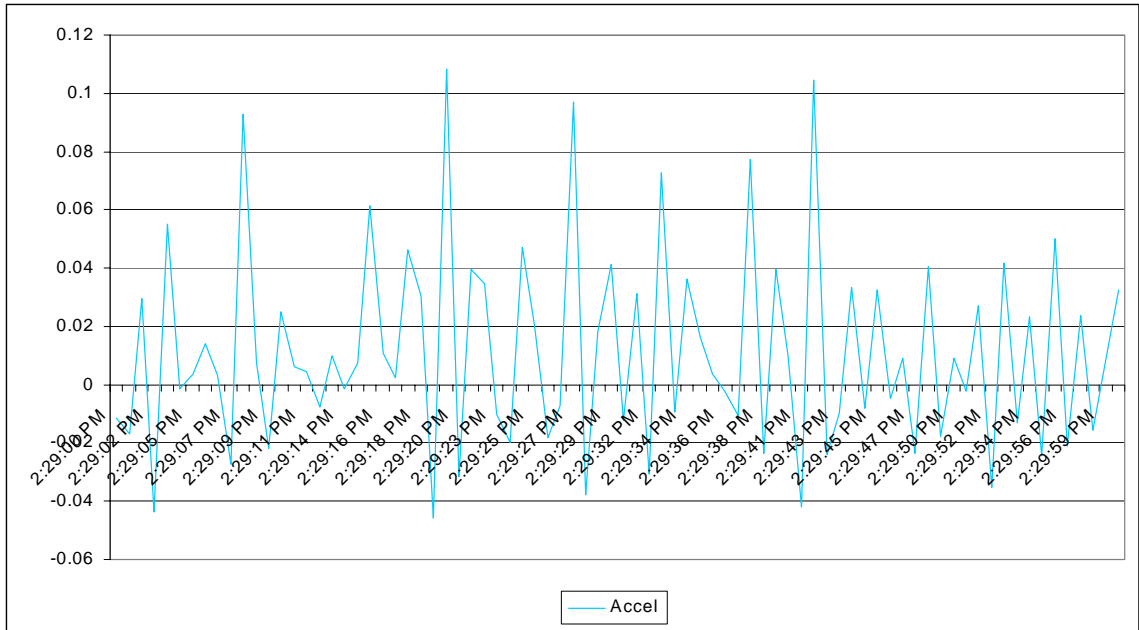


Figure 8-15: Accelerometer Data from Underway Testing

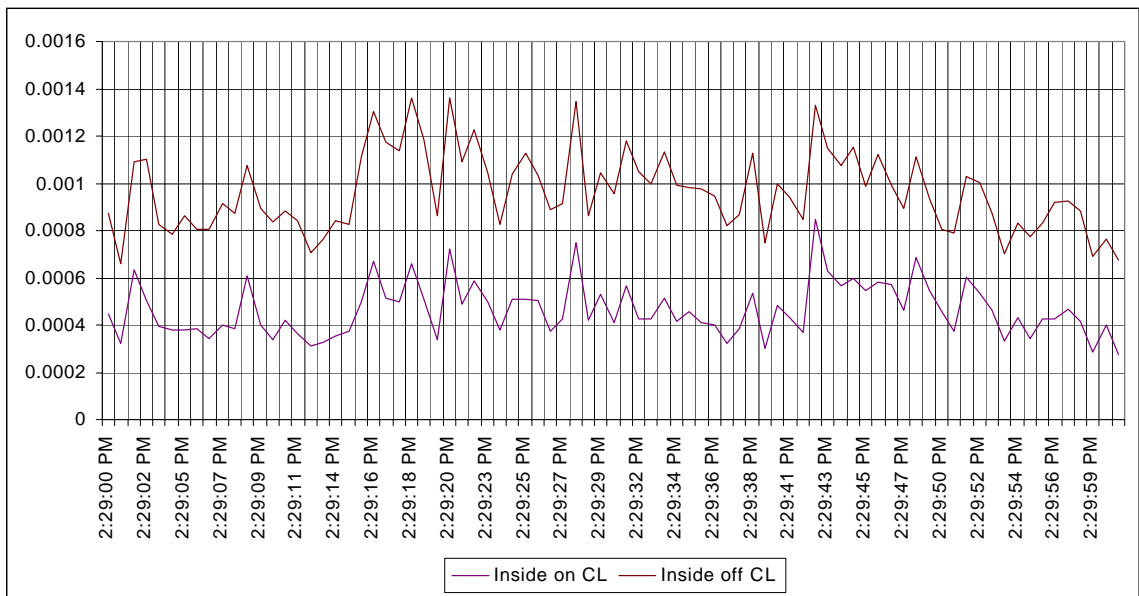


Figure 8-16: Inside Hull Laminate Strain Gauge Data from Underway Testing

9.0 Finite Element Analysis

Finite element analysis (FEA) has rapidly grown in its use as a design tool for marine applications where structural complexity and a requirement for accuracy precludes the efficient use of closed-form solutions. The goal of using FEA in this project was to validate its use in predicting strains related to vessel loading therefore allowing accurate correlation between coupon tests and actual vessel performance. This confidence would then allow for FEA strain prediction to be used in fatigue analysis of composite vessels.

The basic concept of FEA is that a global structure may be represented by a large assembly of small, interconnected individual components. Each of these elements has equations and values describing its stiffness. These elements can be related to each other by a combined stiffness matrix that can be solved for deflections by using standard matrix methods.

Element stiffness equations can be either linear or nonlinear and solutions can be found for structural, vibration, and heat transfer problems. Anisotropic, orthotropic and isotropic element formulations are all possible. A full description of the method is beyond the scope of this paper, so only those aspects related to the selection of certain FEA options are discussed here. Further treatment of the topic can be found in the references [58, 110, 135].

Due to the large number of degrees of freedom resulting from the large number of elements required to accurately model a ship, FEA of composite vessels was limited to mainframe and workstation-type computers until the mid-1990's. Now with more capable desktop computers, numerous analysis possibilities are within the reach of the average designer.

The greater potential accuracy of FEA over other design methods can drastically reduce the level of uncertainty when used properly. Designers must always remember the limitations of FEA however and avoid problems such as those of Sleipner A [136]. For example, composite vessel global FEA does not accurately model joints and compression buckling, and the designer must analyze these separately or include adequate factors of safety. The commonly used plane stress

elements also are limited to in-plane stress results, ignoring dominant failure modes in core materials. In all cases it must be remembered that FEA assumes a material continuity in both geometry and material properties. “Low-tech” composite materials however, have sufficient manufacturing variances that this assumption is often suspect. Property variation of up to 10% is common in many low-tech laminates [4, 15, 54, 137]. Although FEA is often used in the analysis of composite vessels, the extension to composite vessel fatigue analysis is unpublished and unknown.

Due to the complexity of the structural system, FEA was used extensively in this project to correlate and predict strains. This included coupon, panel and full-scale vessel analysis. Although the primary FEA code was an off-the-shelf code named COSMOS/M, the code was verified using standard element robustness and accuracy checks [110]. As noted in Section 3.2.2, in addition to the Tsai-Wu criteria included in COSMOS/M, post-processing using the Hashin failure criteria and the fatigue analysis was performed using spreadsheets. More discussion of the analytical methods used in the complex FEA models is described in Section 9.4.

The selection of the COSMOS/M software was due to software flexibility, availability at no cost, and the author’s familiarity with the code. The software was limited to three element types for composite analysis: linear plane stress, nonlinear plane stress and solid. All use CLT as the basis for their element stiffness calculation and the determination of directional stresses and strains. The plane stress elements are based on Mindlin shear deformation theory. The difference between the two plane stress elements is that the nonlinear element allows for nonlinear in-plane shear deformations. The solid element allows for linear out-of-plane shear deformations. The analysis itself could be either linear or nonlinear, with the nonlinear effects of large deformation and modulus included.

Other finite element codes have more options for composite analysis, however in the period from 1995-1999 no other PC-based code had more features, and the project resources did not allow for more sophisticated platforms or code.

9.1 Tensile and Compressive Coupon Correlation

The material properties derived from the coupon tests described in Section 6 were used to provide inputs to the FEA. Table 9-1 shows the final values used. Plywood and aluminum values were taken from standard references [34, 138]. As the laminates were comprised of different fiber formats, each material property set was adjusted by micromechanics using their base properties, the estimated fiber volume and relative laminate thickness. These were checked using CLT-based symbolic spreadsheets and FEA models of the various coupons and adjusted until differences of less than 1% were achieved.

Material	Gelcoat	1.5oz Mat	2,415	Balsa	10oz Boat	24oz Woven	Plywood	Aluminum	Paint
			Fabmat	Core	Cloth	Roving			
FEA MPROP#	1	2	3	4	5	6	7	8	9
Ex, Ey [psi]	490,000	920,000	1,400,000	25,000	2,450,000	2,450,000	945,000	10,000,000	100,000
Ez [psi]	490,000	490,000	490,000	370,000	490,000	490,000	47,000	10,000,000	100,000
ν_{xy}	0.300	0.361	0.108	0.300	0.067	0.070	0.050	0.330	0.300
Gxy [psi]	245,000	437,500	700,000	10,000	700,000	700,000	400,000	3,800,000	50,000
Gxz, Gyz [psi]	245,000	437,500	700,000	18,000	700,000	700,000	400,000	3,800,000	50,000
Xt, Yt [psi]	11,000	9,427	30,300	1,320	49,000	45,000	6,000	35,000	10,000
Xc, Yc [psi]	18,000	21,238	24,000	1,187	43,000	40,000	6,000	35,000	5,000
XYt [psi]	6,000	4,928	14,000	315	14,000	14,000	250	15,000	2,000
Ply thickness [in]	0.012	0.047	0.073	0.365	0.013	0.038	0.500		0.050
Density [lb/in ³]	0.0400	0.0570	0.0590	0.0048	0.0610	0.0610	0.0185	0.0966	0.0400
Density [mass]	1.04E-04	1.48E-04	1.53E-04	1.24E-05	1.58E-04	1.58E-04	4.79E-05	2.50E-04	1.04E-04
Failure Strain	2.2%	1.0%	2.2%	5.3%	2.0%	1.8%	0.6%	0.4%	10.0%

Table 9-1: Final Material Properties for J/24 FEA

The lamina density was based on micromechanics and published values and was checked against the 24" square panels. The total laminate areal weight was 1.60 lb/ft².

As a second check, comparisons were made between the wet and dry tensile and cored (dry only) compressive specimens and a "rule of mixtures" micromechanics method simulating the laminate used in the finite element analysis. Table 9-2 shows the hull laminate and resulting test values and predictions. The finite element models were revised to use the as-tested wet properties below the waterline.

Hull Laminate			Rule of Mixtures Stiffness		
Material	Thickness		Modulus	E*t (no core)	E*t (w/ core)
Gelcoat	0.000	0.000	490,000	0	0
Chop fibers	0.005	0.005	920,000	4,600	4,600
3/4 oz gun roving	0.023	0.023	920,000	21,160	21,160
1.5 oz mat	0.044	0.044	920,000	40,480	40,480
3/4 oz mat	0.023	0.023	920,000	21,160	21,160
3/8 balsa core	0.000	0.365	1,000	0	365
1.5 oz mat	0.044	0.044	920,000	40,480	40,480
10 oz cloth	0.013	0.013	2,450,000	31,850	31,850
resin	0.000	0.000	490,000	0	0
			sum	159,730	160,095
thickness	0.152	0.517			
			E uncured	1,050,855	
Specimen Averages			E cured	309,662	
Tensile	0.154				
Shear	0.152		Test Values		Difference
Cored Comp	0.512		E tensile dry	1,190,000	13%
Uncured Comp	0.135		E tensile wet	1,050,000	0%
			E comp dry	300,635	3%

Table 9-2: Test Values vs. Rule of Mixtures Prediction of Laminate Stiffness

Figures 9-1 and 9-2 show the tensile FEA model used to validate the tensile test results and design values. The elements are 2-D plane stress, laminated shells⁸. Figure 9-1 shows the resulting displacements, illustrating the bowing and warping due to the unbalanced laminate. The test fixture had universals at both top and bottom to allow the material to warp. Figure 9-2 shows the Tsai-Wu failure criterion plot, showing that outside of the grip area the stress field is almost uniform ($R=1.0$, indicating failure). Note that in this model the extra tabbing is not included as the load is applied at the ends, and as it is a shell element model the clamping effects of the grips are ignored. Next to the grip the FEA model predicted a 23% stress concentration factor due to the grips constraining Poisson's effects.

⁸ In this study flat "shells" are used. The software applies both membrane and bending stresses to 2D elements.

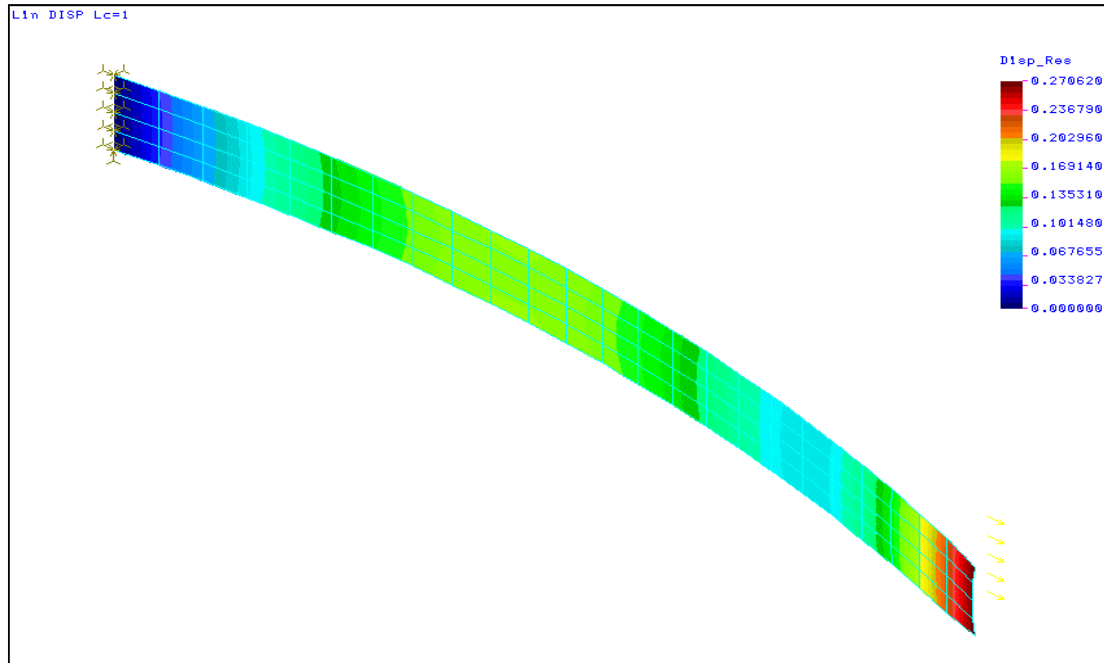


Figure 9-1: Tensile Coupon FEA Displacements (in)

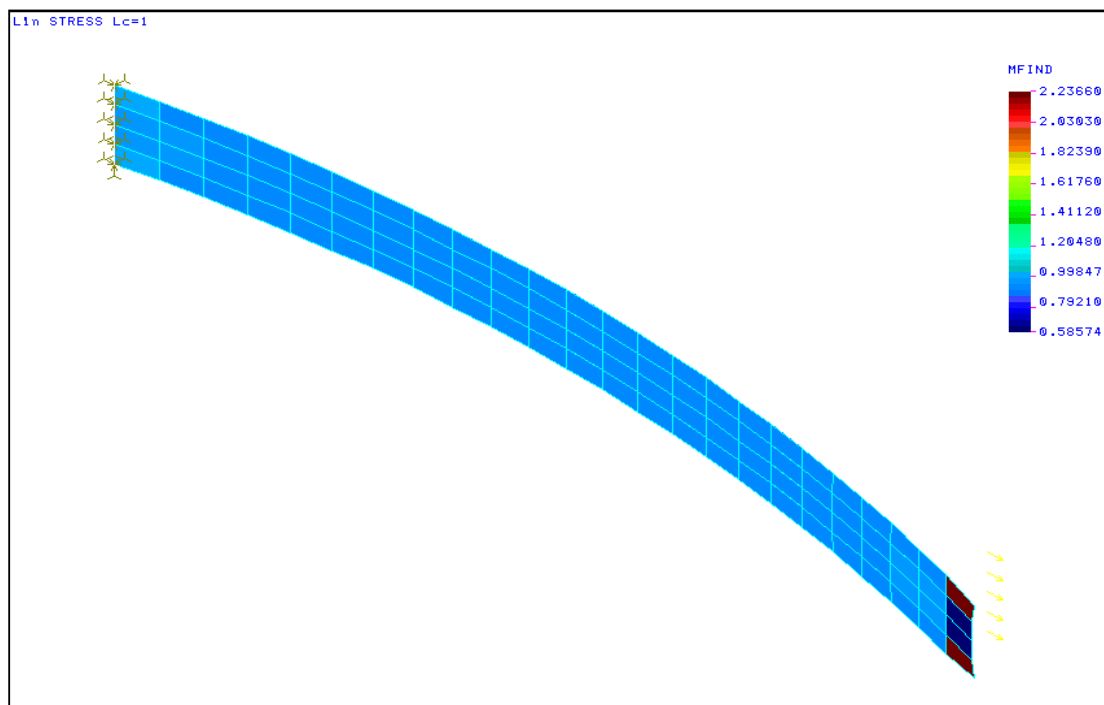


Figure 9-2: Tsai-Wu Plot of Tensile Coupon at Failure

9.2 Flexural Coupon Correlation

As with the tensile, shear and compressive models, the initial flexural FEA models were constructed of 2-D laminated shell elements. To match the ASTM C393 tests, the 3-point models had a 9" span and the 4-point models were set at 16", quarter-point loading.

Figures 9-3 to 9-6 show the 2-D flexural FEA models used to correlate the flexural test results. The boundary conditions are also shown. One support restrained the specimen in all translations and the other restrained it in only the vertical direction. In reality however the second constraint offers some lateral restraint due to friction. To take this into account an axial force equivalent to the static friction reaction force was applied at the support. This also added a slight non-linear in-plane stiffening effect that reduced the vertical deflections by as much as 3%. The measured coefficient of friction between the steel rod and the boat cloth surface was 0.43 as determined by a pull test.

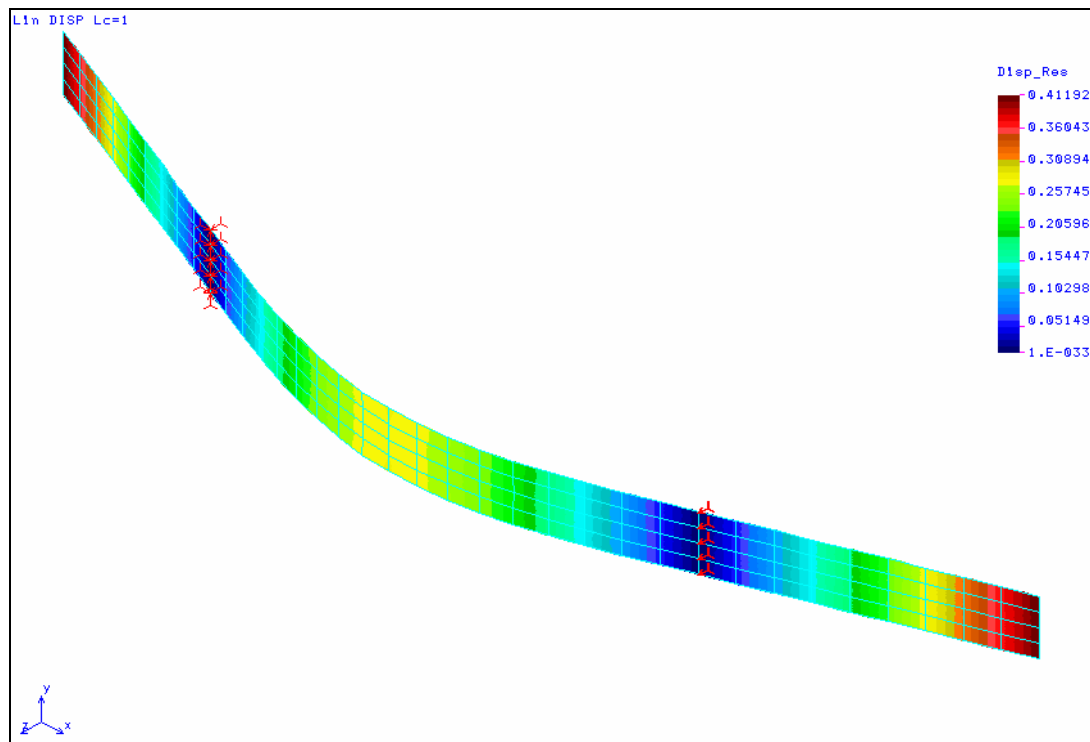


Figure 9-3: 3-Point Coupon FEA Displacements at Predicted Failure (in)

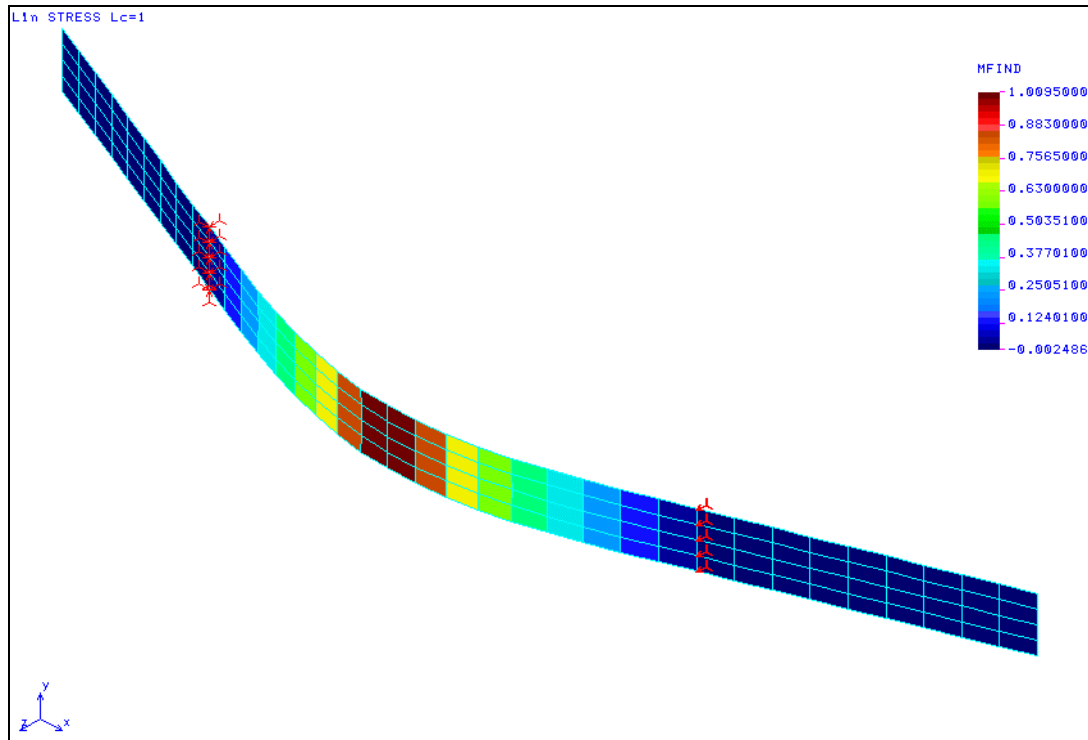


Figure 9-4: Tsai-Wu plot of 3-Point Coupon at Predicted Failure

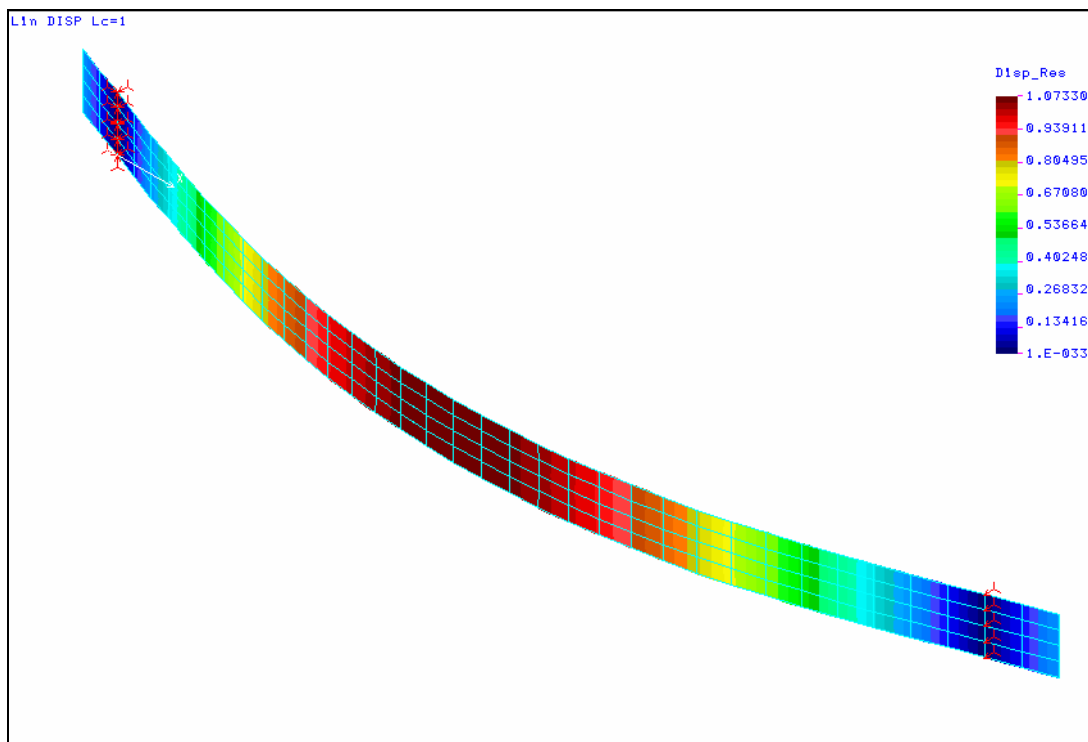


Figure 9-5: 4-Point Coupon Displacement (in)

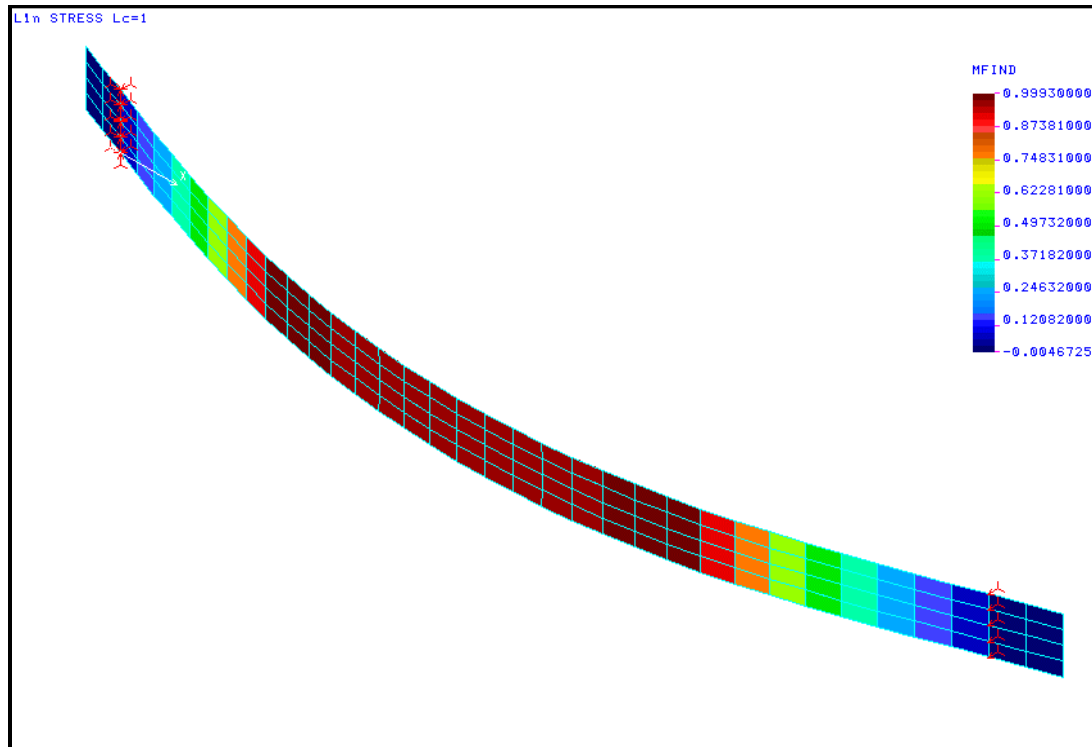


Figure 9-6: Tsai-Wu Plot of 4-Point Coupon at Failure

Table 9-3 compares the combined 3 and 4-point C393 test and the 2-D FEA results at the point where the Tsai-Wu criterion predicted failure.

	D	G	Flex Str	τ
Tests	10242	18019	11947	484
FEA	9631	18545	8116	329
difference	6%	-3%	32%	32%

Table 9-3: Tested and Predicted (2-D FEA) Panel Stiffness, Core Shear Modulus and Strength

The results show the 2D FEA closely predicted the panel stiffness, but significantly underestimated the failure strengths of the skins and core. The predicted deflections for the 4-point tests were within 3% of the average measured values and the 3-point models were within 7%.

One reason for the strength discrepancy is the inherent uncertainty in the tensile testing, which provided the material property input to the FEA. The straight-sided tensile specimen results in a stress concentration at the edge of the grip tabbing. Although needed to avoid a through-the-thickness stress concentration from the grips, the structural transition led to early failure in some tensile specimens. As the flexural specimens also failed in tension, this lower measured tensile value had a significant impact on the predicted flexural strength. For example, if the actual tensile strength (X_t) were 23% higher (the value calculated by the FEA for the stress concentration in the tensile specimen), the predicted flexural strength would be within 5% of the measured flexural strength.

Another reason for the discrepancy is the way the FEA shell elements are formulated in COSMOS/M. Linear shell elements tend to underestimate membrane stresses when the deflections are greater than the thickness of the laminate, leading to larger predicted deformations [110]. Additionally, though the elements include bending and some membrane stresses (through an in-plane stiffness addition term), the linear shell elements used in COSMOS/M are based on Mindlin rather than DiScuiva formulations that better account for the core contribution (see Section 4.1.2). Regardless, an accuracy of 6% is sufficient for most engineering applications as long as it is included in the reliability analysis.

One solution would be to use a different element formulation, such as laminated solids, but as the required material properties for balsa are also suspect due to the test methods for cores [74], an increase in accuracy is not ensured. Figure 9-7 shows the deflected FEA model using linear solid elements. Table 9-4 compares the results with the measured values.

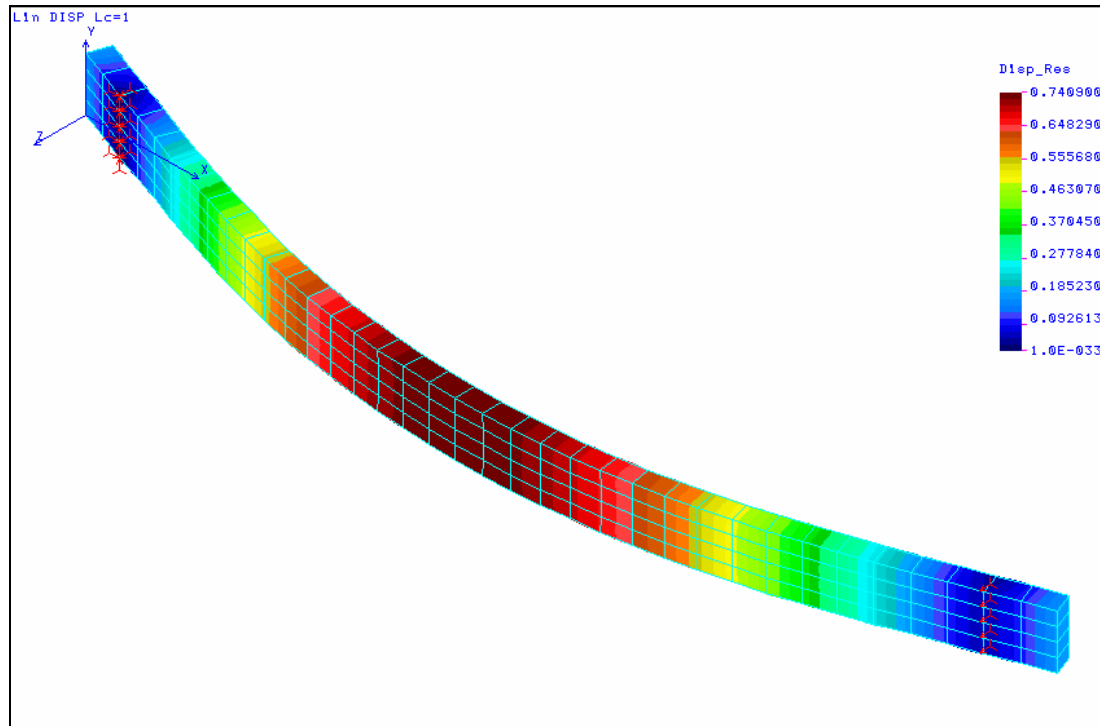


Figure 9-7: Deformed Linear Solid Element Flexural FEA Model (4-point) (in)

	D	G	Flex Str	τ
Tests	10242	18019	11947	484
FEA	8034	38564	7352	298
difference	22%	-114%	38%	38%

Table 9-4: Tested and Predicted (3-D FEA) Panel Stiffness, Core Shear Modulus and Strength

The solid model under-predicted the stiffness by 22% versus 6% for the shell model. In flexural strength the solid model under predicted the strength by 38%, which was also mainly influenced by the tensile test results. In general the poor correlation by the linear solid element and the increased difficulty in application make its use a questionable value.

In vessel design trade-offs exist in selecting element formulations. Although shell elements are significantly faster to model and process, some accuracy relative to the core stresses is lost in out-of-plane analysis. In particular, as the elements use the plane-stress assumption, the

through-the-thickness stresses vanish. Of particular importance is the loss of shear stress information for the core, as this is a major design consideration.

Another way to increase FEA accuracy (although still without core shear information) is to perform a geometric⁹-nonlinear analysis using shell elements. For a simple coupon this does not require significant computation power, but for a model with as many degrees-of-freedom as a global hull model this leads to long analysis times. For the simple flexural model a non-linear analysis improved the stiffness prediction accuracy from 6% error to 4% (at failure deflection), but increased the processing time by a factor of 20. The small increase in accuracy was due to the fact that although the deflections were greater than half the laminate thickness, the resulting strains were still less than 2%. A solution with greater promise if the increased accuracy is needed is a global linear model combined with a local nonlinear or solid model. This is discussed further in Section 9.4.2.

Finally, it is important to note that the flexural coupons were loaded with only out-of-plane loads, and the deflection-to-span ratio was high. In the actual vessel the strains from the hydrodynamic out-of-plane loading were on the same order of magnitude as the rig-induced in-plane strains, and the out-of-plane deflections were small compared to the span. With the 2-D FEA model showing much greater in-plane accuracy, the overall FEA predictions using shell elements is not as bad as indicated by the flexural results alone.

9.3 Finite Element Panel Study

Panel finite element analysis was performed with two goals in mind. The first was to determine the mesh density needed in the global model, and the other was to correlate the panel tests to

⁹ A “material” nonlinear analysis that takes into account a nonlinear stress-strain curve was not required as the polyester/glass laminate is linear up to first-ply failure. See Figure 6-12.

the FEA results. This test program also served as a “bridge” of test results between the coupon and full-size testing.

9.3.1 Mesh Density Study

The general FEA procedure to verify the mesh density and element accuracy followed these steps:

1. Create a linear static FEA model of the HTS method described in Section 4.2 for a 24 inch square panel.
2. Run the model with finer mesh densities until the results approached a constant value.
3. Compare the results with closed form solutions for fixed-fixed and simply supported edges.

Table 9-5 presents the center deflection for a 5 psi distributed load versus the mesh density. The load was chosen to generally agree with marine practices, which are often designed for center deflections on the order of $1/50^{\text{th}}$ of the panel length, and is also of the same order of magnitude of the slamming loads experienced by small vessels. Table 9-6 shows the deviations from predicted stresses. The material properties corresponded to 0.25" aluminum, as an isotropic shell is more easily verified with closed form solution. A comparison with composite elements is presented in the following section. Figure 9-8 shows the stress convergence. The FEA predicted the highest Von Mises stress for the simply-supported panel in the corners and the highest normal stress in the center. All the stresses were highest at the center of the edges for the fixed-fixed boundary conditions.

	Deflection	Deflection
Mesh	Simply-Supported	Fixed Edges
4x4	0.445	0.158
8x8	0.464	0.150
12x12	0.468	0.148
16x16	0.469	0.147
20x20	0.470	0.147
30x30	0.470	0.147
50x50	0.471	0.147

Table 9-5: Mesh Density Verification of Deflections

	Max Von Mises Stress	Max Von Mises Stress
Mesh	Simply-Supported	Fixed Edges
4x4	0.445	0.158
8x8	0.464	0.150
12x12	0.468	0.148
16x16	0.469	0.147
20x20	0.470	0.147
30x30	0.470	0.147
50x50	0.471	0.147

Table 9-6: Mesh Density Verification of Stresses

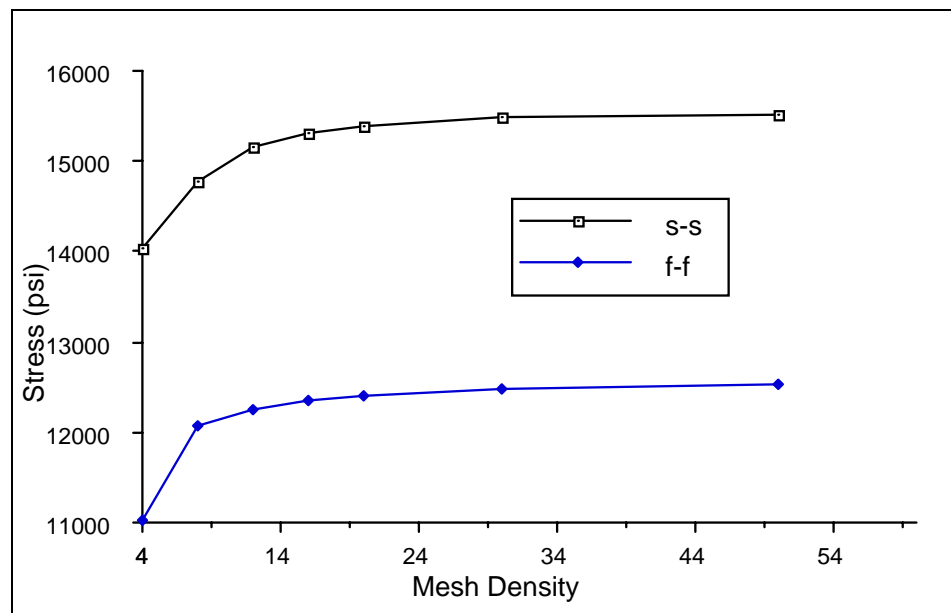


Figure 9-8: Convergence of Stresses

The deflections also converge, although from different directions. The simply-supported panel converged from below, while the fixed edge panel converged from above. Normally the predicted deflection is always less than reality as the linear formulation of the elements causes the strain energy of the elements to be less than the strain energy of the real structure. This was the case with the fixed-fixed case. For the simply-supported case the corner conditions restricted element deflection in that area.

Comparing Tables 9-5 and 9-6, note that the deflections converge more rapidly than the stresses. This is also due to the linear FEA formulation. As the fatigue analysis is mainly stress-based, either a finer mesh density or nonlinear elements are required than for displacement-based analysis. As the stresses nearly reach their asymptote when using a mesh between 20x20 and 30x30, a mesh density of anything greater than 20x20 would give sufficient accuracy. The trade-off was computation time.

Figure 9-9 shows the panel finite element model using a 24x24 mesh density and showing the pressure load and boundary conditions. Figure 9-10 is a plot of the stress contours for a 24x24 mesh with simply supported edges. Figure 9-11 is a plot of the stress contours for a 24x24 mesh with fixed edges.

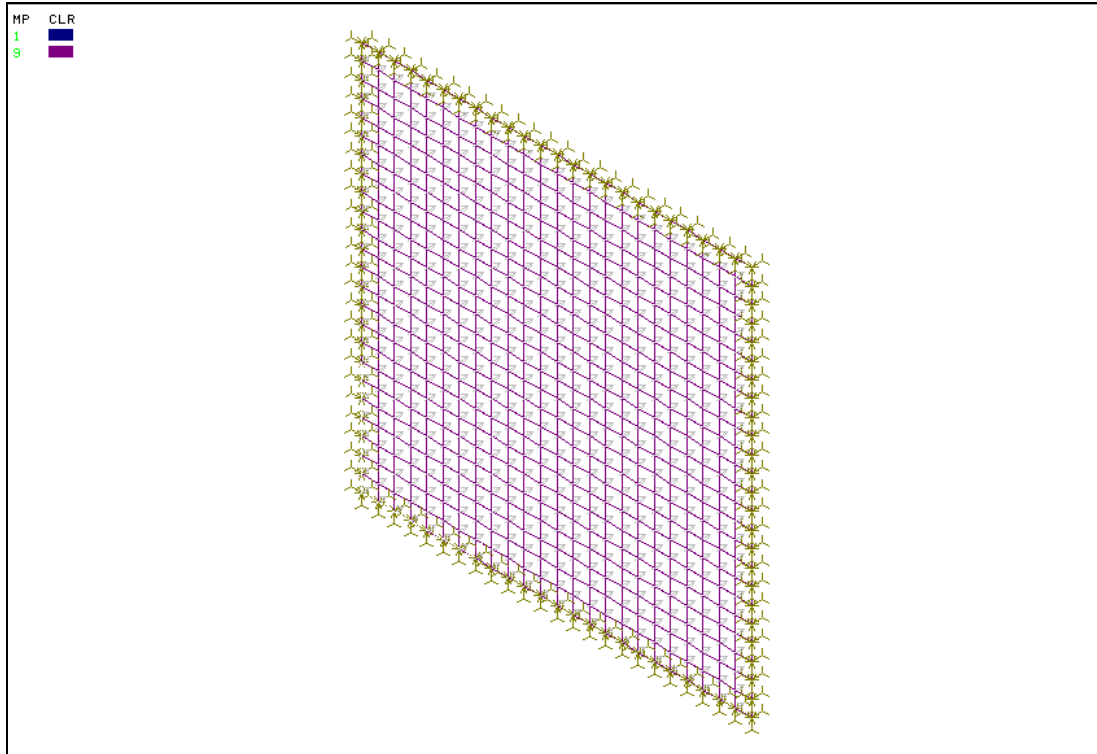


Figure 9-9: Final Panel Verification Model Showing Loading and Boundary Conditions

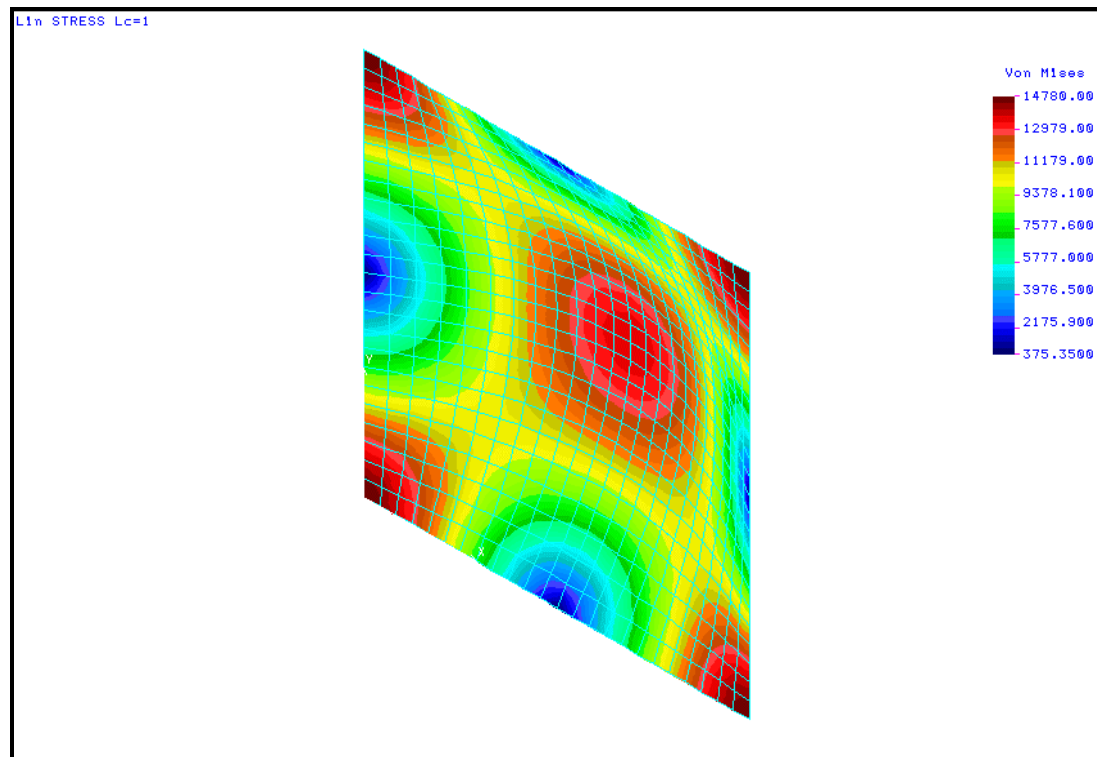


Figure 9-10: Stress Contours for Deformed Simply-Supported Panel

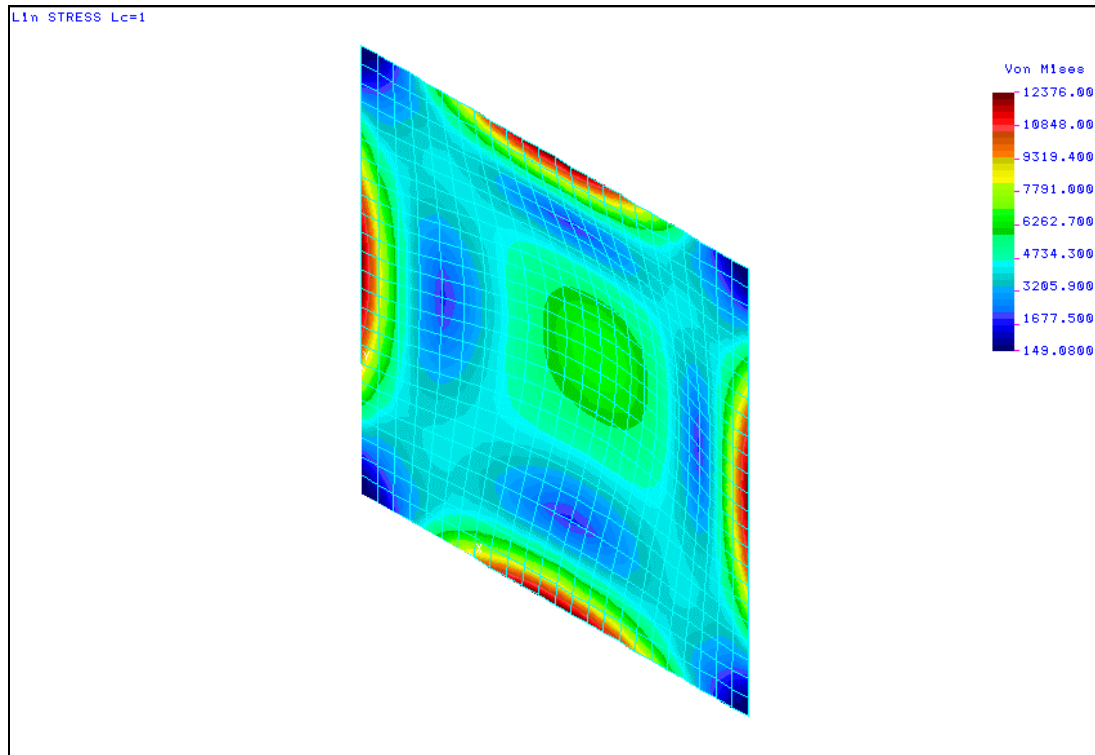


Figure 9-11: Stress contours for Deformed Fixed Edge Panel

Comparing the FEA predictions of the final mesh to the closed form linear solution used in the ABS calculations (also from [139]) showed the correlation was excellent. Table 9-7 presents the linear normal stresses and deflections compared to linear plate theory.

	Defl (FEA)	Defl (ABS)	%	Stress (FEA)	Stress (ABS)	%
S-S	0.470	0.470	0.00	13260	13240	0.15
F-F	0.147	0.147	0.00	14080	14200	0.85

Table 9-7: Comparison of FEA and Linear Plate Theory Predictions

As the predicted deflections are greater than one-half the plate thickness and the element size is approaching the plate thickness, corrections must be made for large deflection characteristics

and thick plates. Tables 9-8 and 9-9 show the effects of including large deflection theory (adding membrane strains) and thick plate formulation (adding transverse shear deformation) for a 24x24 mesh. Note that with the thick plates shear deformation is allowed, which both increases deflections and decreases stresses. This effect is also present when comparing shell and solid elements.

	Thin Element (Large Disp)	Thick Element (Large Disp)
Deflection	0.470	0.474
Stress	15441	13895

Table 9-8: Effects of formulation corrections on 24x24 simply supported panel

	Thin Element (Large Disp)	Thick Element (Large Disp)
Deflection	0.147	0.147
Stress	12435	10467

Table 9-9: Effects of formulation corrections on 24x24 fixed-fixed panel

The results from the panel study indicate the 24x24 mesh and the linear element formulation is adequate to produce results closely matching the closed form solution. In the case of the aluminum shell, large deflection theory was needed to improve the stress predictions as they were greater than one-half the plate thickness. These deflections were based on ultimate strength criteria however rather than the normal working stress used for fatigue analysis. As the strains causing high-cycle fatigue result in small deflections, using small deflection theory in predicting strains is acceptable for this study.

Another element formulation verification tested the composite shell element. For this test aluminum properties were entered as an orthotropic material in a $\pi/8$ quasi-isotropic laminate.

The results indicated negligible deflection and stress differences compared to the isotropic element.

9.3.2 Correlation with Panel Tests

The mesh density study was performed with an isotropic material (aluminum) as this allowed for an easy closed-form solution check. The actual material tested in this study was the J/24's hull laminate, consisting of a balsa-cored polyester resin and E-glass sandwich laminate. TPI supplied panels measuring 24" x 24", but to allow for edge overhang the support jig was made 23" square.

Based on the results from the tensile, compression, shear and flexural coupon studies a FEA model was created using 2-D laminated shell elements. The chosen coordinate system had the panel in the X-Y plane and pressure was applied in the Z-axis. To closely represent the panel jig (see Figures 7-1 and 7-2 for the jig), simply-supported boundary conditions were modeled by constraining the panel edges in Z-axis translation. To prevent rigid body rotation one corner node was also constrained in X and Y translation and rotation about the Z-axis. With the panel overhanging $\frac{1}{2}$ " this required a 48x48 FEA mesh with one element on the overhang.¹⁰

As with the flexural coupons the initial analysis was linear-geometric and additional runs were completed using in-plane stiffness effects and full non-linear geometric effects. The linear runs neglected the membrane forces caused by the in-plane stress created by the large deformations and edge effects. This stiffening effect is similar to that of a guitar string, where the tighter the string is pulled, the greater the out-of-plane stiffness becomes.

The basic panel differential equation is [88]:

¹⁰ Having only one element representing the overhang meant that displacement and stress predictions for the overhanging portion were not very accurate, although they gave a better indication of the edge reaction than not having any elements.

$$\frac{\partial^4 w}{\partial x^4} + 2 \frac{\partial^4 w}{\partial x^2 \partial y^2} + \frac{\partial^4 w}{\partial y^4} = \frac{q}{D}$$

If the membrane forces are included, a nonlinear equation is created [110]:

$$\frac{\partial^4 w}{\partial x^4} + 2 \frac{\partial^4 w}{\partial x^2 \partial y^2} + \frac{\partial^4 w}{\partial y^4} = \frac{1}{D} \left(q + n_x \frac{\partial^2 w}{\partial x^2} + 2n_{xy} \frac{\partial^2 w}{\partial x \partial y} + n_y \frac{\partial^2 w}{\partial y^2} \right)$$

The solution of this equation in general cases is unknown, and apart from a few exceptions, approximation methods are used. The most common approximation method used to solve this equation employs the energy method. The total strain energy is obtained by summing the parts due to bending and stretching of the middle plane. The solution finds the lowest potential energy. In FEA, the analysis is performed using incremental formulation, where the loading is increased in a step fashion and the linearized equation is solved for each load step. To reduce computation time an iterative method such as Newton-Raphson or Quasi-Newton is often employed [140].

The change in stiffness due to membrane forces is influenced by the boundary conditions, loads and especially, the deformed shape. This implies that a geometric non-linear solution is necessary, which as discussed in the flexural coupon section means that significant computational resources are required. For many design applications where the linear assumption is not sufficient, reasonable accuracy can be achieved by using a single-step differential stiffness approach [110, 141]. This approach approximates the full solution by adding a geometric stiffness matrix K_G to the standard structural stiffness matrix, K . Displacements are computed with respect to the original structural configuration and the geometric effects are reflected in the geometric stiffness matrix. This method assumes that the load magnitude and direction do not change but the application point changes with geometry.

Linear analysis with the in-plane stiffness effects is performed in two steps. As with normal linear analysis the global stiffness matrix K is first established and is used to compute the displacements, u_i , from the external forces, R .

$$[K]\{u\} = \{R\}$$

The second step involves forming the $K_G(u_i)$ matrix based on the computed displacements and solving the updated, combined stiffness matrix,

$$([K] + [K_G(u_i)])\{u_{i+1}\} = \{R\}.$$

Multiple repetitions of this process could follow until a given tolerance is reached. This is the general method for a full geometric-nonlinear analysis. Results however show that the one-step iteration provides an acceptable level of approximation for many design cases [142]. A reasonable check would be to see if the results from the linear and in-plane analyses vary significantly. If they do, a non-linear analysis is prudent. The flexural coupon studies for instance, had good correlation with the linear analysis, and adding the single-step in-plane stiffness approximation improved the accuracy by less than 1%.

The magnitude of difference between the linear and non-linear approaches for a pressure load on a 10 mm thick fiberglass panel (with $E_x=E_y=9.0$ GPa (1.3 msi)) is shown in Figure 9-12 [140]. The modulus used in that study is that of a single-skin panel with a low fiber volume fraction. In this study the “Prevented” results show the full influence of membrane stresses on stiffness, with all translations fixed in the FEA. The “Free” solution shows unconstrained in-plane translations in a fully non-linear analysis. The “Linear” case does not include any membrane effects.

In reality, the actual boundary conditions typically fall between the prevented and free conditions. By calculating both, the engineer can determine the test’s sensitivity to boundary conditions. In this study the boundary conditions as well as the analysis methods were investigated.

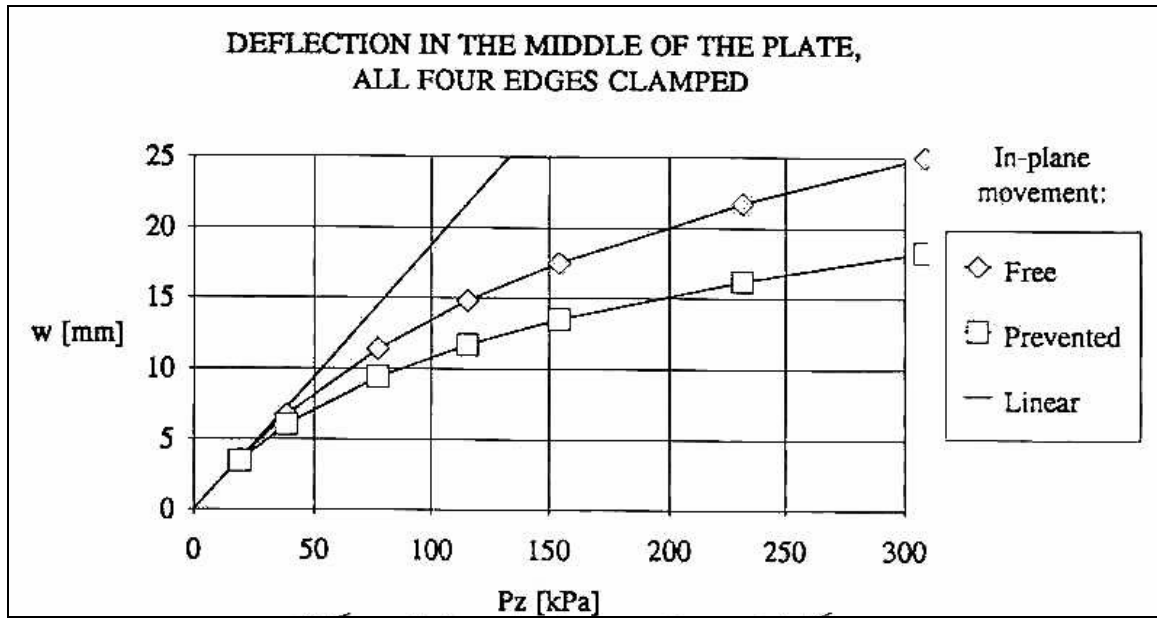


Figure 9-12: Center Deflection of an Edge-Clamped Panel Versus Pressure Loading.

The Figure 9-13 shows the panel deflections at predicted failure, for an 8.35 psi loading using a linear analysis with in-plane stiffness effects considered. A 2% reduction in deflection was seen from the linear analysis. With a 15 psi load the difference was 5%. This indicates that the panel geometric effects are more significant than those seen in the flexural coupons.

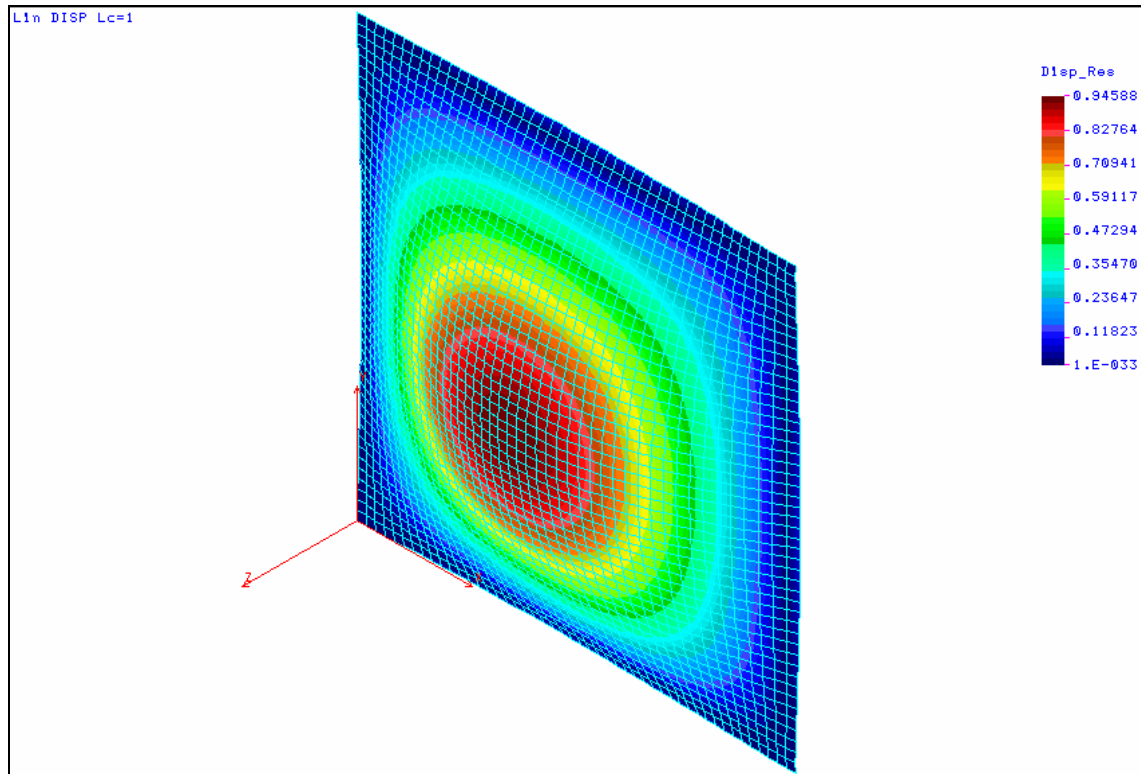


Figure 9-13: Deflections for Deformed J/24 Laminate Simply-Supported Panel (8.4 psi load)

Figure 9-14 shows the primary stresses for the same case for the ply closest to failure. In both the flex coupon and panel models this was Layer 7, a chopped mat layer. This layer is on the inner laminate just inside the boat cloth layer, making it the chopped mat layer farthest from the neutral axis.

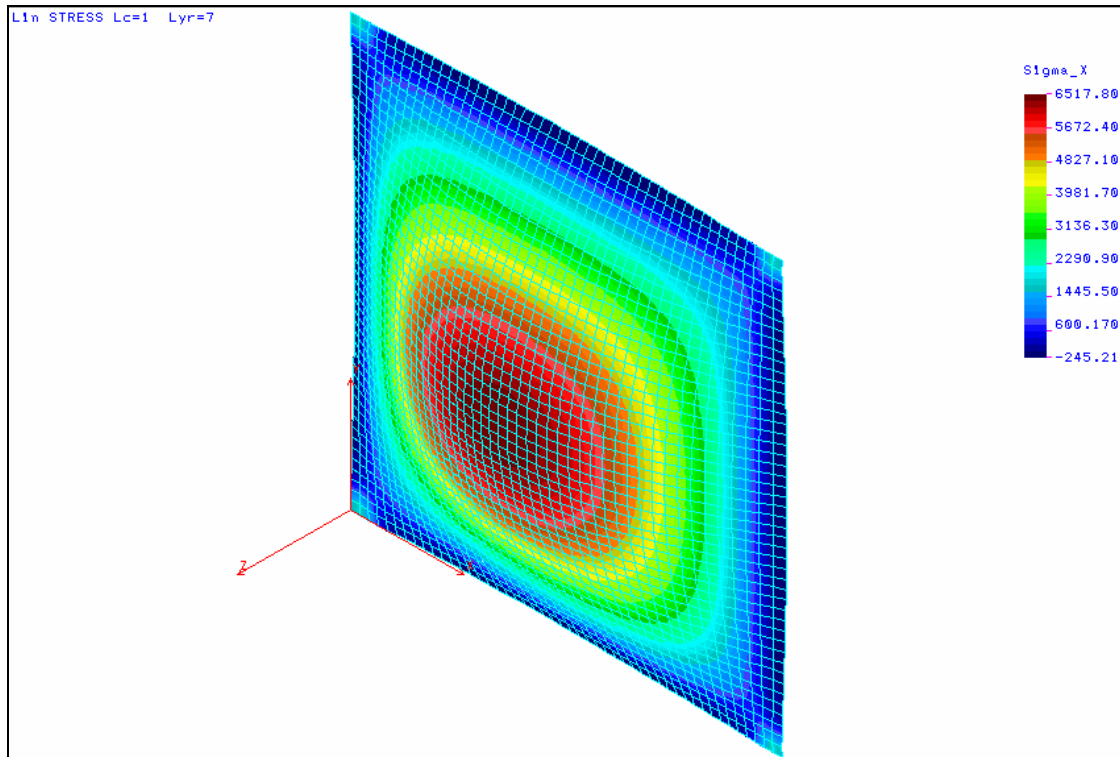


Figure 9-14: Layer 7 Stress Plot for Deformed J/24 Laminate Simply-Supported Panel (8.4 psi load)

The Tsai-Wu plot at the linear predicted failure (8.35 psi) is shown in Figure 9-15. Initial failure was predicted to occur in the corners, followed by the plate center. The corner failure index values were 1.7% higher than the center value.

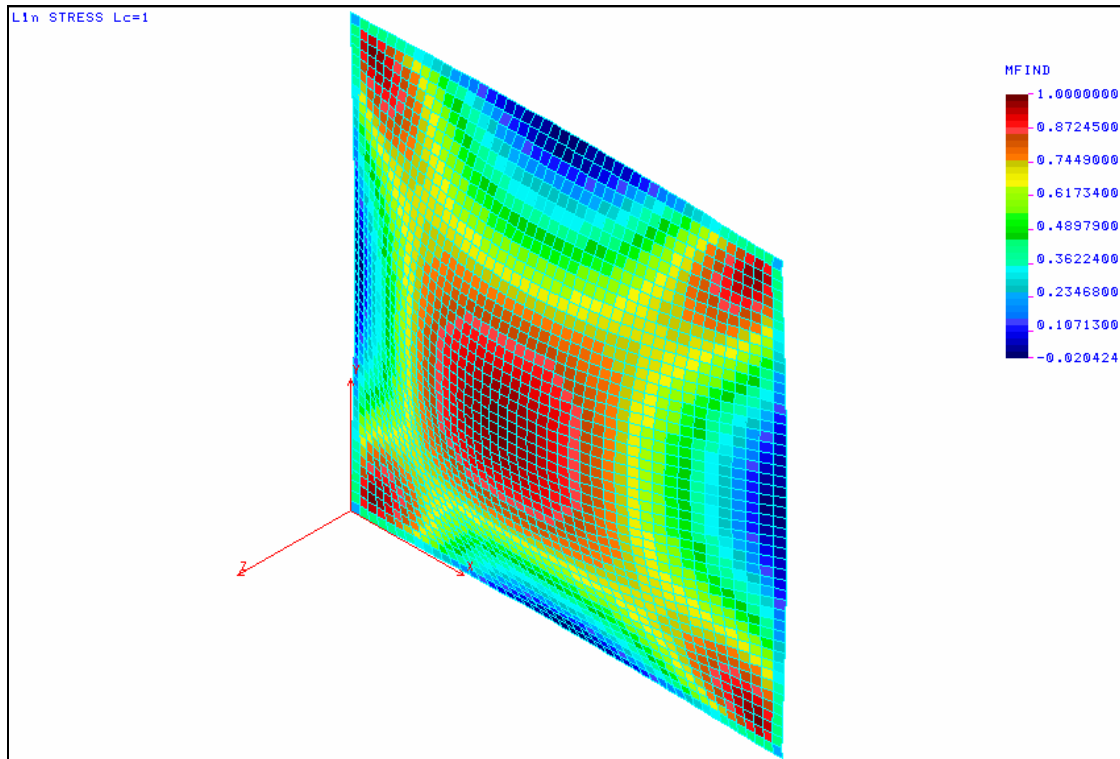


Figure 9-15: Tsai-Wu Plot at Predicted Failure (8.4 psi)

Figure 9-16 shows the predicted load-displacement curves compared to the measured values. The plot shows the wet and dry panels had similar stiffness, and the deflections were decidedly non-linear. The linear FEA closely predicted deflections up to about 20% of the maximum load. The similarities between Figures 9-16 and 9-12 are striking.

The accuracy of the linear (with the single-step in-plane effects) was sufficient at the stress levels corresponding to high-cycle fatigue, however, low-cycle fatigue and both strength and deflection design criteria required more accuracy. To accomplish this a fully geometric non-linear analysis was performed for the panel. The thicker dashed line (the lowest curve in Figure 9-16) shows the predicted deflection for the simply-supported panel. This analysis over-predicted the stiffness.

As the stiffness was over-predicted but the curve's shape was correct, the feeling was that the deflections in the aluminum frame might be causing the error. Figure 9-17 is the displacement plot of the FEA model modified to include the frame. The panel and frame elements were connected through coupling equations that allowed for relative rotations but no translations. This

duplicated the simply-supported boundary conditions in the original panel models. The small dashed line located between the wet and dry deflection curves in Figure 9-16 is the nonlinear analysis when the frame is included.

Figure 9-18 shows the measured and predicted strains for the panel. As with the deflections, the correlation between this model and the wet and dry strain measurements is excellent. This illustrates the importance of boundary conditions in panel tests and in correlating measurements to FEA predictions.

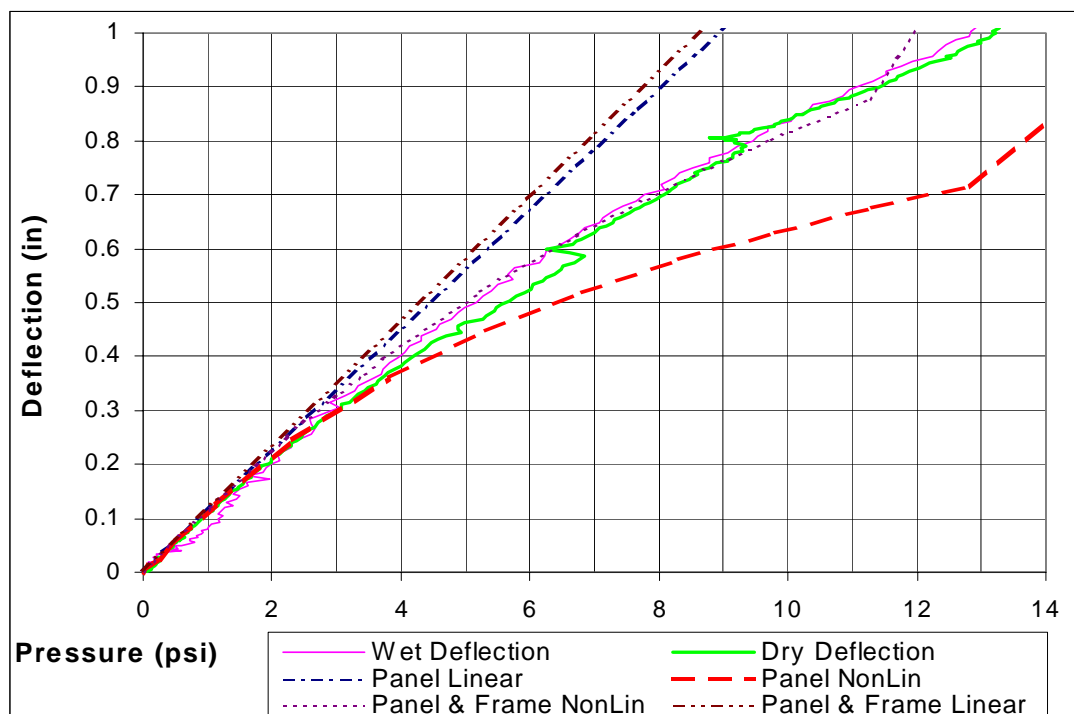


Figure 9-16: Load-Deflection Curves for Pressure Loaded J/24 Hull Panel vs. FEA Predictions

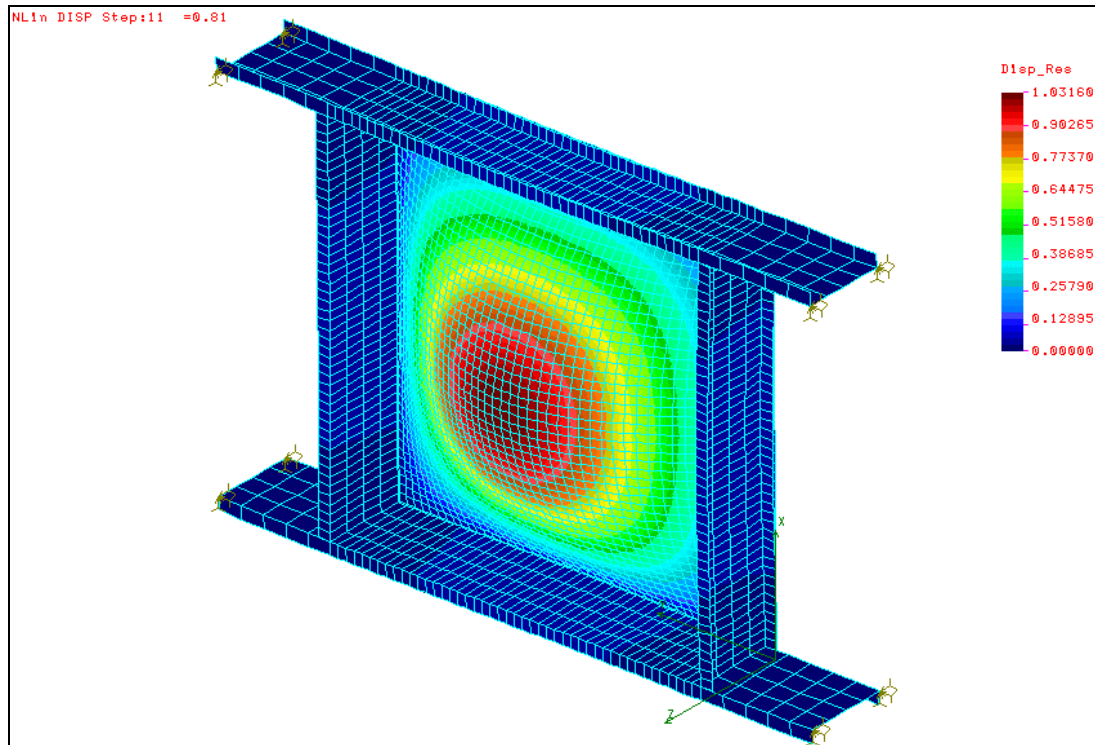


Figure 9-17: Deformed Displacement Plot of Nonlinear Panel and Frame Model (13 psi)

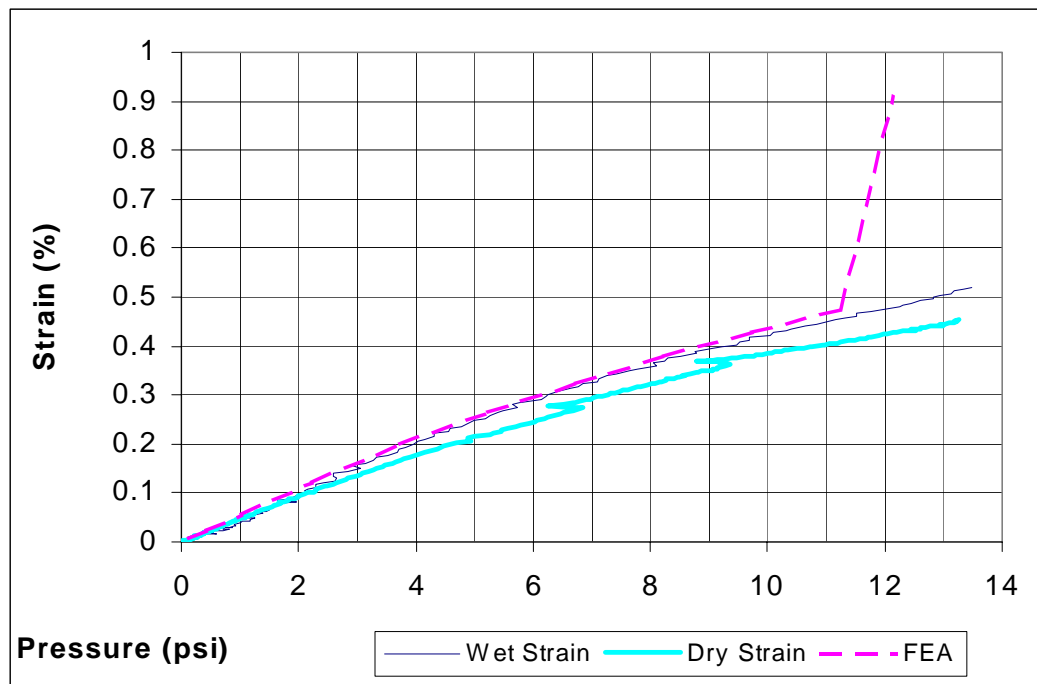


Figure 9-18: Measured and Predicted Strains in J/24 Hull Panel

The non-linear analysis also included a progressive ply-failure routine, which is reflected in the jump in deflections near 11 psi on the non-linear “frame and panel” curve in Figure 9-16. As with the linear analysis initial failure was predicted in Ply #7, a ply that was not the one farthest from the neutral axis. The non-linear analysis increased the failure limit by roughly 50%, illustrating the importance in design of using the appropriate analytical tools. As the actual panels did not fail at the point predicted by the nonlinear FEA, and due to the test machine’s limit of 15 psi, the error in the analysis is not known. As with flexural coupons the error is likely caused by the too low strength values obtained from the tensile tests.

The improved accuracy capable from the non-linear analysis for both strength and deflection limited design criteria is clear, but does come with a price. The non-linear panel analysis took over 50 times longer to execute than the linear analysis. The value of this approach will depend on the application, materials, costs, etc. As one example, the use of carbon fiber with it’s significantly lower strain-to-failure and higher modulus will often mean deflections are within the acceptable limits of a linear analysis.

A sensitivity study of the boundary conditions (in-plane free vs. fixed translations) produced results indicating negligible difference in predicted deflections. This differed from the study associated with Figure 9-12. Unfortunately that reference did not provide full details on the laminate studied, which may have shed light on possible reasons. The most likely reason is the difference in coupling response.

As presented in the analytical background section (3.2.2), the constitutive relations for a plane-stress laminate are:

$$\begin{bmatrix} N_x \\ N_y \\ N_{xy} \\ M_x \\ M_y \\ M_{xy} \end{bmatrix} = \begin{bmatrix} A_{11} & A_{12} & A_{16} & B_{11} & B_{12} & B_{16} \\ A_{12} & A_{22} & A_{26} & B_{12} & B_{22} & B_{26} \\ A_{16} & A_{26} & A_{66} & B_{16} & B_{26} & B_{66} \\ B_{11} & B_{12} & B_{16} & D_{11} & D_{12} & D_{16} \\ B_{12} & B_{22} & B_{26} & D_{12} & D_{22} & D_{26} \\ B_{16} & B_{26} & B_{66} & D_{16} & D_{26} & D_{66} \end{bmatrix} \begin{bmatrix} \epsilon_x^0 \\ \epsilon_y^0 \\ \epsilon_{xy}^0 \\ \kappa_x \\ \kappa_y \\ \kappa_{xy} \end{bmatrix}$$

In the case of a sandwich laminate with equal faces the B_{ij} terms are zero and no coupling exists between the in-plane and out-of-plane responses [56]. This can lead to a variety of responses influenced by boundary conditions. For instance, with a balanced laminate or an isotropic material, uniform Poisson’s effects cause the laminate to contract at the edges when a normal pressure is applied. An unbalanced laminate such as the J/24 hull will have a coupled response

between the moments and in-plane responses. This leads to responses where the direction of normal load is also important. If the thicker skin is in compression, an apparent “negative” Poisson’s effect is present for the entire laminate due to bend-extension coupling, whereas if the thicker skin is in tension the laminate behaves “normally.” This was apparently the case for this laminate, where the bend-extension coupling partially cancelled the Poisson’s effects and reduced the sensitivity to boundary condition fixity.

The panel studies illustrated a number of important elements in marine composites design. One was the effect of large deformations combined with selecting the proper finite element parameters and analysis models. The need for non-linear responses from both strength and deflection criteria are not addressed by the linear beam and panel models used in many design codes and in practice. Additionally, the complex nature of coupled response caused by the typically unbalanced marine laminates negates the use of any “blended properties” structural methods. Finally, the combination of a low-strain-to-failure material such as chopped mat in an inner ply, when used with a higher strain material (cloth) as the outer ply, illustrates the potential case where the outer fibers are not the first to fail in bending. Nonetheless, in conservative design applications where the maximum strains are less than 20% of the material’s failure strain, or when high-cycle fatigue is the design driver, the linear approach appears to yield sufficiently accurate predictions.

9.4 Full Scale Test Correlation

Full-scale results relied on a global model of the J/24. This was compared with results from the coupon and panel tests and data from the on-the-water testing. The model represented an unfatigued vessel where the laminate had reached moisture equilibrium.

9.4.1 FEA Methodology for Complex Structures

The global finite element model of the J/24 was designed to represent as accurately as possible the vessel geometry, construction using composite material properties, and load and boundary conditions of the actual vessel. The selected analysis methods were chosen based on accuracy and computational resources.

The accurate use of a cumulative fatigue damage theory like Miner's Rule relies heavily on the accurate determination of the stresses in the structure and reliable S-N data [62, 143]. The principal drivers of the stress prediction are:

- assumed loads
- material properties
- boundary conditions
- method of structural analysis

Current industry practices for large ships use finite element methods to model the structural response, yielding displacements and stresses [113]. These approaches, exemplified by the ABS "SafeHull" program, replace the empirical design code methods based on beam theory. Although not commonly used for small craft, FEA has been successfully used in high-performance small craft applications such as racing yachts [7, 90, 91, 114, 144]. Current code practice for small craft however, still relies on linear beam and plate theories. In many cases this is acceptable when used with appropriate safety margins. As shown in the coupon tests the flexural results were closely predicted with linear FEA. The important aspect missed in some of the linear beam equations is the same problem as the ASTM C393 calculations, namely that the skin is considered homogenous.

In virtually all FEA for ships and small craft constructed of composite materials the basic approach uses linear shell elements developed for laminated materials. This allows for efficient use of computational resources and provides better deflection and stress prediction than was available using beam theory methods. Coarse meshes are used which provide acceptable deflection predictions and relatively quick computational turnaround. Uncertainties in stress predictions due to the coarse mesh or element selection are compensated for by factors of safety.

Small deflection theory is typically used even though for some high-strain laminates the out-of-plane deflections often exceed half the laminate thickness, limiting the accuracy [110]. Again, this inaccuracy is addressed through factors of safety. As the stress accuracy requirements of this project are more stringent than that for a design case, a more rigorous method was used.

Options to improve the modeling uncertainty address the fundamental problems inherent in the linear shell element formulation. The available options include:

- Higher-order (non-linear) shell elements, solid elements and non-linear analysis
- Higher density meshes using linear or non-linear elements.
- Global/local refinement.

The typical approach generally uses some aspects of all three methods combined in a way to minimize computational requirements. A global model is constructed using linear 2-D shell elements. From that model a local area model is generated using either higher order elements or a significantly more refined mesh. The displacements and rotations or the forces at each node are transposed from the global to the local model and more accurate stress predictions result.

The difference between the first two choices: non-linear or more refined mesh, are based on two limitations, namely whether the deflection is nonlinear. Refining the mesh solves the problem of the piecewise approximation of the panel, but does not fully take into account the reduced deflections caused by membrane stresses. The effects of membrane stresses were discussed in Sections 9.2 and 9.3.2.

The choice of which methods to use depend on the material choices, stress level and deflection information. As a component of this study is to verify the stress prediction by using strain gauges, the reduction of deflection uncertainties is important. If large deflections are expected, such as for low-cycle fatigue of single-skin glass laminates, then non-linear analysis or solid element formulation is required. If expected deflections are small (less than 40-50% of the laminate thickness), such as for high-cycle fatigue of sandwich structures made of the majority of marine composites, then linear theory with a refined mesh is acceptable.

9.4.2 Global/Local Finite Element Model Methodology

The global model is primarily used to identify the areas requiring detailed analysis. In some cases (for instance where deflections rather than strength are the driver) a global model is the only model required. For detailed stress analysis of complex structures the required construction of the global model is limited by the computational power available. In general a sufficiently detailed global model that does not require a separate local model analysis is limited to four specific cases:

- nearly unlimited computational power
- a priori knowledge of the stress area
- deflection driven design
- small deflections (less than 40-50% of the skin thickness)

The level of detail in the global model can depend on the goals of the model and will strongly influence the computational requirements. A global model may also have multiple objectives that influence the design. Some of these may be overall structural response, load distributions during intact or damaged states, stress predictions, or even fluid/structure damping problems.

For this study the initial plan was to use a global model with input to a local model. Due to the increased capability of desktop computers during the study, a larger, more complex global model was constructed and the local (panel) model was only used to correlate the panel study results. For larger or more complex ships the global/local approach still works.

As the highest stresses were in the bow slamming area (noting also that the laminate also increases in thickness in this area) a refined mesh was constructed in that part of the global model which then transitioned to a coarse mesh outside the area of interest. A number of problems existed with this solution. These included the need to taper and skew elements in the transition zone, which affects their accuracy, and the other was the increased time spent creating the transition zone, rather than relying on built-in meshing algorithms. For complicated shapes

such as a vessel, less time may be spent modeling a new local model rather than refining the transition zone in a global model.

A local finite element modeling and analysis can be created to perform a detailed analysis of the local structural region. As with the global model the geometry, boundary conditions, materials and loading of the local model duplicates the physical structure as closely as possible. The amount of detail in the mesh discretization is influenced by the type of element and the amount of accuracy desired. Higher order elements can be used with efficiency. Three methods can be used to create the mesh for the local model [145].

- a high number of finite elements across the model
- a graduated mesh determined by engineering judgment
- multiple global/local analyses

The local refinement affects only the local model and therefore does not increase the computational requirements for the global model. A key decision is the determination of the bounds of the local model and the degree of refinement needed. Using a graduated mesh for the local model based on engineering experience can save significant computational requirements while allowing for sufficient detail. The same methods used to check on the refinement of the mesh, as presented in Section 9.3.1, can be used with success. Additionally, by checking on the stress gradients between elements, a measure of the error is possible. One way to check this easily is to check the difference by reporting stresses as "element stresses" versus "nodal stresses." The element stress calculation averages the nodal stresses over the element. If adjoining elements have stresses that vary by more than 15%, the mesh may be considered too coarse [142].

A major requirement for the successful application of the global/local approach is the successful transfer of the displacements or forces from the global model to the local. Definition of the boundary between the two models is dependent on the geometry of the particular structure. St. Venant's principle applies in this case [110]. The more accurate the global model's results are, the closer the local model's boundary to the point of interest can be. Another way to look at it is

that the stresses are derived from differentiation of the displacement field, so the boundary should be placed in an area where the displacement gradient is small.

Transfer of the global results can be made by either displacements (including rotations) or forces. Normally the input to the local model comes from the displacement field of the global model. As the number of nodes at the boundaries are different, and the element shape functions may also be different, an interpolation scheme is needed which will translate the nodal displacements from one boundary to the other. This can be stated as,

$$\delta_g(x, y, z) \Rightarrow \delta_l(x, y, z)$$

Where the subscripts refer to the global and local models' displacement fields. The interpolation scheme is a set of functions that map the two displacement fields, so mathematically this can be written as:

$$\{\delta_g(x, y, z)\}[S(x, y, z)] = \{\delta_l(x, y, z)\}$$

Where S is a matrix of interpolated functions for the number of displacements (and rotations) in the local model displacement field. A number of interpolation functions are used in finite element analysis. These include:

- linear
- Lagrangian
- least squares fit
- splines

Linear works fine for linear elements and where the local boundary is far from the point of interest. In other cases a mathematical spline is generally used [145]. This is somewhat analogous to a draftsman's spline, where a curve is drawn connecting a number of points on the drawing. Spline functions are piecewise polynomials of degree m that are connected together at points called knots so as to have $m-1$ continuous derivatives. Numerous spline functions are

available, each with their advantages and disadvantages, and the selection is predominantly based on matching their capabilities to those of the element shape functions. By correctly interpolating the results from the global to the local level, the output from the local model will produce results with the minimal possible modeling uncertainty.

9.4.3 J/24 Global Finite Element Model

The global J/24 FEA model was developed using construction drawings and data provided by TPI and boat checks performed at OCSC. All meshing for composite materials used laminated shell elements, with 95% quad elements and 4% triangular elements. The triangular elements were used to transition the mesh density. Isotropic materials used regular shell elements. Some rigid bar elements were used to connect a mass node simulating the center of gravity of the lead keel to the composite keel stump. Mass nodes were also used to represent other heavy, nonstructural components such as the rudder and outboard motor bracket. The mainsheet traveler and jib tracks were modeled using beam elements as detailed stresses were not needed for these components. The mesh density is increased in the slamming area. Table 9-10 shows the element types and real constant sets for the global model. Complete copies of the detailed element groups, real constants, material property sets and model geometry are included in the appendix along with the construction information from TPI.

Component	Ele. Type	El Gr.	Real Const
Hull	Quad	1	1
Hull	Triangle	2	2
Lead keel	Mass	3	3
Hull shell at keel	Quad	4	4
Foredeck	Quad	5	5
Foredeck	Triangle	6	6
Cockpit aft of trav	Quad	7	7
Cockpit aft of trav	Triangle	8	8
Hull shell at keel	Triangle	9	9
Keel flr/bow bkhd	Quad	10	10
Lead keel	Rigid Bar	11	11
Keel flr/bow bkhd	Triangle	12	12
Mast bkhd	Quad	13	13
Mast bkhd	Triangle	14	14
Keel bkhd and liner	Quad	15	15
Keel bkhd and liner	Triangle	16	16
Alum mast step	Quad	17	17
Sliders and tracks	Pipe	18	18
Rudder 1 & mast 4	Mass	3	19
Misc 10 lb weight	Mass	3	20
Main trav	Pipe	18	21

Table 9-10: Element Groups and Real Constant Sets for Global Model

Various structural details were modified during the J/24's production run and as these could influence the structural predictions a second model was created reflecting these changes. With this second model both the old and new J/24's were represented by dedicated structural models. The primary difference between the models is the absence of cockpit lockers in the new boats, and small changes in internal structure. No significant difference in global bending was seen between the two models. As it turned out, the last-minute switch of the newer J/24 with *Imagination* meant that all final analyses were carried out with the model representing the older style J/24.

The "older J/24" model included:

- 8424 elements
- 7940 nodes

- 46728 degrees of freedom

Figure 9-19 shows the global FEA model representing the older style J/24. The different element groups are represented by different colors. Triangle and quad elements with the same properties (real constants) have the same color. The increase in mesh density for the slamming area can be seen. The results of the mesh density study were used to ensure that at least 24 elements were located between structural supports.

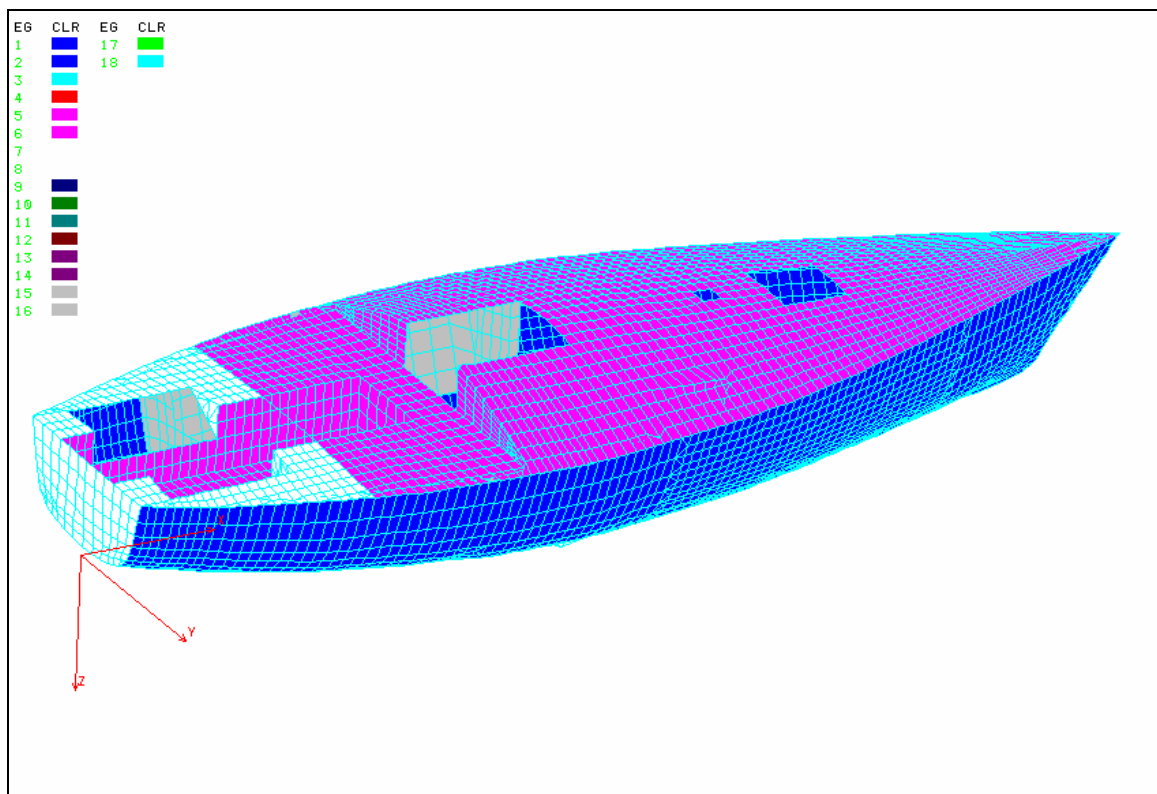


Figure 9-19: FEA Model of the J/24.

Figure 9-20 shows the interior of the global model. Each piece that could possibly provide structural support was modeled. In some cases the drawings and the vessels were slightly different due to manufacturing variances or owner modifications due to repairs. These deviations were included in the FEA model. None were considered structurally significant.

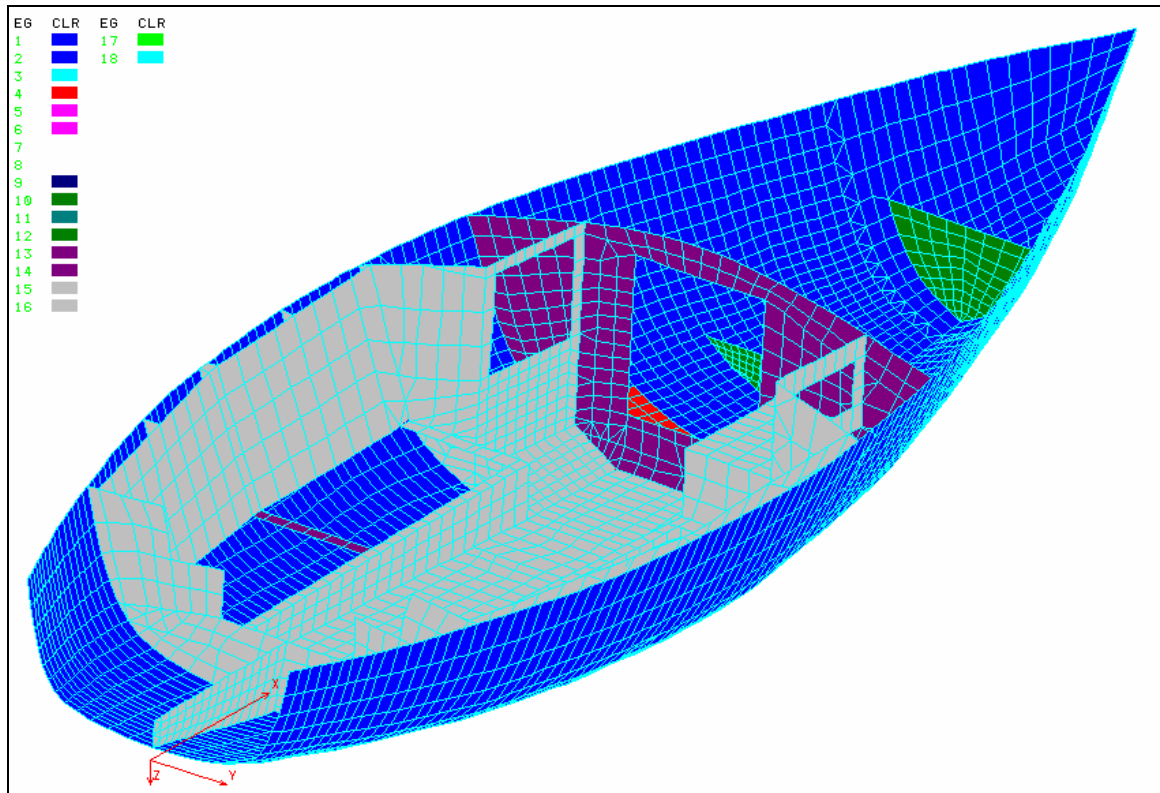


Figure 9-20: Interior Components of the J/24

To verify the accuracy of the FEA global model a simplified version of the model (no internal structure) with simple loading was compared to a detailed MathCad analysis. The results showed a difference of 4%, which is reasonable considering the assumptions in the MathCad analysis. A copy is included in the appendix.

The model represented all structural components as stiffness elements, and included mass nodes to represent the non-structural weight. These items included deck hardware, cushions, sails, the anchor and rode, outboard and fuel tank, safety equipment and other items as determined by an inventory taken just prior to the sailing trials. The final predicted weight was 2831 pounds, versus the 2800-pound class rule minimum weight.

9.4.4 Dockside Test Correlation

To provide a further verification of the global model as well as a baseline for the sailing tests, dockside bending tests were performed on the boats (see Section 8.3.3). The test included two parts; an on-the-water test performed at dockside that measured the global hull change due to imposed rig loads, and correlation of those results to the global FEA models (see Section 9.4.5).

The steps involved in the FEA correlation of the dockside tests duplicated those performed dockside on the real boats, with the exception of needing to balance the gravitational and buoyancy forces. The FEA correlation procedure was:

1. Apply hydrostatic pressure to the hull bottom elements and numerically trim the vessel so that negligible (<5 pounds) reaction forces were seen.
2. Compare trim to observed trim and adjust until no significant differences were seen.
3. Apply rig loads representing condition with zero backstay tension. Check reaction forces for imbalances. Adjust loads as necessary to maintain equilibrium. The rig forces applied to the FEA model were never greater than 2% different from those measured on the Loos Gauge, which was within the gauge's measurement error. Note deflections at bow, stern and mast step.
4. Apply rig loads representing condition with backstay tension. Check reaction forces for imbalances. Adjust loads as necessary to maintain equilibrium. Note deflections at bow, stern and mast step.
5. Determine change in the global bending of the vessel by comparing bow, stern and mast step predicted deflections.
6. Compare to measured deflections.

Table 9-11 shows the dockside static test results compared to the FEA. As described in Section 8.3.3, both boats were loaded and measured identically. Based on the actual measurements the heavily used boat was approximately 33% less stiff in global bending than the lightly used boat. The FEA model predictions based on the unfatigued coupon properties indicated a new,

unfatigued boat would be 14% longitudinally stiffer than *Imagination* and a significant 52% stiffer than J6¹¹.

Load Case 2: Old J Loose Rig			Load Case 3: Old J Tight Rig		
Location	Node	Deflection	Location	Node	Deflection
Stem	1950	6.99E-03	Stem	1950	-8.65E-02
Stern	3018	1.14E-03	Stern	3018	-1.40E-02
Mast step	5082	5.14E-03	Mast step	5082	2.62E-02
	Overall	0.010		Overall	-0.031
				"J6"	"Imagination"
			Measured	-0.063	-0.047
			Calculated	-0.041	-0.041
			Difference	-52%	-14%

Table 9-11: Correlation of Dockside Static Test (Displacements in inches) Versus a Hypothetical New Vessel

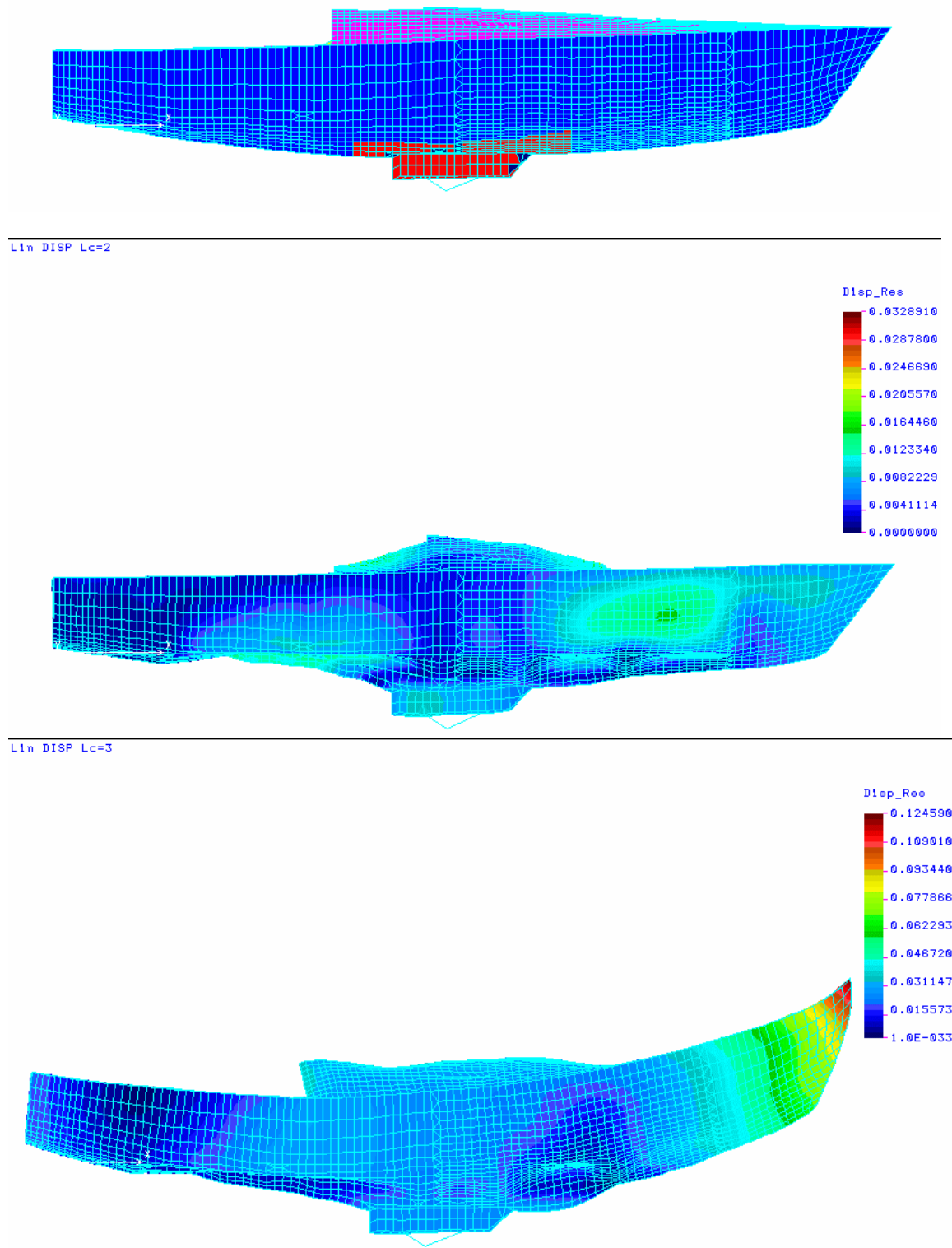
Figures 9-21 to 9-23 show the corresponding displaced conditions of the FEA model:

- a) without loads
- b) floating dockside with slack rigging (Load Case 2)
- c) floating dockside with a tight backstay (Load Case 3)

The FEA analysis clearly shows the hogging effects of flotation and the sagging effects of rig tension. The effect of mast compression on the hull is dramatic, although highly exaggerated by the plotting scale.

¹¹ Although not included in this project, global bending of sailing yachts is a significant factor in boat speed. Structurally stiff boats have longer waterline lengths and more controllable rigs. The sailors onboard during the tests noted a qualitative difference in forestay sag while sailing through waves with the more fatigued boat having greater dynamic forestay movement. Using similar sails, *Imagination* was clearly faster upwind than J6.

Figures 9-21 to 9-23: J/24 Unloaded, and Floating with Slack and Tight Rigs (in)



9.4.5 Underway Test Correlation

The final finite element analysis was to compare the vessel's predicted bending response in the wind and sea conditions seen during the on-the-water testing to measurements taken from the strain gauge and accelerometer data. Rig loads were based on an equilibrium analysis using the shroud and forestay strain gauge readings as the primary inputs. Hydrostatic loading was based on wave elevation profiles scaled off photographs of the boat sailing. Figure 9-24 shows the load application points (green arrows) and wave surface elevation (yellow arrows representing pressures) for the maximum loads seen during the on-the-water testing. The loads and heel reflect the vessel is close-hauled on port tack. The wave elevation was scaled off photos and was adjusted slightly to achieve equilibrium.

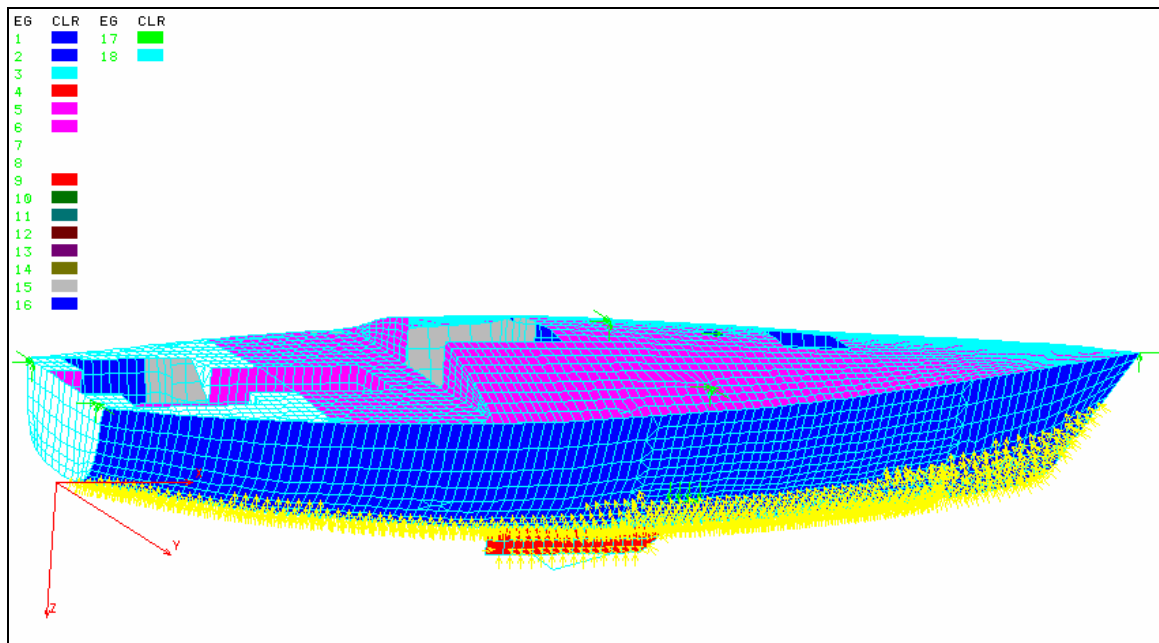


Figure 9-24: Wave Elevation and Rig Loads Simulating Test Conditions

Hydrodynamic slamming loads used the Von Karmen pressure equation with the vertical acceleration components derived from the accelerometer data. The area subjected to slamming

was based on analytical and experimental studies of sailing vessels of similar shape [13, 91].

Figure 9-25 shows the slamming area. The total pressure at any point was a summation of the individual pressure components.

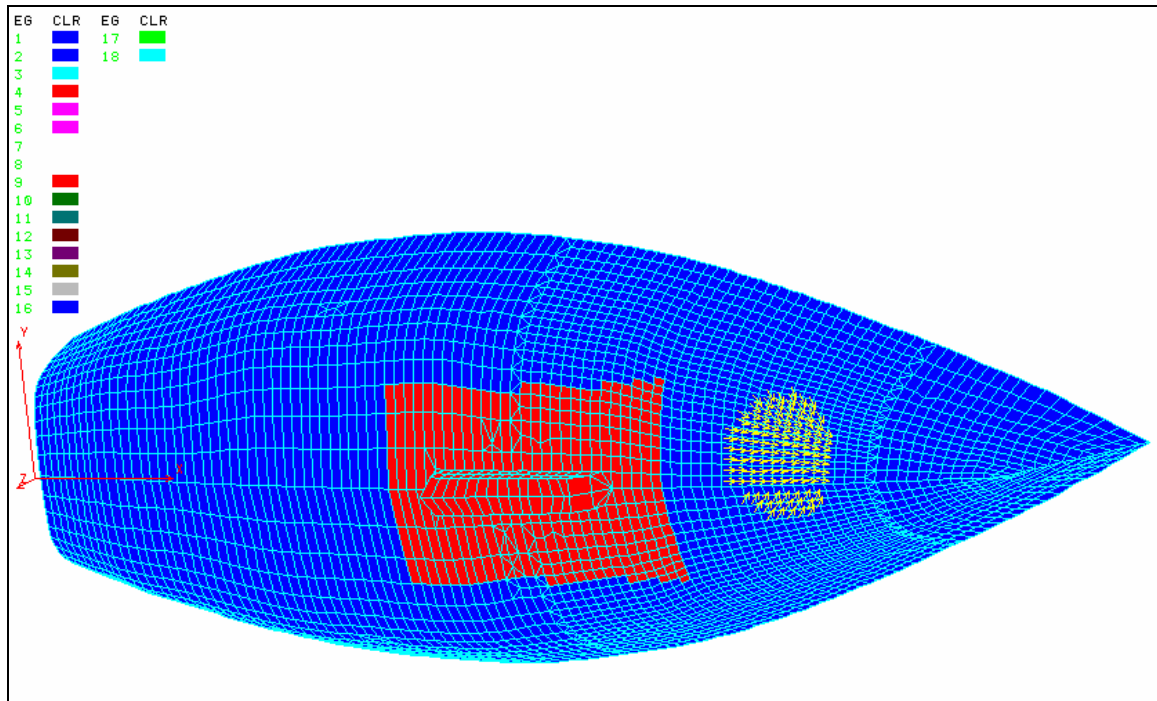


Figure 9-25: Slamming Pressure Application Point

With significant dynamic (transient) pressure loads the FEA analysis needed to match the vertical and rotational accelerations experienced by the vessel. As any body is in instantaneous equilibrium, the method to check the model's accuracy was to eliminate excessive boundary condition reaction forces.

Load cases simulated both ends of the wind and wave energy spectra, as well as one condition seen during the testing. This provided lifetime, in-service strain bounds for the laminates. The need for strain gauges on both the inside and outside of the vessel is evident from the results, which like the actual measurements, show different strains on the two surfaces. The cause of this

is the presence of two different, but related, load conditions. One is the global longitudinal hull bending caused by the rig and wave loading, and the other is the wave slap load.

In this case the maximum forefoot pressure was 6 psi in the slamming area and the maximum wave elevation resulted in a minimum freeboard forward of 1 foot.

Figures 9-26 and 9-27 show the inner and outer layer strain plots resulting from the slamming. The 17% greater strain on the inner skin was due to the combination of the unsymmetric laminate construction and rig and wave loads discussed in previous sections. Away from the slamming area, for instance near the stem and along the hull centerline, the strains experienced by the inner and outer skins are nearly equal.

The maximum predicted strain for the 12.5 knots of wind and 1 foot seas was 0.12%. As the failure strain is 0.93% for the dry condition and 0.90% for the wet condition this means that in moderate conditions the hull is routinely seeing strains equal to 13% of failure strain. As the flexural fatigue experiments presented in Section 6.7 showed the endurance limit was near 25% of the failure strain, this means no significant fatigue would occur on J/24's sailing in winds below 13 knots.

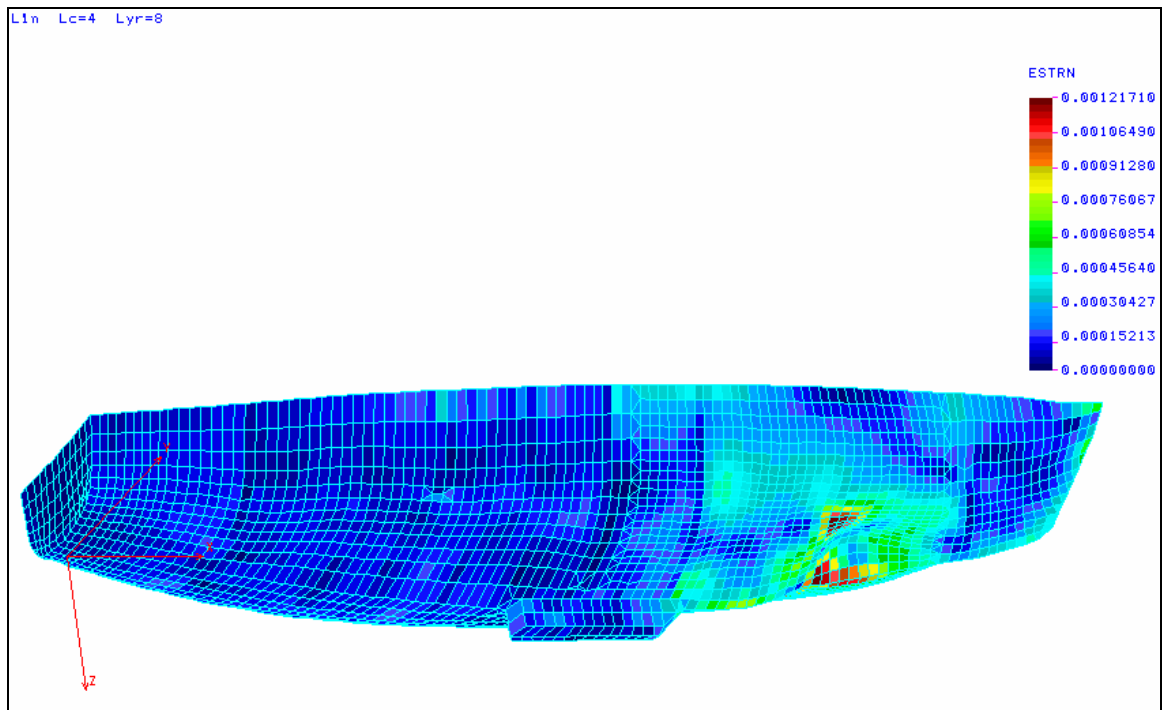


Figure 9-26: Slamming Strain Plot for Inner (cloth) Layer, WS=12.5 knots, Hs=1 foot

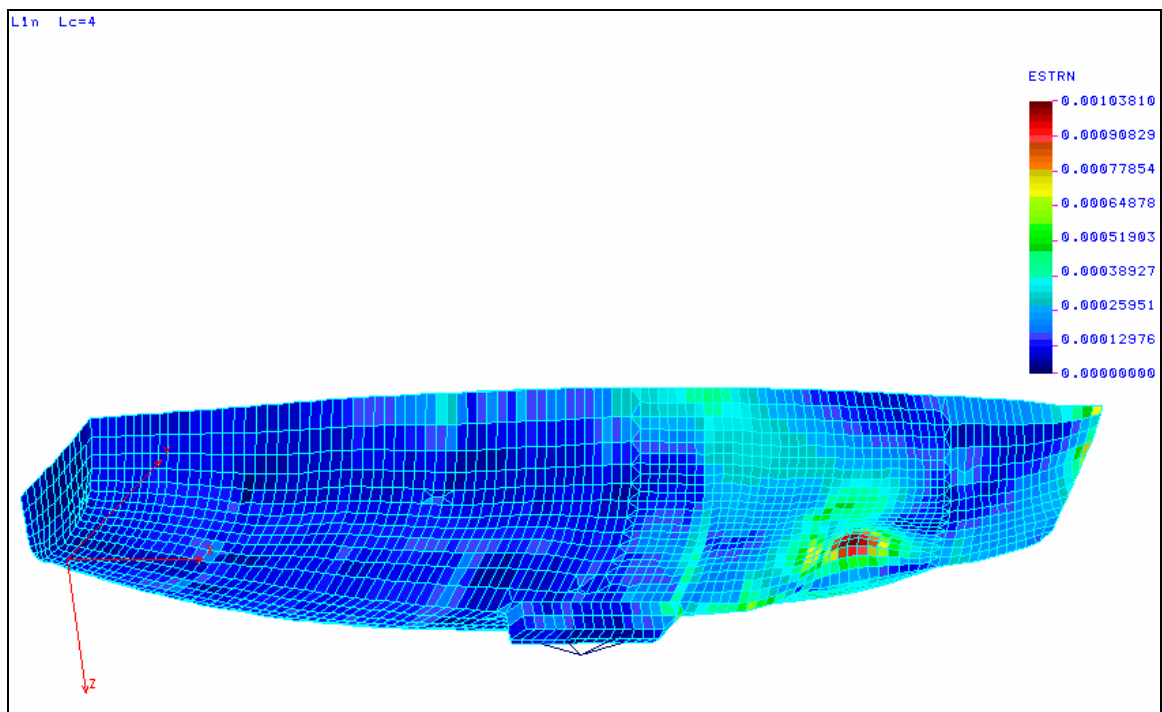


Figure 9-27: Slamming Strain Plot for Outer (mat) Layer, WS=12.5 knots, Hs=1 foot

To model the maximum conditions routinely seen by the vessel, 22 knots and 2.5 feet seas, the vessel was heeled 25 degrees and the freeboard forward was zero, corresponding to the bow nearly burying itself in a wave. Freeboard aft was greater, with the transom bottom submerged only four inches. Again, these wave surface elevations were scaled off photos and the model was balanced for instantaneous equilibrium. Figures 9-28 and 9-29 show plots similar to those presented for the 12.5-knot condition. In these stronger conditions the maximum strain was 0.214%, corresponding to 24% of failure strain. Based on the flexural fatigue coupon results, fatigue will occur.

To develop the stress response distribution, models were run for wind conditions ranging from 10 knots to 25 knots. Corresponding to the wave height distributions (see Table 8-5), the stress distribution was grouped in 5 knot increments with the mean stress at the middle of the range (i.e. 12.5 knots, 17.5 knots, 22.5 knots). The maximum strains, as a percentage of failure, were 13%, 19% and 24%.

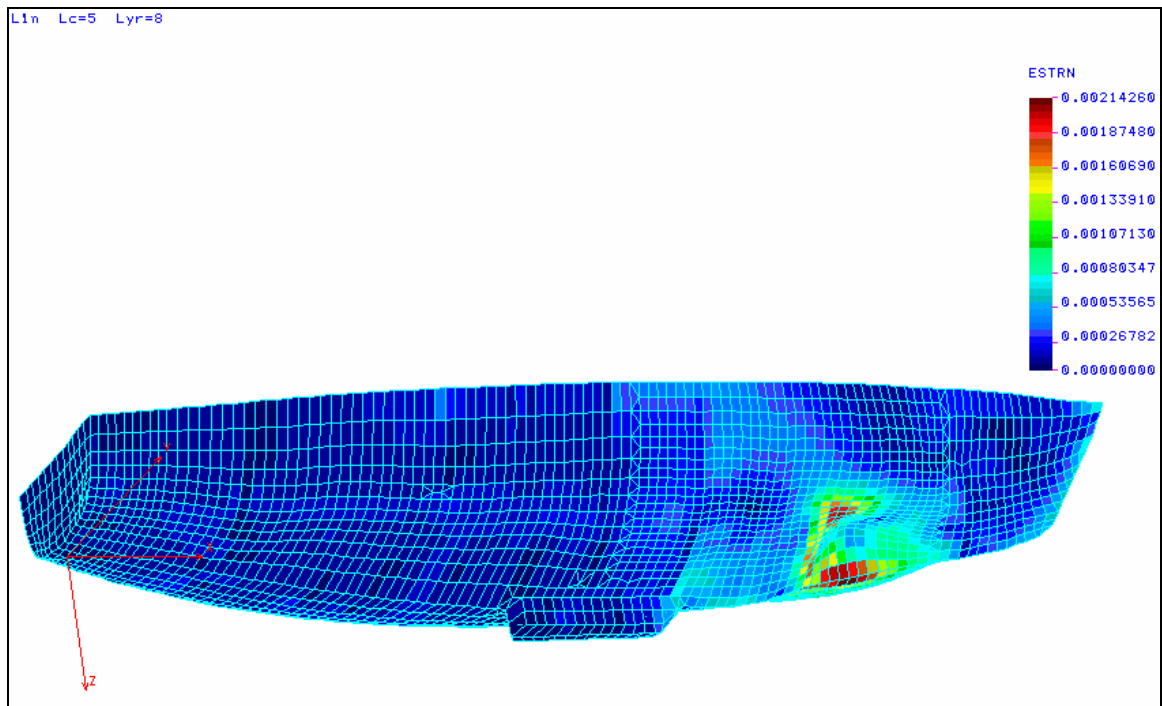


Figure 9-28: Slamming Strain Plot for Inner (cloth) Layer, WS=22.5 knots, Hs=2 feet

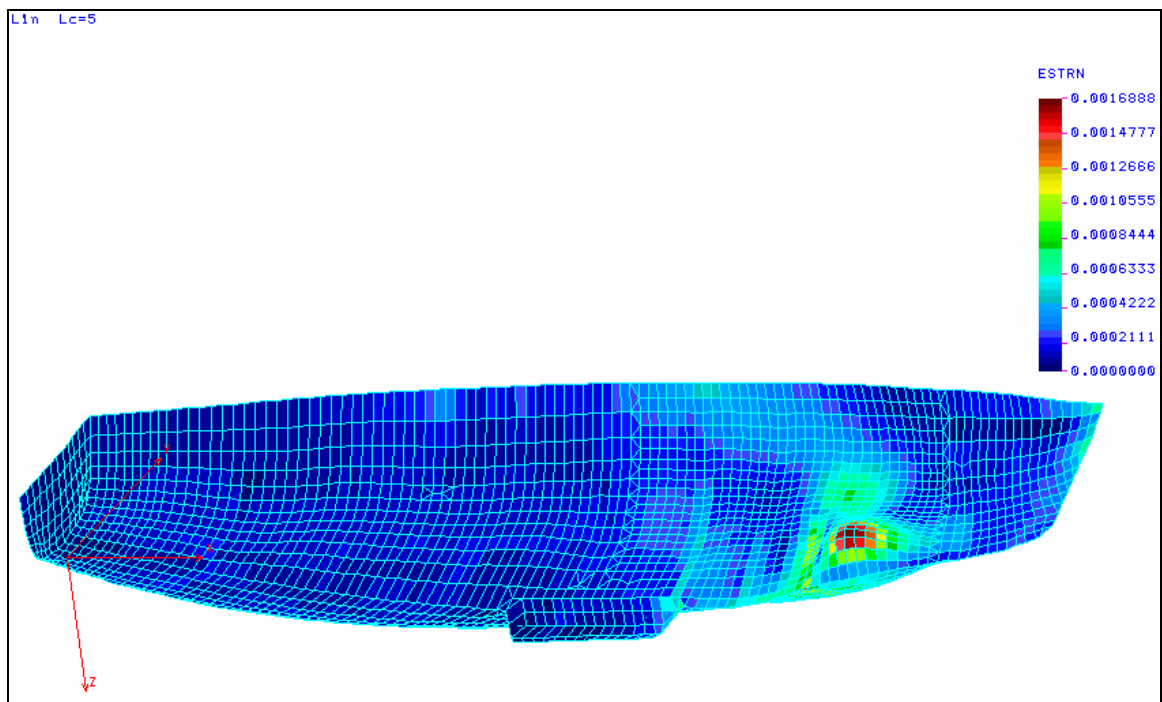


Figure 9-29: Slamming Strain Plot for Outer (mat) Layer, WS=22.5 knots, Hs=2 feet

9.4.6 Cumulative Stiffness Reduction

The final step in correlating the predicted stiffness reduction was to discretize and solve for the total stiffness reduction. Recalling from Section 4.1.3, the total expected damage during T is:

$$E[D] = T \cdot f \int_0^{\infty} \frac{p(s_i) ds}{N(s_i)}$$

and from Section 8.2.2

$$T \cdot f = p(\phi) \cdot p(m) \cdot p(U_{ws}) \cdot \left[f(U_{ws}) + \frac{U(\phi, U_{ws}) \cdot \cos(\phi)}{U_w(U_{ws}) \cdot T_s(U_{ws})} \right]$$

By discretizing, the integration is replaced by a summation in terms of functional relationships

$$D = \sum_{i=1}^j p(\phi)_i \cdot p(m)_i \cdot p(U_{ws})_i \cdot \left[f(U_{ws})_i + \frac{U(\phi, U_{ws})_i \cdot \cos(\phi_i)}{U_w(U_{ws})_i \cdot T_s(U_{ws})_i} \right] \frac{n(s_{fi})}{N(s_{fi})}$$

Where

D = the accumulated damage ratio (stiffness or strength)

p() = the probability distribution function result for that component

ϕ = heading angle relative to upwind

m = the monthly usage

U = boat speed ("ws" refers to wind speed)

U_w = wave speed

T_s = significant wave period (see Figure 8-5)

$n(S_{fi})$ = the number of stress cycles at stress f_i

$N(S_{fi})$ = the number of cycles to failure at stress f_i

As the equation shows, to find the residual stiffness includes summing a series of stress cycles caused by wave encounters. The primary factors include:

- wind speed, which drives wave height, wave period and boat velocity
- course relative to the waves
- time of day
- month of the year

Table 9-12 compares the predicted and measured stiffness reductions for J6 and Imajination compared to an unfatigued vessel.

	New Boat	Imajination	J6
Predicted Stiffness Reduction	0%	3%	14%
Measured Stiffness Reduction - String	-	14%	52%
Measured Stiffness Reduction - Strain Gauge	-	4%	18%

Table 9-12: Predicted and Measured Stiffness Reduction for J6 and Imajination

Using the predicted history of J6 and the flexural fatigue coupon results, the predicted flexural stiffness reduction is 14%. This compares to the peak strain differences between the measurements taken on-the-water and the FEA model predictions of 18%. For Imajination, the predicted stiffness loss was 3% and the measured versus FEA difference was 4%.

The correlation is reasonable given the potential variances in manufacturing between the coupons and the two vessels, and the significance of low-cycle fatigue, where the vessels' histories is unknown. In the case of J6, if, as seen in the flexural coupon studies, a 20% reduction in stiffness signals near-term fatigue failure, then some failures are likely in 5-10 years of continued use.

The simple string test correctly modeled the loss of stiffness trend, but over-predicted the amount significantly. As the string test included components not modeled by the FEA or measured by the strain gauges, such as the mast and pulpits, the higher deflections are not surprising. For those wishing to determine if their vessel has lost stiffness, the simple string test, by amplifying the results to a level measurable by common tools, is a viable option.

10.0 Conclusions and Recommendations

The objective of this study was to document, evaluate and improve the current methods of fatigue analysis for marine composites through a detailed analytical and experimental program. This was satisfactorily accomplished. Additional insight was also developed. Specific conclusions were:

1. “Traditional” single-value reduction factors on composite material properties for fatigue effects are not appropriate in most situations. These can lead to unconservative designs. Four-point bend tests yield acceptable results if the laminate is designed for tensile face failure and the span is large enough that core shear failure is unlikely.
2. Tensile modulus can be determined from tensile tests, but tensile strength is more accurate if derived from flexural tests.
3. Effects of long-term moisture exposure can not be reliably predicted through boil tests. In this case the boil test led to significant conservativeness. For laminates with low fiber volumes tensile properties as well as shear and compressive properties are effected. Significant differences were seen in the number of flexural cycles to failure, even though the inside surface, which failed first, was dry in both cases.
4. Panel testing can be replicated by finite element analysis and coupon tests. In cases where FEA is planned due to the complexity of structure, panel tests are not needed. In other cases, either FEA or panel tests can be used, although FEA offers significantly greater flexibility.
5. Relatively dense meshes are required to accurately model stresses and panel deflections when using linear shell elements. For high-cycle fatigue applications this is acceptable as in-plane deflections remain in the linear range of composites. Low-cycle applications should use a non-linear modulus profile to accurately model deflections and stresses.
6. COSMOS linear solid composite elements provided marginally accurate out-of-plane deflections and stresses, while linear shell elements can provide accurate results. Linear shell analysis can be improved by applying a single-step, in-plane, added-stiffness

- approximation. In cases where large deformation is combined with multi-axis loading, such as boundary constraints, geometric non-linear analysis is required.
7. Four-point flex tests return more consistent results than 3-point tests.
 8. To match core shear vs. skin failure modes in an application, coupon spans must be sized large enough to eliminate premature shear failure.
 9. Contrary to common opinion, edge-sealing does not influence moisture absorption rates of uncured polyester laminates. Varnishing the edges of balsa-cored laminates prevents moisture absorption while not significantly effecting stiffness.
 10. The common marine practice of having thicker outer skin laminates can be justified for more than just abrasion resistance. The thicker outer skin is in compression when exposed to hydrostatic and dynamic loads. With reduced strength due to compression and moisture effects, and for practical reasons of water integrity, the common practice leads to first failure occurring with tensile failure of the inner skin.
 11. Moisture absorption by the outer hull-skin did not significantly effect panel bending or strength, although it did effect the number of fatigue cycles to failure.
 12. A simple, visual clue as to the onset of rapidly increasing fatigue failure is the onset of “whitening” of the resin. The size of the initial failure spots corresponds to the weave crimp dimensions. This could be used by surveyors to identify fatigue failure onset.
 13. Stiffness reduction due to fatigue can be significant on small craft made of composites. In the case of some racing sailboats this verifies a commonly held opinion of boats going “soft.” Design load reduction factors of 4-8 are needed with polyester/E-glass (mat/cloth) laminates to avoid service-life stiffness reduction.
 14. Dharan's proposed fatigue criteria of 40% of neat resin values appears unconservative in this application, where a value of 25% seems more appropriate. This may be due to the

- significantly higher cycles experienced in marine applications, the detrimental effects of moisture and most likely, the lower quality resins and fabrication methods than those used in other (such as aerospace) applications.
15. Polyester resins, which have failure strains of approximately 1% are not well matched to E-glass, which has a failure strain of nearly 5%. This leads to microcracking at a small portion of the fibers' ultimate strength and large moisture absorption. Better combinations would include epoxy and vinyl ester resins which have failure strains of 4-7%.
 16. Standard methods used for fatigue analysis of metal vessels can be applied to composite vessels, but unique S-N curves must be developed for each laminate.
 17. A "Miner's-type" damage accumulation approach can also be applied to stiffness reduction. Like the strength reduction, stiffness reduction in marine composites is dominated by low-cycle events. A few "significant events", such as collisions, can cause the same amount of stiffness reduction as millions of cycles of wave slap.
 18. A relatively simple "string" test can be used to check a vessel's static stiffness. This also gives a good indication of the dynamic global bending stiffness. The string test may over-predict the loss of stiffness however, as it also includes the mast and pulpits and their connections to the hull and localized stress risers such as the laminate below the mast step and the stem fitting.
 19. The "service-life" of recreational craft is difficult to predict. Designers should realize that some vessels may experience 10^8 significant wave loading cycles. As most composite fatigue data only carries to 10^6 cycles this requires a higher safety margin.

Although this project necessarily looked at an application that was commonly used 15 years ago, current technology has relegated the J/24 laminate to low-cost marine applications. Follow-on studies should look at generating S-N curves for currently used laminates. These would include laminates using woven roving, boat cloth, unidirectionals, epoxy, and vinyl ester resins, honeycomb and foam cores, and fabrication methods such as vacuum-bagging, SCRIMP, and pre-pregs.

11.0 References

1. Cauffman, S. and M. Derstine. *Three-Dimensional Braided Composites for Marine Applications*. in *International Conference on Marine Applications of Composite Materials*. 1990. Melbourne, FL.
2. *Offshore One-Designs*, in *Sailing World*. 1991. p. 49.
3. Curry, R. *Fiber Reinforced Plastic Sailing Yachts - Some Aspects of Structural Design*. in *The Ninth Chesapeake Sailing Yacht Symposium*. 1989. Annapolis, Maryland: SNAME.
4. Greene, E., *Marine Composites*, . 1990, Ship Structures Committee.
5. Hellbratt, S.E. and K.E. Makinen. *Design and Production of GRP-Sandwich Vessels*. in *Fifth International Conference on Marine Applications of Composite Materials*. 1994. Melbourne, Florida: Composites Education Assoc.
6. Hepburn, R.D., G. Magliulo, and T. Wright, *The U.S. Navy's New Coastal Minehunter (MHC): Design, Material, and Construction Facilities*. Naval Engineers Journal, 1991(May).
7. Miller, P.H. and D.L. Dillon, *The International Sailing Canoe: A Technical Review*. Marine Technology, 1994. **Vol. 31**(October).
8. Mull, G.W. *Small Craft Structures for the Eighties and Beyond (draft)*. in *The New England Sailing Yacht Symposium*. 1988. Mystic, CT.
9. NRC. *Use of Composite Materials in Load-Bearing Marine Structures*. 1990: National Research Council.
10. NRC. *Use of Composite Materials in Load-Bearing Marine Structures*. 1990: National Research Council.
11. Reichard, R.P. *Materials Selection for Boats and Ships*. in *Conference on Marine Applications of Composite Materials*. 1988. Melbourne, Florida: Composites Education Association.
12. Reichard, R.P. *Structural Design of FRP High Performance Sailing Craft*. in *Ancient Interface XVI: Proceedings of the Sixteenth AIAA/SNAME Symposium on the Aero/Hydronautics of Sailing*. 1986. Long Beach, CA: Western Periodicals Company.

13. Riber, H.J., *Strength analysis of the 470 sailing boat*, . 1993, Technical University of Denmark, Lyngby.
14. Smith, C.S. *Structural Problems in the Design of GRP Ships*. in *Symposium on GRP Ship Construction*. 1973: Royal Institution of Naval Architects.
15. Smith, C.S., *Design of Marine Structures in Composite Materials*. 1990, Barking, Essex, England: Elsevier Science Publishers.
16. Spaulding, K.B., Jr., *Fiberglass Boats in Naval Service*. Naval Engineers Journal, 1966(April).
17. Summers, C., *Building the 161' FRP Yacht Evviva*, in *Professional BoatBuilder*. 1994. p. 18-21.
18. Cahill, P., *Composite Materials and Naval Surface Combatants: The Integrated Technology Deckhouse Project*. Journal of Ship Research, 1992(Feb.): p. 1-7.
19. Pattee, W.D. and R.P. Reichard. *Hull-Bulkhead Joint Design in Cored RP Small Craft*. in *The Int'l Conference of Marine Applications for Composite Materials*. 1988. Melbourne, Florida: Composites Education Assoc.
20. Riley, C. and R. Honey, *Construction and Design Details of the 1988 America's Cup Yacht Hull and Deck Structures*, . 1988.
21. Shenoi, R.A. and J.F. Wellicome, eds. *Composite Materials in Maritime Structures*. Cambridge Ocean Technology Series. 1993: Cambridge.
22. Smith, C.S. and D.W. Chalmers. *Design of Ship Superstructures in Fibre-Reinforced Plastic*. 1986. London: Royal Institute of Naval Architects.
23. Wilhelmi, G.F., W.M. Appleman, and F. Loo, *Composite Shafting for Naval Propulsion Systems*. Naval Engineers Journal, 1986(July).
24. Loveless, H.S., L.R. Ingle, and C.E. Gerrard, *Fatigue and its Relationship to End-Use Performance*. Physical Testing of Plastics-Correlation with End-Use Performance, ASTM STP 736, 1981.
25. Davis, G.T. *In service failures from the marine surveyor point of view*. in *Fourth International Conference on Marine Applications of Composite Materials*. 1992. Melbourne, Florida: Composites Education Assoc.

26. *Boating* 1993, . 1994, National Marine Manufacturers Association.
27. Blanc, L.L., *Composites cut riser weight by 30-40%, mass by 20-30%*, in *Offshore*. 1998. p. 54-60.
28. Miller, P., *Current Technologies Used in America's Cup, IMS, 'Little' America's Cup, and Recreational Naval Architecture*, . 1996: Presentation at Royal Hong Kong Yacht Club.
29. Forbes, H., M. Laing, and J. Myatt, *Fastnet Race Inquiry*, . 1979, Royal Yachting Assoc/Royal Ocean Racing Club.
30. Smith, L.E. *Technical Issues and Design Challenges of Composite Marine Structures*. in *Application of Composites to the Marine Environment*. 1993. Savannah, Georgia.
31. Martinsen, S. and C. Madsen. *Production, Research and Development in GRP Materials at Danyard Aalborg A/S*. in *Third International Conference on Marine Applications of Composite Materials*. 1990. Florida Institute of Technology.
32. Lubin, G., *Handbook of Composites*. 1982: Van Nostrand Reinhold Company.
33. Hashin, Z., *Analysis of Composite Materials-A Survey*. Journal of Applied Mechanics, 1983. **Vol. 50**(September): p. 481-505.
34. *Forest Products Laboratory: The Encyclopedia of Wood: Revised Edition*. 1989, New York: Sterling Publishing.
35. Tsai, S., *Composites Design*. 4th ed. 1988, Dayton, Ohio: Think Composites.
36. Lu, X.S. and e. al. *Weight Critical Structures*. in *12th International Ship and Offshore Structures Congress*. 1994. St. John's, Newfoundland, Canada.
37. Rajapakse, Y.D.S. *The U.S. Navy's Composites Research Program*. in *International Conference in Advances in Marine Structures*. 1991. Dunfermline, Scotland: Elsevier Applied Science.
38. Hertel, T.W. *Advanced Composites Economic Analysis Model*. in *Ninth Composites In Manufacturing Conference*. 1990. San Diego: Society of Materials Engineering.
39. Rohan, N., *Fatigue Testing of Low Styrene Content Resin Composite Laminates*, . 1992, Florida Institute of Technology.
40. *GRP Minehunter Launched*, in *Workboat*. 1994. p. 180.

41. *Shipyard Contracts*, in *Marine Log*. 1994.
42. *Title XI catapults U.S. yards into the export market*, in *Marine Log*. 1994.
43. Helme, S., *North American Sailing Industry Study*, . 1993, International Marine.
44. Greene, E., *Investigation of FRP in Marine Structures: Results from an Industry Survey*, . 1990, Eric Greene Associates, Inc.
45. Margolis, J.M., *Advanced Thermoset Composites*. 1986, New York: Van Nostrand Reinhold.
46. Pfund, B., *The Blister Phenomenon*, in *Professional BoatBuilder*. 1992. p. 60-68.
47. Morgan, K. *Design to the Limit: Optimizing Core and Skin Properties*. in *International Conference on Marine Applications of Composite Materials*. 1990. Melbourne, FL.
48. *Rules for Building and Classing Reinforced Plastic Vessels*, . 1978, American Bureau of Shipping.
49. *Guide for Building and Classing Offshore Racing Yachts*, . 1986, American Bureau of Shipping.
50. Curry, R. *The Small Craft Industry and ABS: The Last Ten Years and the Future*. in *International Conference on Marine Applications of Composite Materials*. 1990. Melbourne, FL.
51. Bea, R.G., *Reliability Based Design Criteria for Coastal and Ocean Structures*. 1990, Barton, Australia: The Institution of Engineers, Australia. 221.
52. *Notes on Ship Slamming*, . 1993, The Society of Naval Architects and Marine Engineers: Jersey City. p. 80.
53. Warren, Q., *A Builder's Designer*, in *Professional Boatbuilder*. 1999. p. 66-80.
54. Gibbs & Cox, I., *Marine Design Manual for Fiberglass Reinforced Plastics*. 1960, New York: McGraw-Hill Book Co.
55. Sponberg, E.W., *Carbon Fiber Sailboat Hulls: How to Optimize the Use of an Expensive Material*, . 1985: New London.

56. Whitney, J.M., *Structural Analysis of Laminated Anisotropic Plates*. 1987, Lancaster, PA: Technomic Publishing Co.
57. Jakubowski, J.C. *Stiffness Reduction of Marine Laminates Due to Constant Amplitude Deflection Fatigue Loading*. in *International Conference on Marine Applications of Composite Materials*. 1990. Melbourne, Fl: Composites Education Association.
58. Hughes, O.F., *Ship Structural Design*. 1988, Jersey City, New Jersey: The Society of Naval Architects and Marine Engineers.
59. Cox, G., *Marine Design Manual for Fiberglass Reinforced Plastics*. 1960, New York: McGraw-Hill Book Co.
60. *Engineer's Guide to Composite Materials*. 1987, Metals Park, Ohio: American Society for Metals.
61. Hofer, K.E., M. Stander, and L.C. Bennet. *Degradation and Enhancement of the Fatigue Behavior of Glass/Graphite/Epoxy Hybrid Composites After Accelerated Aging*. in *SPI Annual Conference*. 1977. Washington DC: Reinforced Plastics/Composites Institute.
62. Collins, J.A., *Failure of Materials in Mechanical Design*. Second ed. 1993, New York: John Wiley & Sons. 654.
63. Schaff, J.R. and B.D. Davidson, *Life Prediction for Composite Laminates Subjected to Spectrum Fatigue Loading*, in *Durability of Composite Materials*. 1994, ASME. p. 89-109.
64. Konor, O. and L. Mathews, *Effect of the Properties of the Constituents on the Fatigue Performance of Composites: A Review*. Composites, 1989. **Vol. 20**(No. 4 (July)): p. 317-328.
65. Burrell, P., T. McCabe, and A. Thomas. *Vinyl Esters (Epoxy Acrylates) in Marine Composites; Studies in Blister and Fatigue Resistance*. in *British Plastics Federation Congress*. 1988.
66. Chamis, C.C. and C.A. Ginty, *Fiber Composite Structural Durability and Damage Tolerance: Simplified Predictive Methods*, . 1987, NASA-Langley.
67. Cable, C.W., *The Effect of Defects in Glass-Reinforced Plastic (GRP)*. Marine Technology, 1991(March): p. 91-98.

68. Howson, J.C., R.J. Rymill, and R.F. Pinzelli, *Fatigue Performance of Marine Laminates Reinforced with Kevlar Aramid Fibre*, . 1990, Lloyd's Register of Shipping.
69. Kovach, B. *The effects of voids on the mechanical properties of fiber-reinforced plastics*. in *Fifth International Conference on Marine Applications of Composite Materials*. 1994. Melbourne, Florida: Composites Education Assoc.
70. Springer, G., ed. *Environmental Effects on Composite Materials*. . 1981, Technomic: Westport, CT.
71. Hashin, Z., *Cumulative Damage Theory for Composite Materials: Residual Life and Residual Strength Methods*. Composites Science and Technology, 1985. **Vol. 23**: p. 1-19.
72. Phelan, R. *Design, Analysis, Fabrication and Testing of a Composite Control Surface for a Small Submersible*. in *Fifth International Conference on Marine Applications of Composite Materials*. 1994. Melbourne, Florida: Composites Education Association.
73. ASTM, *ASTM Standards and Literature References for Composite Materials*, . 1978, American Society for Testing and Materials.
74. Pfund, B., *Testing Composites*, in *Professional BoatBuilder*. 1990. p. 22-29.
75. Fried, N. *Degradation of Composite Materials: The Effect of Water on Glass Reinforced Plastics*. in *Fifth Symposium on Naval Structural Mechanics*. 1967: Pergammon Press.
76. Kienast, G., *Drying Dove's Feathers*, in *Epoxyworks*. 1995. p. 19-21.
77. Sloan, F.E., *The Effects of Long-Term Seawater Exposure on Graphite/Epoxy Composite Materials*, . 1991, University of California at San Diego.
78. Macander, A. and M. Silvergleit, *The Effect of the Marine Environment on Stressed and Unstressed Graphite/Epoxy Composites*. Naval Engineers Journal, 1977(August).
79. Miller, P.H., *Corrosion of a Carbon/Epoxy Skin Laminate with an Aluminum Honeycomb Core Subjected to Seawater Immersion*, . 1994, University of California at Berkeley.
80. Branner, K., *Simulation of Fatigue in the Foam Core of Sandwich Beams*, . 1993, The Technical University of Denmark.

81. Kellas, S. and J. Morton, *Strength Scaling in Fiber Composites*. AIAA Journal, 1991(91-1144).
82. Olsson, K.-A. and A. Lonno. *Shear Fatigue of the Core and Peeling of Skins in GRP-Sandwich*. in *Third International Conference on Marine Applications of Composite Materials*. 1990. Florida Institute of Technology.
83. *Structural Reliability Methods*, . 1991, Det Norske Veritas.
84. Chamis, C.C. and M.C. Shiao, *Probabilistic Assessment of Composite Structures*, . 1993, NASA.
85. Ochi, M.K., *Wave Statistics for the Design of Ships and Offshore Structures*. SNAME Transactions, 1978.
86. Johnson, J.W., *Summary of Wave Data for San Francisco Bay and Vicinity*, . 1953, University of California at Berkeley.
87. Chou, S.J., *Ship motions and capsizing in astern seas*, . 1974, University of California at Berkeley.
88. Lewis, E.V., ed. *Stability and Strength*. Third ed. Principles of Naval Architecture. Vol. 1. 1988, The Society of Naval Architects and Marine Engineers: Jersey City, NJ.
89. McCurdy, R., *Safety From Capsizing: Final Report of the Directors*, . 1985, Society of Naval Architects and Marine Engineers/United States Yacht Racing Union.
90. Pedrick, D. *Advanced Technology in Yacht Design*. in *Incontri in Terra di Sienna*. 1993. Castelluccio di Pienza, Italy.
91. Hamilton, J. and J. Patterson. *America's Cup Yacht Structural Design: Finite Element Analysis and Laminate Optimization*. in *SAMPE*. 1992. Anaheim, California: Society for the Advancement of Materials Processing and Engineering.
92. Morison, J.R., *et al.*, *The Forces Exerted by Surface Waves on Piles*. Transactions of AIME, 1950. **189**: p. 149-157.
93. Hayman, B., T. Haug, and S. Valsgard. *Response of Fast Craft Hull Structures to Slamming Loads*. in *FAST '91*. 1991. Trondheim, Norway: Tapir Publishers.

94. Lind, W. and D. Novak. *ABS Rules for Composite Marine Structures*. in MACM '96. 1996. Cocoa Beach, Florida: Composites Education Assoc.
95. Chiu, F.C. and M. Fujino, *Nonlinear prediction of vertical motions and wave loads of high-speed crafts in head sea*. International Shipbuilding Progress, 1989. **Vol. 36**(No. 406): p. 193-232.
96. Mansour, A.E., *Extreme Loads and Load Combinations*. Journal of Ship Research, 1995. **39**(1): p. 53-61.
97. Mansour, A.E. and J.-P. Wasson, *Charts for Estimating Nonlinear Hogging and Sagging Bending Moments*. Journal of Ship Research, 1995. **39**(3): p. 240-249.
98. Mansour, A.E. and J.J. Jensen, *Slightly Nonlinear Extreme Loads and Load Combinations*. Journal of Ship Research, 1995. **39**(2): p. 139-142.
99. Stenseng, A., *Cracks and Structural Redundancy*. Marine Technology, 1996(October 1996): p. 290-298.
100. Mansour, A.E., *Probabilistic Design Concepts in Ship Structural Safety and Reliability*. Transactions of the Society of Naval Architects and Marine Engineers, 1972. **79**: p. 64-88.
101. Lewis, E.V., ed. *Motions in Waves and Controllability*. Third ed. Principles of Naval Architecture. Vol. 1. 1988, The Society of Naval Architects and Marine Engineers: Jersey City, NJ.
102. Gilmer, T.C., *Modern Ship Design*. Second ed. 1975, Annapolis, Maryland: Naval Institute Press.
103. Young, I.R., *The determination of spectral parameters from significant wave height and peak period*. Ocean Engineering, 1992: p. 497-508.
104. Pond, S. and G.L. Pickard, *Introductory Dynamical Oceanography*. 2nd ed. 1983, Oxford, U.K.: Pergamon.
105. *Shore Protection Manual*. Fourth ed. Vol. 1. 1984, Vicksburg, Mississippi: US Army Corps of Engineers.
106. Gilliam, H., *Weather of the San Francisco Bay Region*. 1962, Berkeley: University of California Press.

107. Chakrabarti, S.K., *Hydrodynamics of Offshore Structures*. 1987, Boston: Computational Mechanics Publications.
108. CRC, *Standard Mathematical Tables*, . 1957.
109. Larsson, L. and R.E. Eliasson, *Principles of Yacht Design*. 1994, Camden, Maine: International Marine.
110. Cook, R., D. Malkus, and M. Plesha, *Concepts and Applications of Finite Element Analysis*. Third Edition ed. 1989: John Wiley and Sons.
111. Reddy, J.N., *A Simple Higher-Order Theory for Laminated Composite Plates*. Journal of Applied Mechanics, 1984. **Vol. 51**(December): p. 745-752.
112. DiSciuva, M., *An Improved Shear-Deformation Theory for Moderately Thick Multilayered Anisotropic Shells and Plates*. ASME Journal of Applied Mechanics, 1987. **Vol. 54**: p. 589-596.
113. Taggart, R., ed. *Ship Design and Construction*. . 1980, Society of Naval Architects and Marine Engineers: New York.
114. Hornzee-Jones, C., Y. Harari, and R.A. Shenoi. *Finite Element Modelling as a Design Tool for Advanced Composite Marine Structures*. in *PRADS*. 1992.
115. Ochoa, O.O. and J.N. Reddy, *Finite Element Analysis of Composite Laminates*. Solid Mechanics and its Applications, ed. G.M.L. Gladwell. 1992, Boston: Kluwer Academic Publisher.
116. Hashin, Z., *Failure Criteria for Unidirectional Fiber Composites*. ASME Journal of Applied Mechanics, 1980. **Vol. 47**: p. 329-334.
117. Talrega, R., *Fatigue of Composite Materials*. 1987, Lancaster, Penn.: Technomic. 180.
118. Dharan, H., *Class notes for ME127, Composite Materials*, . 1993, University of California at Berkeley.
119. Riley, C. and F. Isley. *Application of Bias Fabric Reinforced Hull Panels*. in *First International Conference on Marine Applications of Composite Materials*. 1986. Melbourne, Florida.

120. Huss, J.R. *Structural Response of Marine Sandwich Panels to Uniform Pressure Loading*. in *Fourth International Conference on Marine Applications of Composite Materials*. 1992. Melbourne, Florida: Composites Education Association, Inc.
121. Reichard, R. *Pressure Testing of FRP Sandwich Panels*. in *Fourth International Conference on Marine Applications of Composite Materials*. 1992. Melbourne, Florida: Composites Education Assoc.
122. Bertelsen, W.D., C.S. Rau, and D.L. Sikarskie. *On the development of a two-dimensional test fixture for composite panels*. in *Fifth International Conference on Marine Applications of Composite Materials*. 1994. Melbourne, Florida.
123. Lazarus, P., *Comparing (Composite) Apples and Oranges*, in *Professional BoatBuilder*. 1994. p. 3.
124. <http://www.reichhold.com>, .
125. Belanger, B., *e-mail message*, . 1999, Reichhold, Inc.
126. Burke, S., *Fax of July 29*, . 1998.
127. Windcall, *Wind Reports*, . 1999, Call of the Wind, Inc.
128. NCDC, *Daily Summaries for San Francisco Airport*, . 1999, National Climatic Data Center.
129. Sorensen, R.M., *Basic Wave Mechanics for Coastal and Ocean Engineers*. 1993, New York: John Wiley and Sons.
130. Tupper, E., *Introduction to Naval Architecture*. 1996, Jersey City, NJ: The Society of Naval Architects and Marine Engineers.
131. Kerwin, J.E. and J.N. Newman. *A Summary of the H. Irving Pratt Ocean Race Handicapping Project*. in *Chesapeake Sailing Yacht Symposium*. 1979. Annapolis, MD: Society of Naval Architects and Marine Engineers.
132. IMS, *IMS Velocity Prediction Program Speed Predictions for J/24 Class Sailboat*, . 1996, US Sailing: Portsmouth, RI.
133. Powell, T., *e-mail to Paul H. Miller*, . 1999.
134. J/Boats, *Advertisement*, in *Yacht Racing and Cruising*. 1988.

135. Ottosen, N. and H. Petersson, *Introduction to the Finite Element Method*. 1992, Hemel Hempstead: Prentice Hall International (UK) Ltd.
136. Bea, R.G., *The Role of Human Error in Design, Construction, and Reliability of Marine Structures*, . 1994, Ship Structures Committee: Washington DC.
137. Scott, R.J., *Fiberglass Boat Design and Construction*. 1996, Jersey City, New Jersey: The Society of Naval Architects and Marine Engineers.
138. VanVlack, L.H., *Materials for Engineering: Concepts and Applications*. 1982, Reading, Massachusetts: Addison-Wesley Co.
139. Young, W.C., *Roark's Formulas for Stress and Strain*. 6th Edition ed. 1989, New York: McGraw-Hill, Inc.
140. Hentinen, M. and M. Hildebrand. *Nonlinear Behaviour of Single-Skin and Sandwich Hull Panels*. in *FAST '91*. 1991. Trondheim, Norway: Tapir Publishers.
141. *COSMOS/M 2.0 User's Manual*. 1998, Los Angeles, CA: Structural Research and Analysis Corp.
142. *COSMOS/M Nonlinear FE Structural Analysis Training Manual*, ed. A.-S.M. Niaz. 1998, Santa Monica, Calif.: Structural Research and Analysis Corp.
143. Suresh, S., *Fatigue of Materials*. 1991, Cambridge: Cambridge University Press.
144. Houlsten, R. and C.G. DesRochers, *On Analysis of Structural Response of Ship Panels Subjected to Air Blast*. *Computers and Structures*, 1985. **21**: p. 273-289.
145. Ransom, J.B. and J. N. F. Knight, *Global/Local Stress Analysis of Composite Panels*, . 1989, NASA.

12.0 Appendices

MathCad CLT

J/24 Drawings and Specifications

Global FEA Model Element Groups, Real Constants, Material Properties

MathCad J/24 bending